

1-1-2014

Blast-Induced Tinnitus: A Combined Behavioral, Memri, And Electrophysiology Study

Jessica Pengyun Ouyang
Wayne State University,

Follow this and additional works at: http://digitalcommons.wayne.edu/oa_dissertations



Part of the [Neurosciences Commons](#), and the [Physiology Commons](#)

Recommended Citation

Ouyang, Jessica Pengyun, "Blast-Induced Tinnitus: A Combined Behavioral, Memri, And Electrophysiology Study" (2014). *Wayne State University Dissertations*. Paper 910.

**BLAST-INDUCED TINNITUS: A COMBINED BEHAVIORAL, MEMRI, AND
ELECTROPHYSIOLOGY STUDY**

by

JESSICA OUYANG

DISSERTATION

Submitted to the Graduate School

of Wayne State University,

Detroit, Michigan

in partial fulfillment of the requirements

for the degree of

DOCTOR OF PHILOSOPHY

2014

MAJOR: PHYSIOLOGY

Approved by:

Advisor

Date

© COPYRIGHT BY

JESSICA OUYANG

2014

All Rights Reserved

DEDICATION

To my family and friends for their constant encouragement.

ACKNOWLEDGMENTS

The dissertation was performed under the supervision of Prof. Jinsheng Zhang at the department of otolaryngology and head-neck surgery, School of Medicine, Wayne State University. First and foremost, I would like to thank Dr. Zhang for his excellent guidance and support during the entire dissertation. I express my gratitude to him for leading me into the field of auditory neuroscience.

Next, I would like to thank Prof. Cala, Prof. DeGracia, Prof. O'Leary, and Prof. Worth for their constructive criticism and guidance. Not only are they the committee members who ensured the quality of this dissertation, but most importantly, they are also mentors who ignite interests, cultivate passions and foster ambition in next generation of researchers like me.

I would also like to thank Prof. Bruce Berkowitz at the department of anatomy, School of Medicine, Wayne State University for his support and collaboration. The manganese enhanced MRI (MEMRI) technique that he helped to implement was an essential component of this research project. This dissertation would not be completed without his helpful suggestions and critiques. Additionally, I would like to thank Dr. David Bissig for his fruitful collaboration and Ms. Robin Roberts for her facilitation in sharing the 7T MRI scanner.

In addition, I owe many thanks to Dr. Pamela VandeVord and Dr. Srinikrishna Kallakuri (Dept. of bioengineering, Wayne State University) for their support in conducting the blast shock wave exposures. Their generous sharing of the facility to conduct Morris Water maze experiment made this project possible. Also, special thanks are due to Dr. Shane Perrine (Dept. of Psychiatry, behavioral and neuroscience, Wayne State University) for his friendly support for the elevated plus maze experiments.

Last but not least, I owe special thanks to the colleagues at Dr. Zhang's lab: Dr. Xueguo Zhang, Mr. Edward Pace, Miss. Laura Lepczyk, Dr. Hao Luo, Dr. John Moran, Miss Wei Zhang, Dr. Bin Li, and Mr. Mike Kaufman. The past five years of working with such an academic family of high intellectual caliber has been the most incredible treasure for me for many years to come. I would also like to extend my gratitude to Miss. Chris Cupps at the department of Physiology, whose patience and support have carried me through the darkest time.

And I would also like to acknowledge my offsprings (Nathan and Jason) for their encouragement.

The Department of Defense and the American Association of Nurse Anesthetists Foundation collectively supported this thesis.

TABLE OF CONTENTS

Dedication.....	ii
Acknowledgments.....	iii
List of Tables.....	viii
List of Figures.....	ix
List of Abbreviations.....	xi
CHAPTER 1: General Introduction.....	1
Part I: Blast-induced Tinnitus.....	1
Auditory System: anatomy and physiology.....	1
Tinnitus.....	4
Blast-induced Tinnitus.....	10
Blast-related PTSD and its Association to Blast-induced Tinnitus.....	14
Electrophysiology of the Auditory System.....	15
Manganese Enhanced Magnetic Resonance Imaging (MEMRI).....	17
Part II: Impacts of Isoflurane and Sevoflurane on Auditory Electrophysiological Signals.....	22
Consciousness.....	22
Relevance to Anesthesia Practice.....	25
CHAPTER 2: Experimental Plan and the Hypothesis.....	29
Part I: Blast-induced Tinnitus.....	29
Experimental Plan.....	28
Hypotheses.....	30
Part II: Impacts of Isoflurane and Sevoflurane on Auditory Electrophysiological Signals.....	31
Experimental Plan.....	31
Hypotheses.....	31
CHAPTER 3: Materials and Method.....	33

Animal subjects.....	33
Behavioral testing for tinnitus and hearing los	34
ABR procedure.....	37
Blast procedure.....	37
Elevated plus maze (EPM).....	39
Morris water maze (MWM).....	41
MEMRI scanning.....	43
Electrophysiology recording, ACES and acoustic masking.....	49
Histology procedure.....	52
CHAPTER 4: Results.....	53
Part I: Blast-induced Tinnitus.....	53
ABR.....	53
Diagnostic behavioral data.....	56
MEMRI.....	57
Electrophysiology data.....	58
Part II: Blast-related PTSD.....	60
Elevated Plus Maze.....	60
Morris Water Maze.....	61
MEMRI.....	62
Part III: Impacts of Isoflurane and Sevoflurane on Auditory Electrophysiological Signals.....	65
Electrophysiological data: Coherence Analysis.....	65
CHAPTER 5: Discussion.....	68
Summary of major findings.....	68
Part I: Blast-induced Tinnitus.....	68
Part II: Impact of Isoflurane and Sevoflurane on Auditory Electrophysiological Signals.....	76

Appendix I: IACUC approval.....	80
References.....	81
Abstract.....	99
Autobiographical Statement.....	101

LIST OF TABLES

Table 1: Common chemical properties of isoflurane and sevoflurane.....	23
Table 2: Signal-to-noise intensity ratio of regions of interest.....	63

LIST OF FIGURES

Figure 1: The schematic diagram of peripheral auditory system	1
Figure 2: A cross section through one of the turns of the cochlea.....	2
Figure 3: Neural wiring diagram of the DCN.....	3
Figure 4: The auditory afferent pathway.....	4
Figure 5: Schematic illustration of the connections from auditory system to amygdala.....	9
Figure 6: Schematic illustration: components of a blast.....	11
Figure 7: Three pressure/time histograms illustrating blast in three different settings.....	12
Figure 8: Distance and explosive energy level vs. possible injuries.....	12
Figure 9: A schematic illustration of the experimental design.....	29
Figure 10: Schematic illustration of a gap/PPI behavioral testing system.....	34
Figure 11: Schematic illustration of principle of Gap and PPI.....	35
Figure 12: Illustration of the shockwave apparatus.....	39
Figure 13: Picture of a rat in elevated plus maze.....	40
Figure 14: A schematic drawing of Morris water maze apparatus.....	42
Figure 15: Regions of interest superimposed on the Atlas of rat's brain.....	45
Figure 16: The RO1 of the hippocampus CA1 and CA2 regions.....	46
Figure 17: Corrected T1-weighted images (DCN, IC, VCN, AC).....	48
Figure 18: Corrected T1-weighted images (AMG, NA, ACC).....	48
Figure 19: Surgical view of the left DCN of the rat.....	50
Figure 20: Photograph showing surgical placement of electrodes arrays.....	50
Figure 21: ABR data at baseline, post-blast day 1 and post-blast day 35.....	54
Figure 22: ABR data for rats that underwent MEMRI at baseline and post-blast day 35.....	55
Figure 23: Amplitude of PIN1 ABR waveforms of the left ear.....	55

Figure 24: Auditory brainstem response waveforms.....	56
Figure 25: Gap and PPI ratios.....	57
Figure 26: Maganese enhanced MRI.....	58
Figure 27: Spontaneous multiunit firing rate in the rat DCN.....	58
Figure 28: Firing pattern plots.....	59
Figure 29: Acoustic masking, coherence coefficient matrix of a rat in tinnitus positive group.....	60
Figure 30: Elevated Plus Maze.....	61
Figure 31: One day Morris water mazes.....	62
Figure 32: MEMRI: SNR of limbic structues.....	64
Figure 33: MEMRI: average of SNRs from both sides of the brain.....	64
Figure 34. Coherence analysis matrices: anesthesia.....	66
Figure 35. Change of coherence coefficient with deepening anesthesia.....	67

LIST OF ABBREVIATIONS

A		F	
ABR	Auditory brainstem response	FID	Free induction decay
AC	Auditory cortex	Floc	floccules
AII	Secondary auditory cortex	G	
ACES	Auditory cortex electrical stimulation	GABA	gamma-aminobutyric acid
AMG	Amygdala	GCD	Granule cell domain
AMPA	α -amino-3-hydroxy-5-methyl-4-isoxazole	GWT	Global war on terrorism
B		I	
BBB	Blood brain barrier	IHC	Inner hair cell
BINT	Blast-induced neurotrauma	IC	Inferior colliculus
C		IED	Improvised explosive devices
CN	Cochlear nucleus	ICXV	Ventralateral region of IC
CTG	Chronic tinnitus group	L	
CVA	Cerebral vascular accident	LC	Locus coeruleus
D		M	
DCN	Dorsal cochlear nucleus	MGB	Medial geniculate body
DPOAE	Distortion product otoacoustic emission	MEMRI	Manganese enhanced magnetic resonance image
DRN	Dorsal raphe nucleus	MR	Magnetic resonance
E		MPRAGE	Magnetization prepared rapid acquisition gradient echo
EPM	Elevated plus maze		

M		R	
MWM	Morris water maze	RF	Radio frequency
N		ROTM	Rupture of tympanic membrane
NLL	Nucleus of lateral lemniscus	ROI	Region of interest
O		S	
OEF	Operation of Enduring Freedom	SOC	Superior olivary complex
OIF	Operation of Iraqi Freedom	Sp5	Spinal trigeminal nucleus
OHC	Outer hair cell	T	
P		TE	Echo time
PET	Positron emission tomography	TR	Repetition time
PPI	Pre-pulse inhibition	TTG	Transient tinnitus group
PTSD	Post-trauma stress disorder	V	
PDGE	Proton density gradient echo	VCN	Ventral cochlear nucleus
Pfloc	paraflocculus	VGLUTs	Vesicular glutamate transporters
Q			
QOL	Quality of life		

CHAPTER 1

GENERAL INTRODUCTION

Part I: Blast-induced Tinnitus

Auditory System: anatomy and physiology

The auditory system consists of conductive system and sensory neural system. The function of auditory system is to transform acoustic signals into neural impulses, and these impulses are then processed by the central auditory nervous system.

The conductive system consists of the outer ear and the middle ear. The outer ear includes the auricle, external auditory meatus and tympanic membrane, and the middle ear includes a chain of three ossicles (malleus, incus and stapes). The stapes attaches to an opening into the inner ear called oval window. Via vibration of ossicles in the middle ear, acoustic energy is converted to mechanic energy, which is then exerted to cochlear fluid in the inner ear.

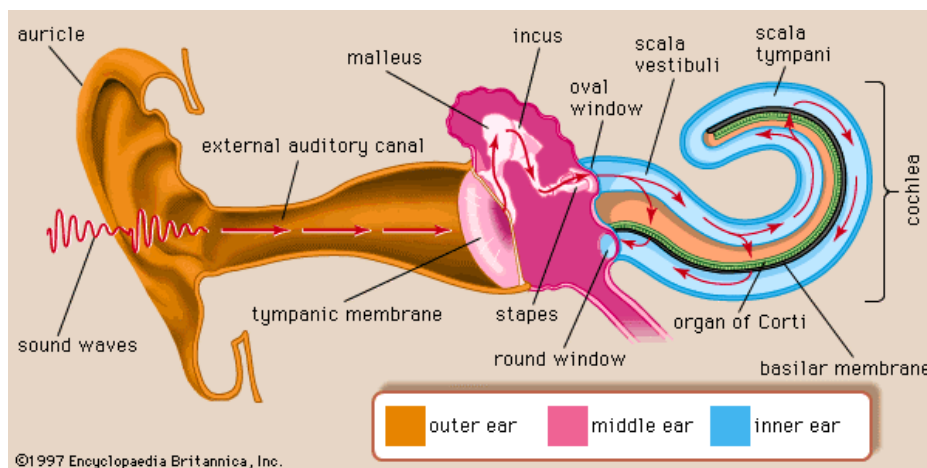


Figure 1. The schematic diagram of peripheral auditory system. The cochlea is shown in uncoiled form. *From ear: hearing mechanism. Art. Encyclopædia Britannica Online.*

Reissner's membrane and basilar membrane divide the fluid-filled cochlear into three compartments. Communicating at the apex, the scala vestibuli and scala tympani contain perilymph. The compartment in the middle is called scala media, which contains endolymph. The vibration of stapes from acoustic stimuli transfers to

perilymph in waves. While traveling down to the apex of the cochlear, the wave grows in amplitude, reaches to the peak then decays rapidly after the peak. The location of the maximum amplitude is dependent to the frequency of pure tone acoustic stimulus. The location of maximum amplitude for high frequency is close to the base, whereas for low frequency it is at apex.

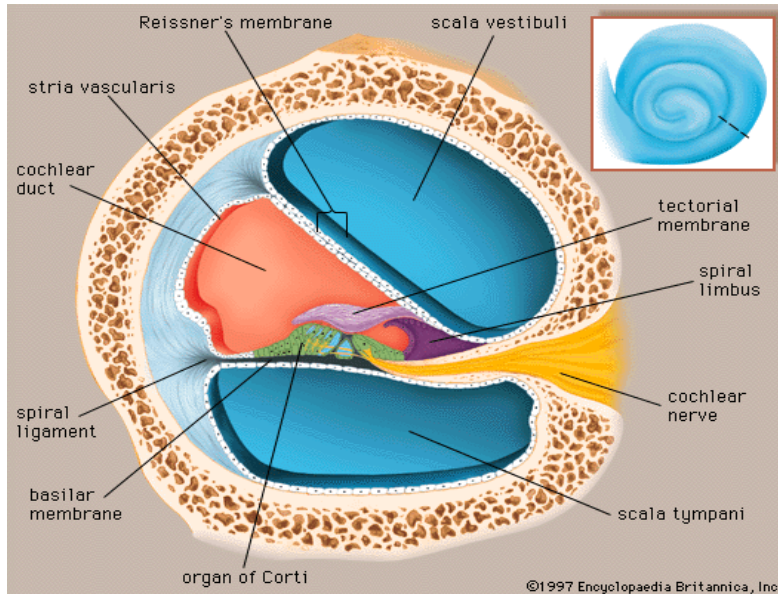


Figure 2. A cross section through one of the turns of the cochlea (inset) showing the scala tympani and scala vestibuli, which contain perilymph, and the cochlear duct, which is filled with endolymph. *Cochlea: cross section.* Art. *Encyclopædia Britannica Online.*

Supported by the basilar membrane and bathed in the endolymph, the *Organ of Corti* is the signal transduction machinery for the auditory nervous system. It contains one row of inner hair cells, three rows of outer hair cells, and several types of other supporting cells. Apical surface of the hair cells contains stereocilia. The horizontal movement of stereocilia, which is caused by vibration of the endolymph, results in a receptor potential in the hair cells. The majority of afferent impulses are propagated to the cochlear nucleus via type I neurons from inner hair cells. Type I neurons excite both fusiform cells and vertical cells; the former are principal cells in the cochlear nucleus and the latter are inhibitory interneurons in the cochlear nucleus. Type II neurons innervate outer hair cells and make excitatory synaptic contacts with granule cells in the

CN. Subsequently, granule cells make *en passant* excitatory synapses with stellate and cartwheel cells, the latter are the inhibitory interneurons for the fusiform cells (Kaltenbach et al., 2005). The outer hair cells and inner hair cells differ in morphology, innervations, and function. The inner hair cell acts as a mechanoreceptor. The outer hair cell may act as a gauging control for the type I neurons, which results in higher sensitivity and sharpened tuning properties (Abbas, 1988; Kaltenbach et al., 2005).

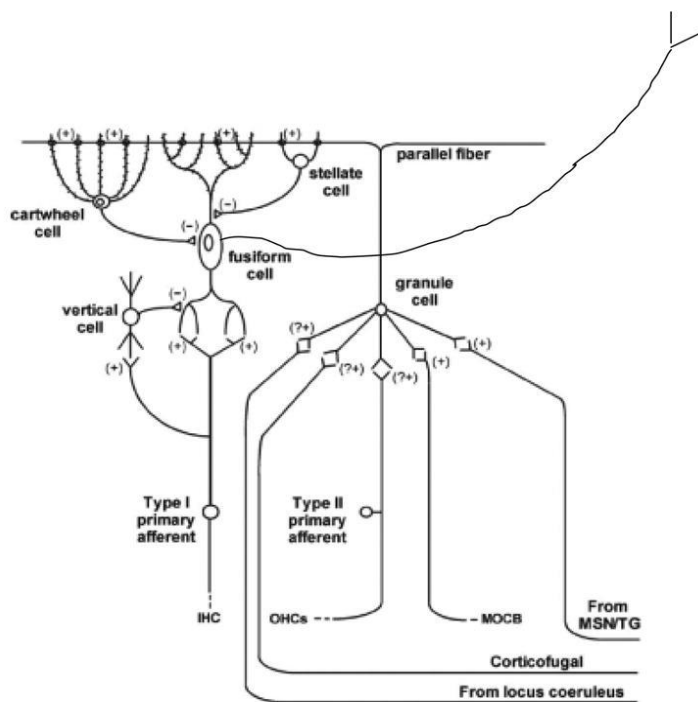


Figure 3. Neural wiring diagram of the DCN, showing inhibitory and excitatory inputs to fusiform cells (principal neuron). Kaltenbach, J.A. et al. *Hearing Research*. 206 (2005).

The cochlea sends afferent signals to the cochlear nucleus. The cochlear nucleus is divided into two subdivisions: the dorsal cochlear nucleus (DCN) and the ventral cochlear nucleus (VCN). The dorsal cochlear nucleus (DCN) sends afferent signals to the contralateral superior olivary complex (SOC) then the nucleus of lateral lemniscus (NLL), en route to the contralateral inferior colliculus (IC). The ventral cochlear nucleus (VCN) projects to both ipsilateral and contralateral superior olivary complex (SOC) then bilateral inferior colliculus (IC). After some crossover at the inferior

colliculus (IC), the auditory afferent signals reach to the medial geniculate bodies (MGB) and finally end at the auditory cortex (AC). Because of crossover at the brain stem and mid-brain, auditory afferent signals are processed in the bilateral auditory cortex (AC) (Abbas, 1988).

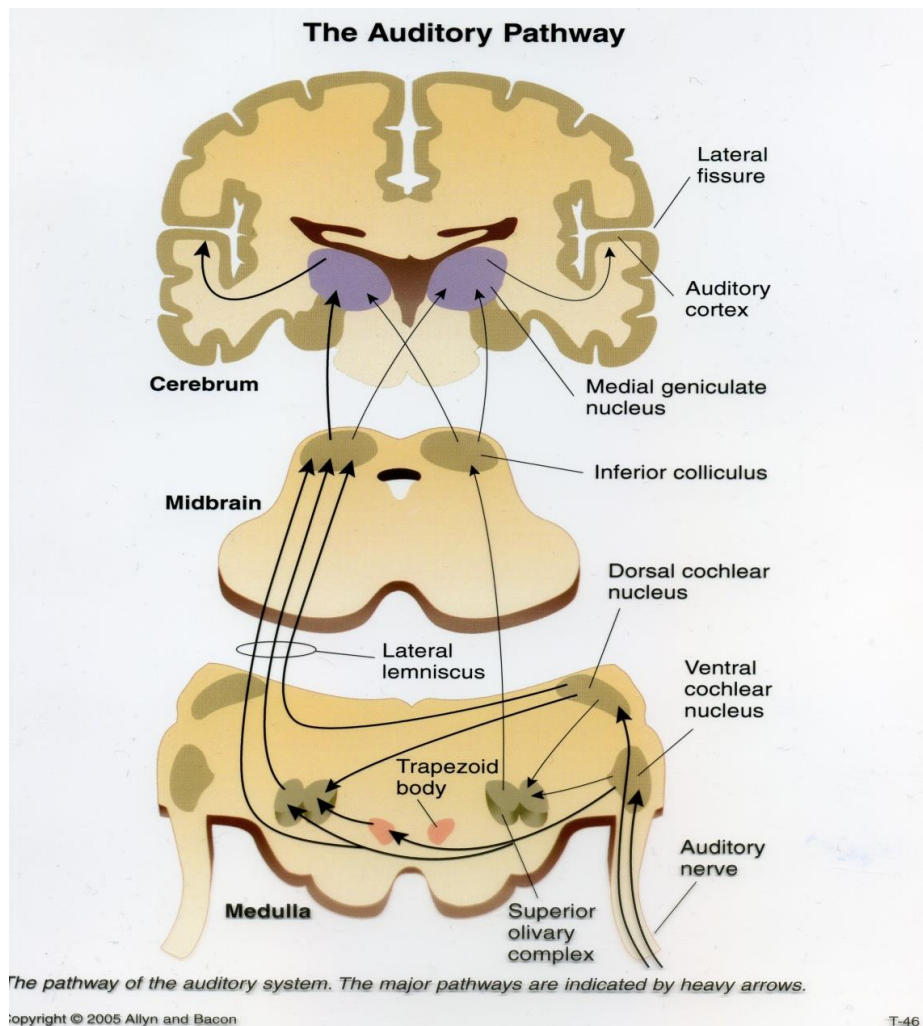


Figure 4. The auditory afferent pathway. The Major pathway is indicated in thick line. Allyn and Bacon (2005)

Tinnitus

The word "tinnitus" roots from Latin *tinnire*, which means, "to ring." Tinnitus is commonly referred to the symptom of "ringing in the ear", and it is scientifically defined as sound perception without an acoustic event. Tinnitus is a waxing and waning

sensation that is universally experienced (Baguley, 2002). Most tinnitus last seconds to hours; however, 42 million Americans suffer from long-term tinnitus, with about 10 million seeking medical help. Elderly people under stress are prone to develop tinnitus; men tend to develop tinnitus more frequently than women (Lockwood, 2005). The prevalence of severe tinnitus that affects sleep is as high as 8%-14% for people that are 50 or older (Nondahl et al., 2002).

Tinnitus is classified as objective and subjective tinnitus. Objective tinnitus is associated with turbulent blood flow, which produces real sounds that are perceived by auditory nerve system. Subjective tinnitus, on the other hand, represents the “phantom” auditory perception (Moller, 2006). The characteristics of perceived auditory sensations described by patients are heterogeneous, ranging from buzzing, humming, whistling, hissing, and to ringing. The severity of the symptoms ranges from no impact on quality of life (QOL), to mild deterioration of the ability to concentrate, to annoyance, frustration, anger, anxiousness, and to depression. In some extreme cases, severe tinnitus leads to suicidal attempts (Adoga et al., 2008; Folmer et al., 1999; Saunders, 2007). Using statistical approaches, symptoms of tinnitus can be categorized into 4 types: constant distressing tinnitus, well-coped varying tinnitus that’s worst in quiet environment, well-coped varying tinnitus that’s worst in noisy environment, and well-coped tinnitus that’s not somatomodulable (Tyler et al., 2008). This classification reflects the plastic property of tinnitus; it also implies that the mechanism of tinnitus may involve the limbic system and somatosensory modulation.

Clinically, tinnitus is associated with the following conditions: intense sound exposure, aging (presbycusis), acoustic neuromas, and exposure to ototoxic medications such as salicylates, aminoglycoside, quinine, and cisplatin. These

conditions share at least one or maybe more of four common triggers, which are hearing loss, injury of the outer hair cells, cranial nerve VIII (auditory nerve) injury, and/or excitotoxic injury (Kaltenbach et al., 2005).

(1) Hearing loss and tinnitus: current evidences indicate that hearing loss is closely correlated with tinnitus. There are two types of hearing loss: conductive hearing loss and sensorineural hearing loss. The incidence of tinnitus associated with conductive hearing loss ranges from less than 10% to 44%, and the incidence of tinnitus associated with sensorineural hearing loss ranges from less than 10% to 79% (Hazell and Jastreboff, 1990; Man and Naggan, 1981; Mills and Cherry, 1984).

(2) The injury of the outer hair cells and tinnitus: changes of amplitude of Distortion Product Otoacoustic Emission (DPOAE) have been shown as indicators of the injury involved outer hair cells but not the injury involved inner hair cells (Probst et al., 1987). Based on the observation that some patients with tinnitus have decreased DPOAE amplitude along with normal hearing, it is postulated that the cochlear mechanism of tinnitus involves damage to the outer hair cells; as matter of fact, a injury associated with outer hair cells is sufficient to induce tinnitus (Shiomi et al., 1997).

(3) Auditory nerve (CN VIII) injury and tinnitus: clinical evidence of new onset of gaze-evoked tinnitus after surgical removal of tumors of auditory nerve strongly suggests that deafferentation of auditory nerves may induce tinnitus. The onset of such tinnitus varies, which indicates plasticity (Lockwood, Wack et al. 2001); moreover, for patients with existing tinnitus due to damage of auditory nerve from the tumor, removing cranial nerve VIII does not alleviate tinnitus. This scenario suggests that the location of tinnitus formation is above the cochlea (House and Brackmann, 1981).

(4) Excitotoxic injury and tinnitus: last but not least, tinnitus can be induced by

excessive acoustic stimulation, which may lead to excessive glutamate release and transient CN VIII injury due to excitotoxicity (Puel et al., 1998). In the laboratory setting, all of above triggers have been used to create animal models for studying the mechanisms of tinnitus.

It has been well established that one of the key structures of central neuroplasticity underpinning tinnitus is the dorsal cochlear nucleus (DCN). DCN hyperactivity was observed to coincide with various aspects of plasticity of tinnitus (Kaltenbach et al., 2005). Hyperactivity in DCN, especially in the fusiform cells, can be induced by surgical removal of ossicles, by noise exposure, and by destroying outer hair cells with cisplatin in animal models (Kaltenbach et al., 2002; Kaltenbach et al., 2005). However, the DCN is not necessarily the feed-forward source of chronic tinnitus. Ablating bilateral DCNs do not improve tinnitus percept in animal model (Brozoski and Bauer, 2005).

As an integrating station for multi-modal interaction in the brain stem, the dorsal cochlear nucleus (DCN) receives nerve inputs from the spinal trigeminal nucleus (Sp5), the dorsal raphe nucleus (DRN), and the locus coeruleus (LC) (Zhang and Guan, 2007). The majority of non-auditory projections to the cochlear nucleus are from the Sp5, which carries sensory inputs such as touch, and proprioceptive inputs from the ipsilateral head, neck, tongue, and temporomandibular joint to the DCN (Zhou and Shore, 2004). Sp5 neurons project to the DCN with two types of terminal endings: small *en passant* fibers and large mossy fibers. Small fibers make synaptic contacts with granule cells in granule cell domain (GCD) and deep layer of the DCN as well, whereas mossy fibers make synaptic contacts mainly in GCD with granule cells (Haenggeli et al., 2005). In a double-labeling fluorescence study in guinea pig model conducted by Zhou et al.

(2007), two types of vesicular glutamate transporters (VGLUTs), a marker for glutamatergic synapses, were found expressed in DCN. VGLUT1 was expressed in deep layer of DCN, and VGLUT2 located in GCD (Zhou et al., 2007). These presumably excitatory mossy fibers in GCD may modulate synaptic strength and DCN output activity; subsequently, somatosensory inputs may play a critical role in initiation and modulation of tinnitus. This plausible speculation is appreciated by the clinical observation that some patients can modulate their tinnitus through movement of ipsilateral muscles in head and neck (Levine et al., 2003). It also has been proved that somatosensory electrical stimulation can suppress the DCN hyperactivity induced by noise exposure (Zhang and Guan, 2008).

As an integrating station for multi-modal interaction in mid-brain, the inferior colliculus (IC) also receives nerve inputs from the spinal trigeminal nucleus (Sp5). Inputs from the cochlear nucleus and the Sp5 converge at the ventrolateral region of IC (ICXV) then relay to bilateral MGB. Insights gained from a recent clinical report applauded a new direction. In this case, the patient suffered a cerebral vascular accident (CVA) that affected thalamocortical radiations and descending corticothalamic projections. The CVA mitigated patient's 40-year-old persistent tinnitus (Lowry et al., 2004). Moreover, a clinical high resolution MRI and voxel-based morphometric study identified increased grey matter in MGB and decreased grey matter in subcallosal area including nucleus accumbens (NA) in patients with tinnitus (Muhlau et al., 2006). The changes in grey matter in these structures reflect reorganization of corticothalamic loops with involvement of limbic system through relays from the MGB. In a review, Møller (2006) laid out two routes that auditory system relays to the limbic system. The auditory input relay in "high route" through first ventral MGB then cortico-cortio modulation (top-

down), and the extralemniscal inputs relay in “low route” through first dorsal medial MGB then subcortical modulation (bottom-up) (Moller, 2007).

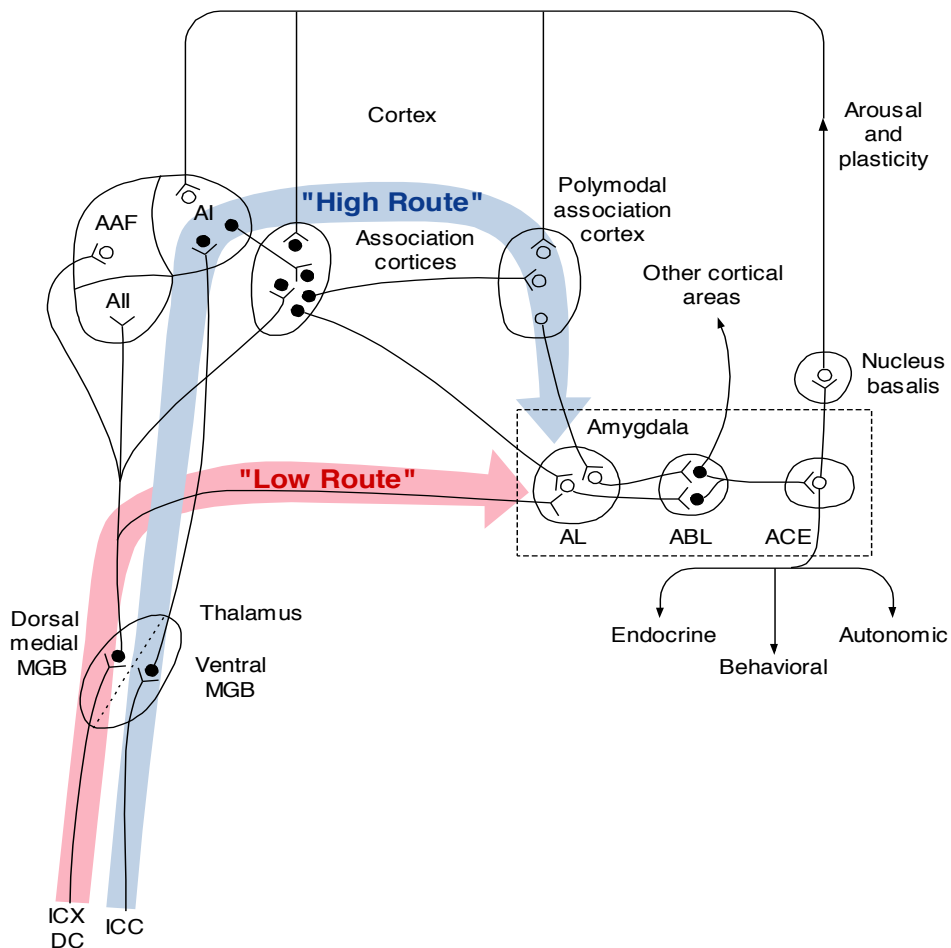


Figure 5. Schematic illustration of the connections from auditory system to amygdala. Moller, A. R. (2006). "Neural plasticity in tinnitus." *Progress in brain research* 157: 365-372

In summary, ample evidence now supports that the mechanism of tinnitus involves maladaptive plasticity in both classic auditory and non-classic auditory pathway. The changes in classic pathway include hyperactivity in the DCN, IC and AC along with increased neuronal synchronization and tonotopic remodeling in the AC (Eggermont, 2003; Norena and Eggermont, 2003). The non-classical pathway is referred to multi-modal sensory inputs to the auditory system, limbic system, and

extralemniscal paths, including the GCD in DCN, DCIC, ECIC, and the secondary AC (All) (Saunders, 2007). Intertwining with each other, plastic changes in these two pathways contribute to the perplexity of tinnitus. Despite its high prevalence and debilitating association with anxiety and depression, there is no treatment modality proven efficacious at the present time for tinnitus. However, rooted from central plasticity model, auditory cortex electrical stimulation (ACES) has shown promising results in an animal study (Zhang et al., 2011) and a number of clinical trials, which currently are in the investigating stage (Seidman et al., 2008).

Blast-Induced Tinnitus

Since 2001, 2.5 million U.S. service members have been deployed to Iraq and Afghanistan; and they have been in constant danger from roadside bombs, so-called improvised explosive devices (IEDs), ambushes and sudden firefights (Hosek, 2009; IOM, 2010). When IEDs are detonated, the sound level can exceed 140 dB SPL (IOM, 2005). Combined with overpressure, blast from IEDs can be extremely damaging to the auditory system. Even though the US Army requires wearing earplugs, almost none of the service members wear ear-protection in combat zone because they are afraid of missing critical sounds made by insurgents. Subsequently, it is not surprising that 49% of service members exposed to IEDs develop tinnitus. Currently, tinnitus is the number one service-related disability from the GWT. In 2006, \$540 million were paid to veterans of Operation of Enduring Freedom (OEF) and Operation Iraqi Freedom (OIF) as disability payments due to tinnitus, and by 2011, payment for service-related tinnitus is expected to reach \$2 billion per year (ATA, 2011).

Blast-induced tinnitus has its own complex characteristics, which dictates its complex underlying mechanism(s). Understanding the physics with regard to a blast

event is fundamental in pursuing knowledge about how blast exposure damages the auditory nerve system. A blast event starts with *detonation*, which generates a *blast flow field*; it ends with a hurricane-like blast wind, which dynamically propagates energy to nearby field (Figure 6). *Detonation* is instantaneous combustion of a solid or liquid explosive material into gaseous products at extremely high pressure and temperature, resulting in a blast wave or “*blast front*” that travels at supersonic speed from a point source. The gaseous products from detonation can reach up to 150k atm (2M psi) in pressure, 3000°K in temperature, and 3000-fold in volume expansion. The blast front is visible in the form of a luminous fireball. It expands and pushes small objects to project faster and further than the gaseous products.

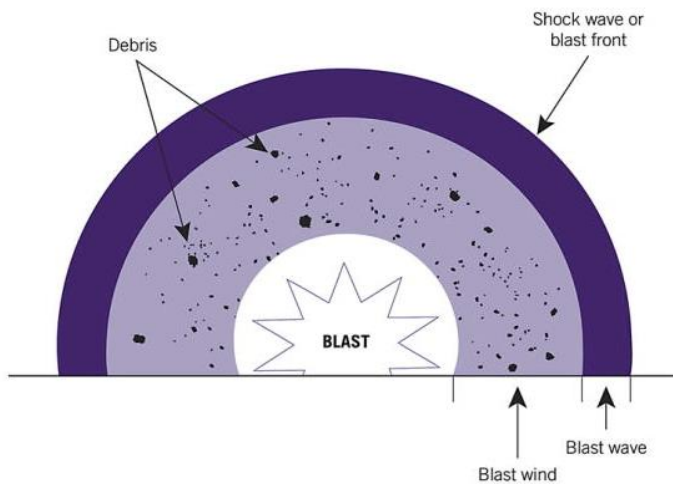


Figure 6. Schematic illustration: components of a blast. *Darley and Kellman (2010)*

At a given point of time and space in the blast flow field, the integrated energy consists of 3 components: kinetic energy from projecting materials, static pressure, and internal energy from high temperature and electromagnetic domains. Over the course of a blast event, the static pressure in the blast flow field exhibits a pattern of “overpressure-underpressure-overpressure” (Figure 7).

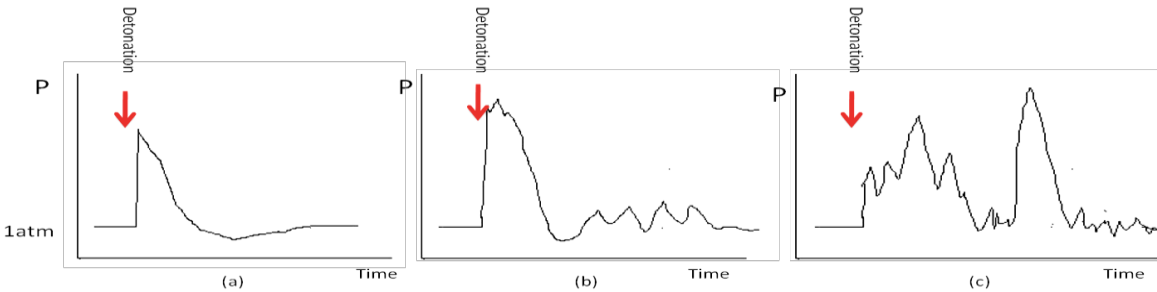


Figure 7. Three pressure/time histograms illustrating blast in three different settings. (a) Friedlander wave: classic biphasic waveform of peak blast overpressure and sub-atmospheric pressure, respectively; (b) simple open field wave: a realistic pattern in open field with ground underneath; (c) complex wave: a realistic pattern in closed field (i.e. room, bunker, foxhole, ally, etc.). *Mayorga MA. The pathology of primary blast overpressure injury. Toxicology 121 (1997) 17-18.*

If the explosive is detonated in a relative closed space, such as in the streets that are lined with buildings, the expanded gas hits the obstacles and reverses direction, the pattern of air pressure change in the blast field can be very volatile and un-predictable. Figure 7 illustrates three pressure/time histograms of blast in different environments. The distance of the victim from the explosive, the energy of the explosive in TNT unit, and the severity of the injuries exhibit a linear relationship, as illustrated in Figure 8 (Mrena et al., 2004).

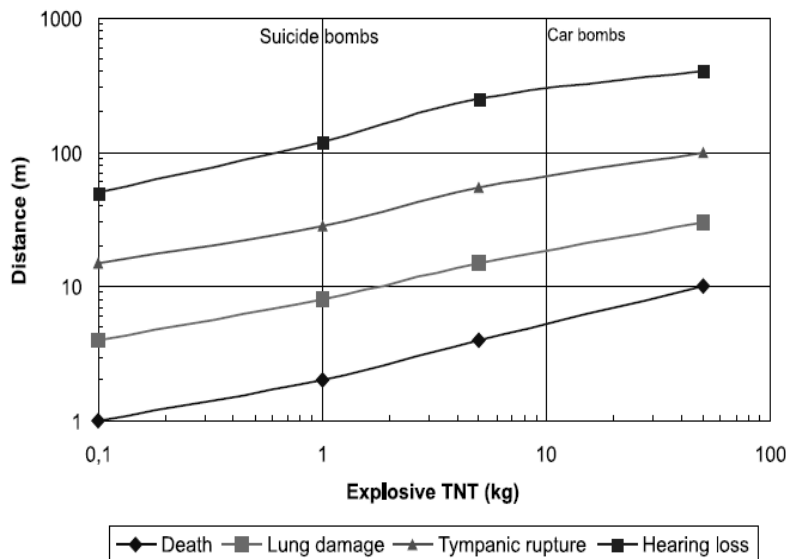


Figure 8. Distance and explosive energy level vs. possible injuries. *Adapted from Mrena, R., R. Paakkonen, et al. (2004). Otologic consequences of blast exposure: a Finnish case study of a shopping mall bomb explosion." Acta otolaryngologica 124(8): 946-952*

Air-filled organs such as ears are most susceptible to injuries inflicted by blast overpressure. All structures of the ear including tympanic membrane, inner and middle ear can be affected. The profile of blast includes basilar membrane shear, rupture of tympanic membrane, and ossicular fracture. The level of energy to inflict injuries for sensory structures on the basilar membrane in the inner ear is the lowest among auditory structures, followed by that of the tympanic membrane and the conductive structures in the middle ear (Fausti et al., 2009).

(1) Basilar membrane shear: blast overpressure causes excessive displacement of the basilar membrane, and this displacement tears the sensory cells off their supporting cell attachment from the basilar membrane. Tissue degeneration and repair from the injury may take up to 10 days (Patterson and Hamernik, 1997). Due to the damages to the inner ear, victims of blast typically experience a temporary hearing loss and/or transient tinnitus; however, some victims develop permanent hearing loss and/or tinnitus (Darley and Kellman, 2010).

(2) Rupture of tympanic membrane (ROTM): for human subjects, the direction of the blast wave in relation to the position of the head, the characteristics of the blast wave, and the conditions of the tympanic membrane affect the prevalence of ROTM (Richmond et al., 1989). Due to the complexity of blast field, it is not surprising that the prevalence of ROTM in several previous cohort studies range from 27.6% to 100% (Cohen et al., 2002; Miller et al., 2002; Mrena et al., 2004; Tungsinmunkong et al., 2007).

(3) Ossicular fracture: ossicular disruption is less common but may occur with higher blast pressure (Fausti et al., 2009).

Damage to the organ of Corti due to basilar membrane shear, ROTM, and

ossicular disruption may contribute to mixed hearing loss in a blast event. The displacement of reticular lamina of organ of Corti alters the endolymphatic milieu, which attributes to temporary threshold shift. Permanent hearing loss is attributed to permanent damage to hair cells (Darley and Kellman, 2010).

Blast is very rare in civilian population. In previous warfare's, blast was commonly associated with lung injuries and fatality. The prevalence of blast-induced tinnitus was significant lower prior to GWT, possibly due to much higher fatality rate associated with blast (IOM, 2005). There was a general lack of interest and funding to study blast-induced tinnitus prior to GWT. Very little is known regarding the impact of blast on central auditory nervous system.

Blast-related PTSD and its Association to Blast-induced Tinnitus

With advanced armors, military members are surviving the blasts that would otherwise have been fatal in the past; nevertheless, no known armor can prevent service members from blast-induced neurotraumas (Cernak and Noble-Haeusslein, 2010). Blast-induced neurotrauma (BINT) and post-trauma stress disorder (PTSD) are called "signature injuries" of global war on terror, with prevalence as high as 16% and 14%, respectively. Symptoms of PTSD include sleep deprivation, outbursts of anger, difficulty concentrating, hyper-vigilance, and exaggerated startle response. Many of these symptoms prevent the returning veterans from having normal social life; sometimes, holding a job and maintaining relationships can be difficult. PTSD and depression are strongly associated with BINT and blast-induced tinnitus. 34% of veterans with tinnitus carry diagnose of PTSD concurrently (Fagelson, 2007). Tinnitus is often intensified by the sounds that trigger "flash-backs"; and service members who carry both tinnitus and PTSD diagnoses reported that their PTSD symptoms are more

intense and frequent than that of whom with PTSD only (Hinton et al., 2006).

Compounded with PTSD, depression, and BINT, blast-induced tinnitus can be very debilitating. The cost of long-term care for veterans that suffer these conditions is astronomical; yet, the knowledge of their underlying mechanisms, interrelation, and treatments remained largely unclear. Coping with their “invisible wounds” with little help is frustrating, so some of the young veterans turned to abusing alcohol and/or other substances, which brings on other societal public health implications. What happened in Fort Carson, Colorado in 2009 was an extreme case, in which 6 veterans from the same infantry committed 8 suicide/homicides within 9 months after returning home, but some aspects of the tragedy are depicting (Army, 2009). Without a thread of doubt, there is an imminent urgency to seek knowledge on the mechanism of blast-induced tinnitus and its interrelations with other blast-related sequalea.

Electrophysiology of the Auditory System

Electrophysiological recordings of neural activity from neurons have greatly contributed to our understanding of the functions of the brain including the auditory system. Recording using microelectrodes is a common approach to obtain detailed information about neural activity under normal or pathological, and awake or anesthetized states. The reason that detailed neural information may be obtained is that the diameter of the tips of these multi-unit platinum-iridium electrodes is less than 10 μm , enabling *in vivo* single-cell recording on multiple neurons simultaneously. Vast electrophysiology data can be extrapolated from the recording regarding the firing rate and the pattern of neurons. If multiple electrode arrays are implanted into various brain structures, the simultaneous recording enables us to explore the pattern of interactions and synchronization of these structures, which offers direct insights to the dynamic of

neuronal network or circuitry.

Relative small brain structures post great difficulties for implantation of multiple electrode arrays to a rodent animal model; in addition, because many events or neurons are recorded simultaneously, large amount on-line data need to be processed with millisecond temporal resolution, which creates another great difficulty in this line of study. Last but not least, the lack of proper mathematical tools to compute and process the enormous amount of digital signals has hindered the progress in the past. Therefore, firing rate, frequency tuning, and topographic organization have been the focuses of auditory electrophysiology studies since the first *in vivo* electrophysiology study conducted in early sixties (Davies et al., 1956; Downman et al., 1960). However, firing rate, bursting events, and tonotopic map organization cannot represent every aspect of coding system in central nervous system (Eggermont, 2001; Eggermont, 2007). With the advancement of powerful personal computers, processing up to 90 channels of electrophysiological signals simultaneously becomes feasible, which provides a superb tool to explore interconnection of correlated heterotopic neurons.

In a review, Eggermont (Eggermont, 2007) proposed that the interconnection of correlated heterotopic neurons acts as the substrate of cortical reorganization and such reorganization with hypersynchrony can be considered the driving force that underlying tinnitus. Functionally, the brain has two types of neuronal maps: topographic map and computational map. Topographic map stems from anatomy axonal circuitry that preserves the orderliness of the central nervous system. However, not all the neurons in the circuitry participate in a specific sensory event necessarily. Neurons that participate in an event may be mapped using a computational tool. Participating neurons that show strong coherency of their firing are functionally related in the

computational map, or vice versa.

The computation of neural coherence involves feeding raw local field potential data from all 90 channels into the logarithm of the peak coherence matrix. The mathematic theory behind constructing such matrix is beyond the scope of this prospectus. In such matrix, the diagonal squares or rectangles represent the amplitude of coherence within and among brain structures, which ranges from 0 to 1. Value 0 represents that the two neuron or two groups of neurons are functionally un-related whereas value 1 refers that two neuron or two groups of neurons are functionally related (Elisevich et al., 2011a; Moran et al., 2004). Computational map is intrinsically plastic; therefore, it is logical to conclude that the plasticity of computational map may be the driving force underpinning tinnitus. Naturally, having the technology advantage of being able to implant 3 structures simultaneously with 16 or 32-channel microwire electrodes, we will focus our efforts on three major structures along central auditory pathway: ipsilateral dorsal cochlear nucleus (DCN), contralateral inferior colliculus (IC) and auditory cortex (AC) in reference to noise/blast exposed left ear.

One of the advantages from the *in vivo* multi-unit electrophysiology study is that the implanted structures can be electrically stimulated, and the effect of such intervention can then be analyzed. By analyzing the spikes of spontaneously activity, the rate of bursting events, and the coherence coefficient of implanted structures, and by comparing such data from control animals, we will potentially be able to objectively evaluate the efficacy of treatment modality in the animal model.

Manganese Enhanced Magnetic Resonance Imaging (MEMRI)

MRI is a non-invasive technique that enables *in vivo* brain studies. Magnetic field strength of the MRI scanner is denoted by the symbol of B_0 . High resolution MRI is

preferentially performed at high magnetic field strength ($B_0 \geq 7.0$ Tesla). A reference coordinate system of three orthogonal axes (x, y, and z) is utilized to define 3-D orientation of the scanner, with z to be the same as B_0 by convention. Hydrogen is the most abundant element in biological organisms. Hydrogen contained only one proton, which spins around its axis. When hydrogen atom is placed in a strong magnetic field, its proton will align in either a parallel or anti-parallel direction in reference with the direction of the magnetic field (B_0). Protons in the anti-parallel orientation are defined to be in a high-energy state, whereas protons in the parallel orientation are defined to be in a low-energy state. Low-energy state is a preferential state for protons. The nuclear spin of excess protons that stay in low-energy state forms a jointed magnetic moment, defined as *net magnetisation* and denoted by M_0 at equilibrium. The higher the magnetic field strength, the more protons stay in low-energy state (Ridgway, 2010).

If a radio frequency (RF) pulse is applied to the magnetic field at an angle (commonly known as *flip angle*), it will “force” the net magnetization to change the direction by Faraday’s Law of Induction. This phenomenon is referred to *precession*. The resulted net magnetization can be split into two components: longitudinal component denoted by M_z and transverse component denoted by M_{xy} . The frequency of such RF pulse is referred to as resonance frequency and is calculated with Larmor equation. For a 7 Tesla scanner, the resonance frequency is 298 MHz. The speed of precession is also 298 MHz. Immediately after the secession of RF pulse, the protons will start to return to their equilibrium state. This exponential process is referred to as *relaxation*. T_1 relaxation refers to the relaxation of M_z to M_0 , and T_2 relaxation refers to the relaxation of M_{xy} back to M_0 (Ridgway, 2010).

By Faraday’s Law of Induction, relaxation induces electrical signals known as

Free Induction Decay (FID). FID can be detected with a receiver coil. The actual magnetic field is by no means homogeneous. The effect of T_2 relaxation combined with the effect of heterogeneity is defined as T_{2^*} relaxation. T_1 relaxation is represented by time constant T_1 , and T_{2^*} relaxation is represented by time constant of T_{2^*} . Both T_1 and T_{2^*} can be extrapolated from actual measured FID. Different tissues have different sizes of molecules that contain hydrogen, therefore, the dissipation of energy during T_1 relaxation is not homogeneous among tissues; in another word, T_1 is tissue-specific. T_1 is shortest for fat tissue. If one specific tissue has high water content, the T_1 of that tissue is long. Additionally, T_{2^*} is tissue-specific due to the fact that molecules in different tissues have different spin-spin interaction. Based on this principle, a computer-generated 3D MRI image can offer excellent spatial resolution for soft tissues (Ridgway, 2010).

When RF is applied at different flip angles, the resulting magnetic field is graded and may interrupt acquisition of FID; therefore, an *echo* instead of FID is used to measure magnetic resonance (MR) signals. The scanning protocol that controls magnetic field gradient is therefore called “*gradient echo*” pulse sequence. *Echo time* (TE) refers to the time that takes to reach maximum gradient echo of M_{xy} from zero. The frequency encoded signals like MR echoes are analyzed using a Fourier transform, which requires the MR echoes to be generated with repeat encoding processes. The *repetition time* (TR) is the time interval between two consecutive encoding processes (Ridgway, 2010).

Weighting refers to the technique that uses different parameters to enhance tissue-specific images. A T_1 -weighted image is obtained, utilizing intermediate TR, large flip angles, and very short TE. Brain grey matter and white matter is best

differentiated with T_1 -weighted images. One of the most commonly used T_1 -weighted sequences with 7T scanners is called magnetization prepared rapid acquisition gradient echo (MPRAGE). A proton density weighted image is obtained with very long TR and very short TE. Proton density weighted images are useful for anatomical reference scans. Example of proton density weighted sequence is proton density gradient echo (PDGE). At high magnetic field, the wavelength of RF may be smaller than the size of biological region of interest (ROI), resulting undesirable intensity variations in the MR images. This phenomenon is commonly termed *intensity field bias*. A prepared over non-prepared (P/NP) ratio image can be used to mitigate intensity field bias. This technique involves dividing a 3D-MPRAGE image with a corresponding 3D-PDGE image ($P/NP = \text{MPRAGE} / \text{PDGE}$). The resulting high resolution T_1 weighted 3D-MPRAGE image is independent of sensitivity of receiver coil, proton density, and T_2^* (Van de Moortele et al., 2009).

Paramagnetic contrast agent can intensify the magnetic field strength when placed in the magnetic field. Mn^{2+} can significantly reduce both T_1 and T_2 , thus is popular to use as a paramagnetic contrast agent in animal studies with 7 T MRI scans. MRI technique that utilizes manganese to enhance the images is called Manganese enhanced MRI (MEMRI) (Silva and Bock, 2008). Manganese is an essential element for human. It is the key component of a number of enzymatic cofactors, including manganese superoxide dismutase, pyruvate carboxylase, and glutamine synthetase (Aschner and Aschner, 2005). After systematically administered, manganese enters brain through blood brain barrier (BBB) at low dose and through choroid plexuses at higher dose (Murphy et al., 1991). In the central nervous system, Mn^{2+} enters neurons through voltage-gated calcium channels, Na/Ca exchanger, Na/Mg anti-transporter, and

mitochondria calcium channels (Crossgrove and Yokel, 2005). Once entering the neuron, manganese is transported anterogradely down axons and released into synaptic cleft with glutamine. The half life of neuronal clearance for Mn^{2+} is 51—74 days, which makes studying task-oriented brain function in moving animals possible; the intensity of the Mn^{2+} enhanced MR signals are used to represent neuronal activities. Indeed, MEMRI is being recognized as an exceptional hemodynamic-independent tool to probe functions of central nervous system in research community (Silva and Bock, 2008).

MEMRI has been used in explore cerebral neuroarchitecture, to map neural tracts *in vivo*, and to probe cerebral function in awake and moving animals (Chuang et al., 2009; Eschenko et al., 2010a; Tucciarone et al., 2009; Watanabe et al., 2008; Yu et al., 2008). The spatial resolution of MEMRI makes *in vivo* layer-specific neuronal activity analysis reality (Bissig and Berkowitz, 2009). MEMRI has been used to probe hippocampal functions with promising results (Jackson et al., 2011). Last but not least, a recent study has utilized 4.7 T MEMRI to explore the circuitry involved in the mechanism of tinnitus induced by noise and salicylates. The study discovered that intensity is high in dorsal cortex of IC in both models show high manganese uptake indicating DCIC is a key player in possibly tinnitus mechanism in at least salicylates and noise induced tinnitus (Holt et al., 2010).

The use of a 7.0 Tesla scanner for MEMRI has further improved the spatial resolution. Nevertheless, the use of MEMRI is currently restricted to animal cerebral study. The major drawback of this technique is manganese's cellular toxicity. Clinically, chronic overexposure to manganese leads to a syndrome, commonly referred to manganism. Typical symptoms of this syndrome resemble many clinical features of

Parkinson's disease. The mechanism of manganese toxicity is not fully understood though progress has been made. Current evidences support that manganese toxicity is associated with mitochondrial dysfunction and endothelial toxicity (dos Santos et al., 2010). Therefore, it is beneficial to use the lowest dosage possible and to carefully plan the timing of MEMRI. In this project, psychobehavioral experiments are conducted before MEMRI. Only electrophysiology recording is conducted after MEMRI. Previous study has demonstrated that at dosage of 0.1mmol/Kg (30mg/Kg) MnCl₂ administrated systematically, MEMRI does not affect electrophysiology signals in central nervous system (Eschenko et al., 2010b). The returning of pre-MEMRI gap/PPI behavioral pattern indicates animal's readiness for recording.

Part II: The Impacts of Isoflurane and Sevoflurane on Auditory Electrophysiological Signals

Consciousness

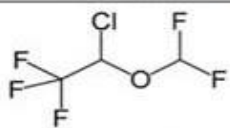
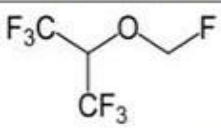

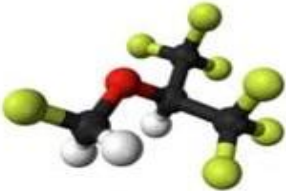


After more than 150 years of clinical application, the physiological mechanism underlying unconsciousness produced by general anesthesia remains unclear. This may be unresolved due to our limited understanding of unconsciousness or the neurobiological events associated with it (Urban, 2002). Thalamo-cortical circuits together with reciprocal cortico-thalamic circuits, commonly known as the thalamo-cortical loop, have received much attention in recent years; these circuits possibly are the key structures for generating consciousness (Butler and Cotterill, 2006; Llinas et al., 1998a).

Since Ramón and Cajal (Romon, 1911) first described the morphology of neocortical neurons, endless efforts have been made to describe specific

electrophysiological qualities of these neurons. The correlation between firing patterns and cortical cell types is; however, much more complex. Not only can morphological similar neurons have different firing patterns; firing patterns of the same neuron are able to transform from one type to another during shifts in the level of consciousness. Characterizing the change in pattern together with correlation in anesthetic depth may offer a theoretic base for developing a clinical tool in order to monitor anesthetic depth.

Isoflurane and sevoflurane were the products of the “Manhattan atomic bomb project” when the fluorine chemical technology became available. Differ from the previous available inhalational anesthetics; isoflurane and sevoflurane are halogenated ether. Their chemical structure and common chemical and biological properties are

Table 1. Common chemical properties of isoflurane and sevoflurane

	Isoflurane	Sevoflurane
Chemical Structure		
		
		
Boiling Point (°C)	48.5	58.6
Blood:gas partition coefficient	1.43	0.69
Minimum alveolar concentration	0.91% -- 1.49%	1.40% -- 2.29%

listed in Table 1.

Isoflurane was synthesized in 1965 and approved by Food and Drug Administration (FDA) in 1979; sevoflurane, on the other hand, was first synthesized in 1968 but approved by FDA in 1995.

Today, isoflurane and sevoflurane are widely used inhalational agents of choice for the

millions of patients around the world who are in need of general anesthesia for their surgeries. (Basak, 1984; Smith et al., 1996).

Current evidence on the topic of halogenated ethers' effects on receptors in the brain may shed lights on the mechanisms underlying the electrophysiological changes induced by halogenated ethers. Isoflurane antagonizes α -amino-3-hydroxy-5-methyl-4-isoxazole (AMPA) receptors in the basal forebrain and suppresses glutamate release, and thus predominantly decreases acetylcholine efflux in the somatosensory cortex (Dong et al., 2006). The agent agonizes gamma-aminobutyric acid (GABA)_A receptors in the cortico-thalamic loop, causing prolonged hyperpolarization and initiating hypnosis (Detsch et al., 1999). Maintenance of such prolonged hyperpolarization may involve a decreased extracellular $[Ca^{2+}]$ as evidenced by decreased membrane conductance. This decrease in extracellular $[Ca^{2+}]$ has been recognized as a mechanism of changing neuronal firing patterns from a tonic pattern to an oscillation at low frequency in anesthetized animals (Alkire et al., 2000a; Nunez et al., 1993; Steriade, 2001).

Several cortical electrophysiology investigations have described similar findings in different sensory pathways. Hudetz and Imas (Hudetz and Imas, 2007) studied visual pathways with an instrumented rat model and found that under a therapeutic concentration of isoflurane rhythmic bursting recorded in the visual cortex can be activated with visual flash stimulus in a dose-dependent manner. In the olfactory pathway, isoflurane induces a synchronized gamma band oscillation in a dose-dependent manner (Hermer-Vazquez et al., 2009).

Auditory sensory inputs have two dimensions: intensity and frequency, both of which are relayed and processed in the auditory pathway in a topographical manner (Hoa et al., 2008). Studies on tone-evoked EEG showed that under various anesthetic

agents, evoked oscillations at a frequency of 5-15 Hz are noted in the cortico-thalamic auditory system (Cotillon-Williams and Edeline, 2004b). The phenomenon is reproducible across various agents and various anesthetic depths. The fact that these tone-evoked oscillations are absent in un-anesthetized animals during wakefulness as well as during natural sleep indicates that this phenomenon reflects cellular changes that anesthetics induce. These oscillations are even detectable at low levels of anesthesia. More interestingly, with the deepening of anesthesia, the frequency of these oscillations decreases, and eventually they are abolished (Cotillon et al., 2000; Cotillon-Williams and Edeline, 2004b).

Several limitations of previous studies in this field have been identified as follows:

- 1) the size of implanted electrodes was quite large as compared to the size of the animal's brain resulting in possible severe trauma to the brain.
- 2) The signal acquisition systems may miss valuable information due to low resolution and computing capability.
- 3) Limited information regarding coherence analysis among brain regions were obtained, possibly due to disadvantages in the data analysis tool. A instrumented rat model with 16-channel platinum-iridium micro-wire electrode implants to various sites within auditory pathway will offer insights into intrinsic neuronal network dynamic, coherence coupling, and topographic mapping of complex sensory inputs (Zhang and Guan, 2007; Zhang and Zhang, 2010). The diameter of platinum-iridium micro-wires is only 50 μm , and the tip of the wire was sharpened to a few μm in diameter, which makes these electrodes superb and minimally traumatic (Zhang et al., 2011).

Relevance to Anesthesia Practice

Despite decades of dedicated research efforts, the mechanisms underlying halogenated ethers such as isoflurane and sevoflurane that produce unconsciousness

remain to be elucidated. A minimally invasive, convenient, reliable and sensitive monitoring modality for consciousness would be advantageous for anesthesia practice; nevertheless, tremendous impediments have been encountered on the journey toward developing such a tool due to a limited understanding of consciousness, the complexity of neuronal network, and a lack of biomedical markers reflecting halogenated ether-induced cellular events.

Even though a very rare condition at estimated incidence of 0.13% in the United States, awareness with recall during surgery under general anesthesia is well publicized and can lead to serious adverse psychological sequelae, including posttraumatic stress disorder (PTSD) (Sebel et al., 2004). Positron Emission Tomography (PET) studies on patients with PTSD showed enhanced thalamo-cortical loop activities associated with flashbacks (Huber et al., 2002); additionally, the thalamo-cortical loop is believed to be a key functional structure of consciousness. Lastly, a pilot study done in our lab showed a novel finding of strong coherence coupling between the thalamo-cortical auditory system and the amygdala; the latter is a major player in emotional learning and fear conditioning. These findings prompted us to further explore relationships among auditory sensory inputs, memory, and emotional responses under general anesthesia. If PTSD is mainly associated with auditory awareness under general anesthesia, diminishing auditory sensory inputs may help to mitigate PTSD associated with awareness under general anesthesia.

Approved by FDA in 1996, Bispectral Index (BIS) is available at the present time to clinicians to monitor consciousness. It utilizes an algorithm that is generated from EEG patterns of a pool of approximately 5000 adult volunteers. A BIS number is then generated by fitting bispectral and power spectral variables into a multivariate statistical

model (Kelly, 2007). Drummond (Drummond, 2000) suggested that a reliable monitoring modality for hypnotic depth should satisfy both of following criteria: 1) the average values measured by the device in two different depths of anesthesia should be statistically different; 2) the type of anesthetic agent should have no effect on measurement-depth correlation. BIS has; however, failed to satisfy both of the aforementioned criteria in a randomized blinded clinical trial (Ibrahim et al., 2001). Clinical trials have showed varying results on its efficacy due to two reasons: 1) the size of the data pool was relatively small for such a rare anesthesia complication; 2) the assumption that frontal lobe EEG data reflects the level of consciousness lacks sound scientific research support. Recently, a multi-center cohort study indicated that an intra-operative low BIS value (<45) was a significant predictor of 2-yr mortality when preexisting malignancy was not among the covariates. The investigators of the study contributed the practice of “treating the BIS value” as one of the reasons (Lindholm et al., 2009). This study showed the potential problems of administering anesthetics using BIS as reference. Since BIS is far from ideal, we, as anesthesia providers, need to be open-minded and keep exploring other options.

It is well known that all halogenated ethers are cardio-depressants (Llinas et al., 1998a; Zucchi and Ronca-Testoni, 1997); therefore, if a monitoring modality is used for monitoring anesthetic depth or consciousness, it must be reliable, sensitive, and clinically practical. How far along are we on the road of developing such a tool? With micro-wire electrodes, researchers were able to implant various cortical regions in chronic animals with minimal damage to cortices. The complexity of the neuronal network and its dynamic has been revealed in recent years. When a patient receives general anesthesia, anesthesia providers often have access to patient's head, which

makes it clinically practical to have a microphone-ear plug to deliver tone burst stimuli and to collect subcutaneous EEG signals from the auditory cortex. If tone-evoked oscillations in the auditory pathway under anesthesia are proven to be reliably sensitive to anesthetic depth and reliably consistent among all commonly used anesthetics, we may be very close to finding that competent monitoring modality.

CHAPTER 2

EXPERIMENTAL DESIGN AND THE HYPOTHESES

Part 1: Blast-induced Tinnitus

Experimental Plan

Sixty male 2-month-old Sprague Dawley rats were used in this project. After baseline auditory brainstem response (ABR) was established for all the rats, rats were trained with gap detection (GAP) and prepulse inhibition (PPI) paradigms, three times a week. Only 46 rats that exhibited stable startle behaviors were selected to proceed with further experimentation. After the baseline responses are obtained, 29 rats underwent blast shock wave exposure with right ear protected using earplugs. 17 rats in control group had sham blast shock wave exposure, in which rats were placed in the shock tube but no shock wave generated and delivered. ABR testing was conducted

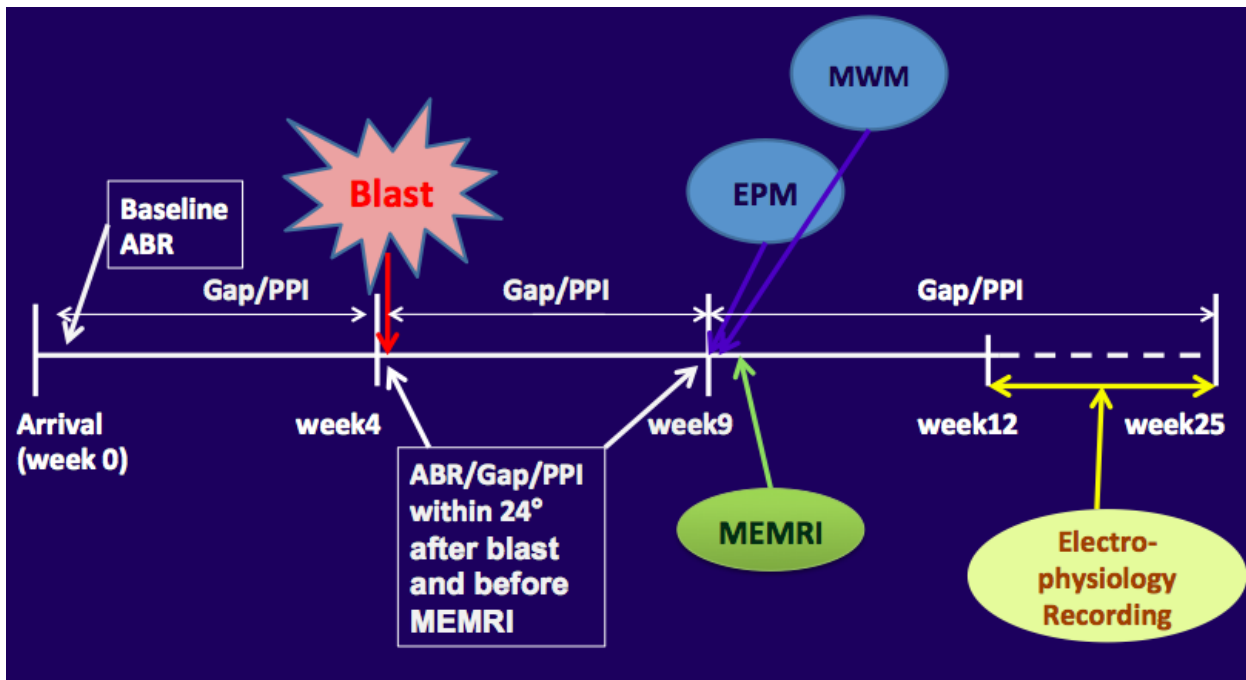


Figure 9. A schematic illustration of the experimental design immediately following blast exposure for the blast group. All selected 46 rats continued

to have GAP/PPI testing twice a week until acute electrophysiology recording for 28 rats and until the MEMRI for the other 18 rats. 4 weeks after the blast, all 46 rats underwent elevated plus maze, Morris water maze, and ABR testing. At week 5 after blast, 41 rats underwent MEMRI scanning, and 18 rats were euthanized after the MEMRI. 4-8 weeks after MEMRI, 28 rats underwent acute electrophysiology recording before they were euthanized. After the rats that had electrophysiological recording were euthanized, a histology study was conducted to confirm the location of electrodes. Figure 9 shows a schematic illustration that illustrates the experiment plan.

Hypotheses

[I] Auditory nerve system changes associated with blast-induced tinnitus:

1. Rats will develop tinnitus after a single blast exposure at 14 psi.
2. Rats with tinnitus will develop hyperactivity in dorsal cochlear nucleus (DCN) and auditory cortex (AC) and have decreased spontaneous activity in inferior colliculus (IC).
3. Both auditory cortex electrical stimulation (ACES) and acoustic masking can decrease spontaneous activity in AC and DCN, but increase spontaneous activity in IC in rats with blast-induced tinnitus.
4. For animals with chronic tinnitus, neuronal hyperactivity as evidenced by higher uptake of manganese in structures like DCN, VCN, AC, and dorsal cortex of inferior colliculus (DCIC) will occur; whereas neuronal hypoactivity will occur in central inferior colliculus.

[II] Neural activity changes in limbic and paralimbic structures associated with the blast-related PTSD:

1. Blasted rats will show the higher anxiety level and worse cognitive functions as

evidence of worse performance in Morris Water Maze.

2. Neuronal hyperactivity as evidenced by higher uptake of manganese in structures such as amygdala (AMG) and nucleus accumbens will be observed; whereas hypoactivity will be observed in structures such as anterior cingulate cortex and hippocampus.

Part II: The Impacts of Isoflurane and Sevoflurane on Auditory Electrophysiological Signals

Experimental Plan

Ten male Sprague-Dawley rats age 60-70 days were used for this study. Isoflurane was utilized for craniotomy to insert electrodes. After rats were ruled out for hearing loss with the auditory brainstem response (ABR) test, three 16-channel platinum-iridium microwire electrodes were inserted into the left dorsal cochlear nucleus (DCN), right inferior colliculus (IC), and right auditory cortex (AC). 2 hours later, after rats recovered from surgery, electrophysiological tests were conducted with first isoflurane then sevoflurane at different inhaled concentrations. For each concentration, a minimum of 10 minutes was used to allow for cerebral-pulmonary equilibrium. A minimum of 30 minutes was allocated to allow clearance of isoflurane before recording data for sevoflurane. Rats then were euthanized, and histology study was conducted to verify the location of electrodes.

Hypotheses

1. Isoflurane and sevoflurane induce a dose-dependent shift of firing pattern from regular tonic firing to bursting with intervals (evoked-oscillation) in the thalamo-cortical auditory system; there is no difference on the dose-response relationship between these two agents.

2. Increased coherence coefficient (CC_{AC_IC}) between auditory cortex (AC) and inferior colliculus (IC), indicating higher level of connectivity, occur with deepening of anesthesia with isoflurane or sevoflurane.
3. Decreased coherence coefficient (CC_{IC_DCN}) between IC and dorsal cochlear nucleus (DCN), indicating functional dissociation in the subcortical auditory pathway, occur with the deepening of anesthesia with isoflurane or sevoflurane.
4. There is no difference in the manner of changes between two halogenated ethers.

CHAPTER 3

MATERIALS AND METHOD

Animal subjects

Animal subjects were male Sprague-Dawley rats (n=60). They were purchased from Harlan Laboratory with age of 60-70 days at the time of arrival. Rats were kept on a 12/12h day/light cycle and were cared for in a federally approved animal vivarium. 4 rats were excluded for their poor startle reflex responses. 29 rats were exposed to blast shock wave, and 17 rats underwent sham exposure. Immediately following blast, all rats in experimental group usually developed tinnitus, but 4 weeks after the exposure, 15 rats retained tinnitus, and 14 rats recovered from tinnitus. The rats that retained tinnitus were grouped into the tinnitus positive group, and the rats that recovered from tinnitus are referred to tinnitus negative group. The rats that underwent sham exposure were referred to the sham (control) group (n=17). 24 rats underwent craniotomy for electrophysiological recordings 9 weeks after the blast or sham exposure. Among them, 8 rats were in the sham (control) group; 8 were in the tinnitus positive group; and 8 were in tinnitus negative group. 2 rats that were in the tinnitus positive group 4 weeks after the blast exposure (at the time of the MEMRI scanning) were grouped into the tinnitus negative group 8 weeks after the exposure (at the time of the electrophysiological recording) because their behavioral evidences of the tinnitus subsided. Likewise, 3 rats that were in the tinnitus negative group at the time of the MEMRI scanning exhibited behavioral evidences of tinnitus at the time of the electrophysiological recording, and they were grouped into the tinnitus positive group for the purpose of data analysis for electrophysiology study portion of this dissertation.

The experimental protocol and all amendments were reviewed and have been

approved by the Animal Investigation Committee at Wayne State University and followed federal animal research guidelines.

Behavioral testing for tinnitus and hearing loss

Each rat was placed in a custom-made conditioning restrainer. During the testing, the restrainer along with the rat was placed in a behavior chamber for gap detection and PPI testing. The gap/PPI testing sessions were conducted 3 times a week (2-3 days between each testing) for 4 weeks before the blast exposure; and they were conducted twice a week (3-4 days between each testing) after the exposure. The first 6 testing sessions were for conditioning training and were excluded from baseline analysis.

Gap and PPI paradigm procedures were conducted with a behavioral testing system (Kinder Scientific, Poway, CA). Figure 10 is a schematic representation of such a system. In the soundproof testing chamber, the startle force (Newton) of the animal was detected with a piezoelectric transducer attached under the platform. Peak-to-baseline startle responses were monitored and recorded in real time using startle monitor software (Kinder Scientific).

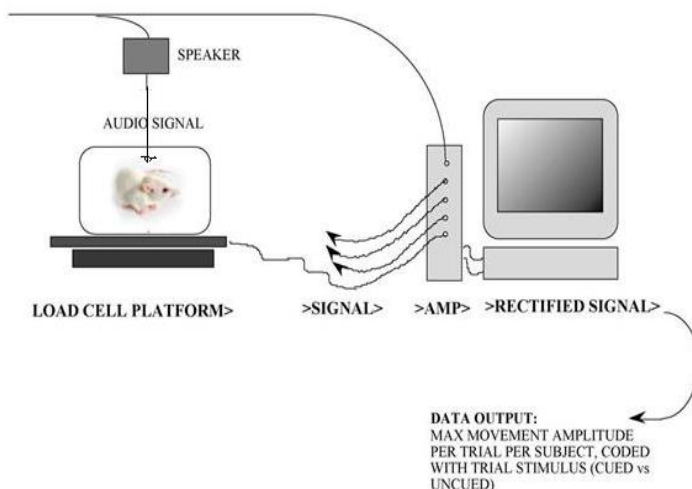


Figure 10. Schematic drawing of a gap/PPI behavioral testing system

Prior to each testing session, calibration of test stimuli was performed using a Newton impulse calibrator and a sound pressure level meter. In the gap detection procedure, each rat was tested in the chamber with a continuous background noise. The noise consisted of 2 kHz bandpass noise signals at 8-10, 12-14, 16-18, 20-22, 28-30 kHz, and broadband noise (2-30 kHz) was delivered at 60 dB SPL. The noise burst of 50-msec duration was delivered at 115 dB SPL with an in-chamber speaker. With the rats with normal hearing and without tinnitus, the presence of a 40-msec silent gap before a startling acoustic stimulus serves as a strong inhibitory signal to suppress the startle reflex after proper conditioning training (B and B' in blue panel in Figure 11), and

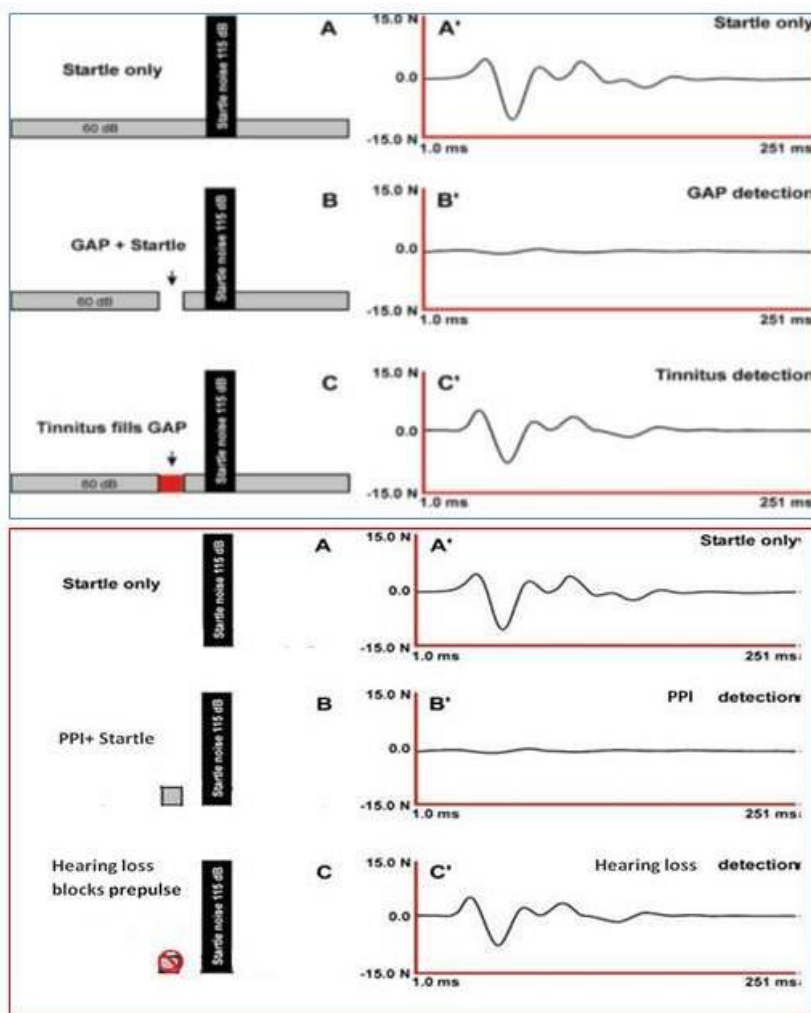


Figure 11. Schematic illustration of principle of Gap and PPI paradigm for diagnosing hearing loss and tinnitus in rodents; Zhang *et al.* *Cortical stimulation suppresses tinnitus in rats.* *JARO.* 12:185-201(2011).

result of the test was referred to a “negative gap test” or “inhibition”. With the rats with tinnitus, when the background sound was similar to their tinnitus, they failed to detect the gap and to suppress the startle reflex (C and C’ in blue panel in Figure 11), and the test was referred to a “positive gap test” or “no inhibition”.

PPI detection was introduced to further differentiate hearing loss from tinnitus. In a PPI paradigm, there was no background noise. The gap was replaced with a 40-msec 60 dB SPL prepulse acoustic signal of 2 kHz bandpass at 8-10, 12-14, 16-18, 20-22, 28-30 kHz, and broadband noise (2-30 kHz). The rats without hearing loss were able to detect a 40-msec noise at 60 dB SPL before the startling acoustic stimulus and to suppress the startle reflex after successful conditioning training (B and B’ in red panel in Figure 11), and the result was referred to a “negative PPI test” or “inhibition”. The rats with hearing loss were unable to hear the prepulse thus were unable to suppress the startle reflex (C and C’ in red panel in Figure 11), and the result of this test was referred to a “positive PPI test” or “no inhibition”. The trials that yielded extreme results (extreme results were defined as higher or lower than Mean+2SD) were excluded from calculation. The corrected results from 4 out of 5 sessions before the experimental time points such as blast, EPM/MWM/MEMRI, and EP recording, were averaged to yield stable behavioral results for “baseline (BL)”, “post-exposure week 5 (PEW5)” and “post-exposure week 8 (PEW8)”; respectively. A negative PPI test (B’ in red panel in Figure 11) and a positive gap test (C’ in blue panel in Figure 11) will confirm the diagnosis of tinnitus for rats. Figure 11 illustrated the principle of gap/PPI behavioral paradigm, a widely accepted diagnostic tool for diagnosing tinnitus in rats (Fitch et al., 2008; Turner et al., 2006)

ABR Procedure

ABR thresholds to clicks and tones were evaluated at the baseline, immediate after blast, and before MEMRI. The general anesthesia was induced with 5% isoflurane/air mixture then maintained with 2% isoflurane/air mixture for this procedure. After sound calibration was done, to record the threshold for left ear, a set of 3 platinum-coated tungsten electrodes were inserted. The locations of the electrodes were as following: the return electrode was inserted to vertex (midline and the between two ears); the active electrode was inserted below the left pinna; and the grounding electrode was inserted into right temporal muscle. To record the threshold of right ear, the returning, active, and grounding electrodes were inserted to vertex, below the right pinna, and into the left temporal muscle; respectively. Click and tone bursts of 10-msec duration at 4, 8, 12, 16, 20, 28 kHz (0.1-msec rise/fall time) were delivered to the ear canal from an electrostatic speaker at intensity level from 100 to 5 dB SPL with 5 dB SPL decrescendo increments. Stimuli were generated by a RX6 Multifunctional Processor and were processed by the SigGenRP software (TDT system 3). Calibration was achieved using SigCalRP[®] software. ABR signals were amplified; they were band-filtered from 0.3 to 3 kHz and notch-filtered at 60 Hz; and they were averaged 300 times as well.

Blast procedure

Shock tube is a commonly used apparatus to generate blast shock wave. To simulate a blast overpressure, the shock tube activated by compressed gas is widely used. The shock wave tube (ORA, Inc) employed in this project was helium-driven, and located in Wayne State University Bioengineering Department. Figure 12-A is the picture of the shock tube. The shock tube consisted of two components: a driver

cylinder (L30 in X D12 in) and a driven cylinder (L242 in X D12 in). The driver cylinder was filled with highly pressurized helium, and the driven cylinder was filled with air. To avoid excessive trauma to the rat, the rat was placed on a mesh platform (C, Figure 12) 198 inches downstream from the bursting membrane and 44 inches upstream from the open end of driven cylinder. The 44 in of open cylinder was important to prevent excessive underpressure (Leonardi et al., 2011).

After the rat was anesthetized with ketamine/xylazine (0.1ml/kg with concentration of 100/20 mg/ml) intraperitoneal injection or 5% isoflurane/oxygen mixture, the right ear of the animal is plugged with a Mack's[®] earplug, sealed with mineral oil, and sutured closed at the pinna with one stitch. The rat was then wrapped in protective garment and secured on a holder in the driven cylinder as in the picture (lower corner of panel A of Figure 12). A Mylar membrane was placed between the driver cylinder and driven cylinder (left lower corner of panel A in Figure 12). When the membrane burst, a uniform shock front quickly propagated down the driven cylinder. Because the area of the cross section for the cylinder stayed the same, the speed of the shock front stayed the same until the reflected rarefaction from the closed end of the driver overtook it. In this design, the waveform of static pressure had a decaying profile similar to a free-field blast wave (B in Figure 12) (Leonardi et al., 2011).

The simulated blast was delivered at 14 pounds per square inch (psi) overpressure, which was comparable to be around 96.5 kPa or 194 dB SPL. The positive phase duration was 10 msec (B, Figure 12). After the exposure, each rat was carefully monitored until they regained consciousness.

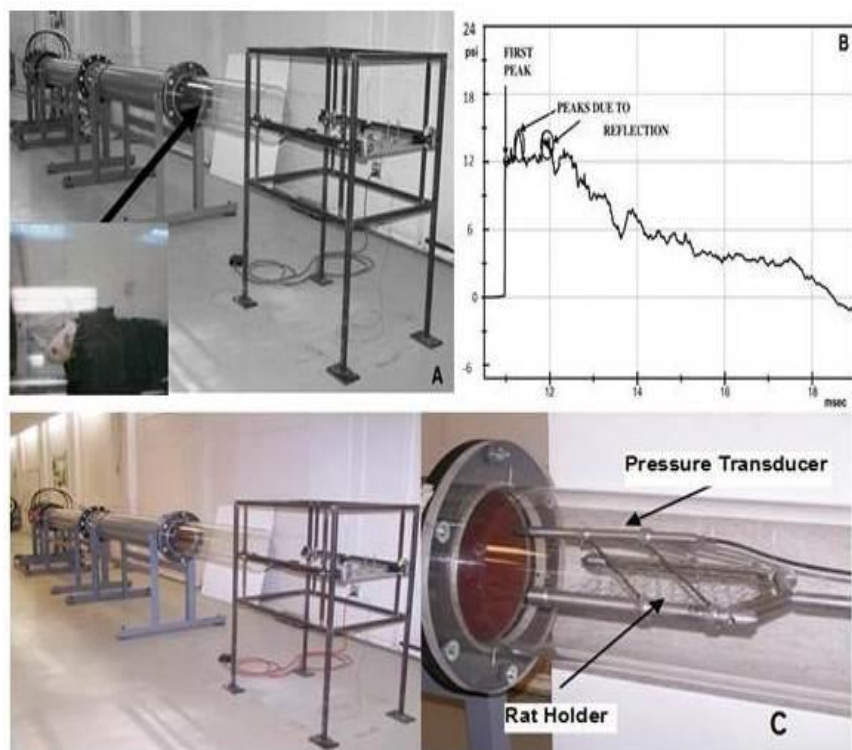


Figure 12. (A) A photo of a shockwave tube in WSU; the arrow points to the position of animal loading mesh platform. The insert shows the picture of a rat in protective wrap. (B) A shockwave profile generated by the WSU shock tube. The first peak is the overpressure created by the blast; later higher peaks are due to reflections of the shockwave against the animal. (C) A photo of the mesh platform, showing the pressure transducer.

The rats in the control group (n=17) received sham exposure. The rats were anesthetized with ketamine/xylazine (0.1ml/kg with concentration of 100/20 mg/ml) intraperitoneal injection or 5% isoflurane/oxygen mixture, the right ear of the animal is plugged with a Mack's[®] earplug, sealed with mineral oil, and sutured closed at the pinna with one stitch. The rat was then wrapped in protective garment and secured on a holder in the driven cylinder. However, no shock wave blast was delivered. The rats were then carefully monitored until they regained consciousness.

Panel B in Figure 12 showed an overpressure graph measured by the sensors in the driven cylinder of the shock wave tube. The x-axis indicates time (msec), and the y-axis indicated the overpressure (psi above atmospheric pressure).

Elevated plus maze (EPM)

All 46 rats' level of general anxiety was measured with elevated plus maze (Tracoustics Inc., Austin, TX). Panel A in Figure 13 is a picture of the maze. The EPM

consists of four runways (L45 cm X W10 cm). Four runways (arms) are equal in size and height, which is 52 cm above the ground. Two of the arms are enclosed by a black solid wall 30 cm high, and they are referred to closed arms. The other two arms are referred to open arms. Testing room lighting was adjusted from normal level of ~450 lux to a dim setting of 1-5 lux, where the light level in open arms is ~4 lux and the light level in closed arms is ~1 lux.

Prior to testing, rats were handled every day for 5 days by the author who also conducted testing. Each rat received a handling session that lasted 2 minutes each day. On the testing day, rats were transported to the testing room and acclimated in dim light for 4 hours before testing. Each rat was placed on an open arm of the maze facing the center and its behaviors were recorded with a digital camcorder mounted above the EPM on the ceiling. Each testing trial lasted for 5 min. After the trial, the rat was returned to its cage; the maze was cleaned with 70% alcohol; and the maze was allowed air dry after the cleaning. Trials were interspersed with 5-minute-intervals. Each rat was tested for one trial only.

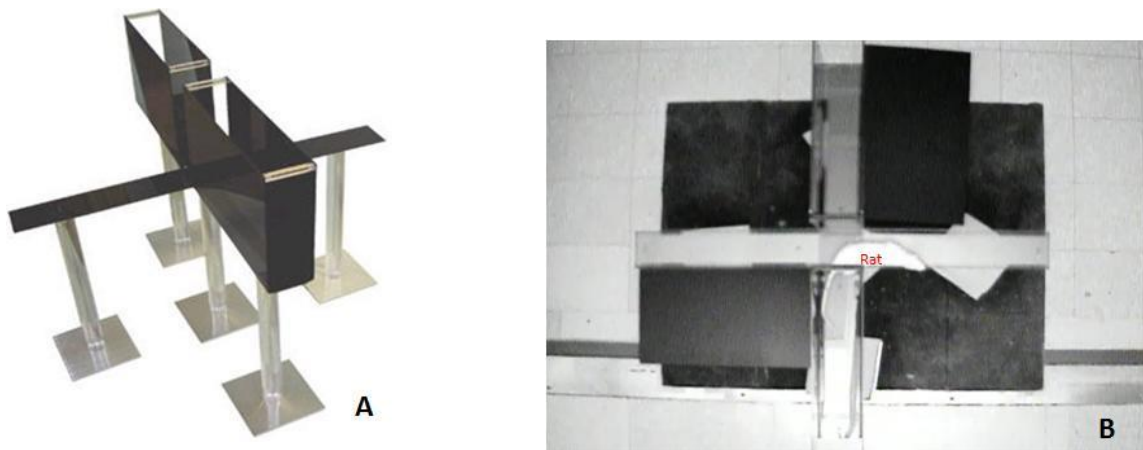


Figure 13. (A) A picture of commercially made elevated plus maze (Tracoustics Inc., Austin, TX). (B) A photo of a rat on the maze stretches forward and leans over the edge of east (open) arm, shot from the high quality digital camcorder placed above the maze.

Two people rated the videos independently. The scores of the two raters were

averaged for each measure. Anxiety-like behaviors were determined by calculating the amount of time and number of entries each rat made to the open arms and closed arms; and the data were reported as a “percentage open time”, “percentage open entry” and “average duration of open entry”. The formula to calculate above-mentioned measures were as following:

$$\text{Percentage open time (\%)} = \frac{\text{total time spent on open arms (sec)}}{300 \text{ sec} \times 100\%}$$

$$\text{Percentage open entry (\%)} = \frac{\text{total number of entries to the open arms}}{\text{total number of entries to open \& closed arms} \times 100\%}$$

$$\text{Average duration of open entry (sec)} = \frac{\text{total time spent on open arms (sec)}}{\text{total number of entries to the open arms}}$$

An *arm entry* was counted when the superior portion of the rat (cranial to the transverse plane or ventral midline), the shoulders (pectoral region), the forelimbs and forepaws, and the thoracic region (anterior to the rib cage) moved into an open or closed arm (Perrine et al., 2006). This measure sufficiently improved the reliability of the test by including open arm risk assessment behaviors, namely stretch attend postures and head dippings. Stretch attend postures referred to rat’s stretching forward without moving its hind-limbs and hind-paws; head dippings referred to rat’s leaning over the edges of the open arms (B, Figure 13) (Dawson and Tricklebank, 1995).

Rats that exhibited very low locomotive motivation as evidenced by very low number of entries to any arm were excluded from the data analysis. Data from 28 rats (10 in tinnitus positive group, 9 in tinnitus negative group, and 9 in the control group) were included for the data analysis.

Morris Water Maze (MWM)

At least 24 hours after the elevated plus maze trial, all 46 rats were tested for

learning and spatial memory using a one-day Morris water maze protocol. Morris water

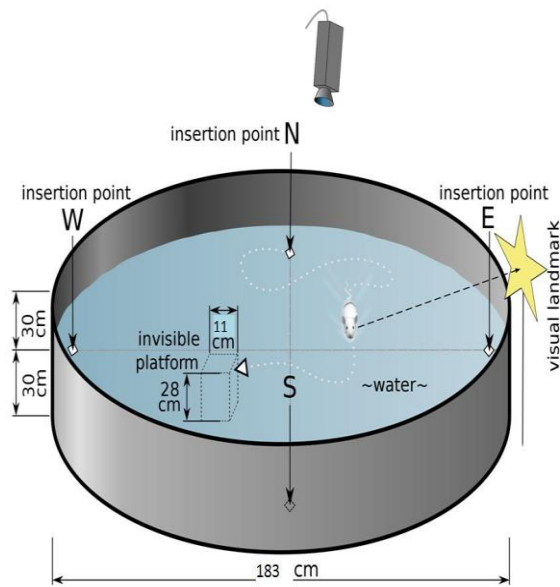


Figure 14. A schematic drawing of Morris water maze apparatus in Bioengineering Dept, Wayne State University.

maze apparatus consisted of a circular fiberglass pool 183 cm in diameter and a flat surface platform. The pool was filled with water that is mixed with commercially made opaque acrylic, non-toxic paint to provide the best contrast for optimum

tracking of animal's swimming trajectory. The platform (11 cm in diameter) was placed inside the circular water tank in the middle of one of four designated quadrants. The pool was filled with water until the surface level reached one inch above the platform (hidden platform). The temperature of the water in the pool was $23 \pm 1^\circ\text{C}$. Visual cues were painted on the walls, and the experiment was conducted in a 3x3 ft room free from other distractions. Figure 14 shows a schematic drawing of the experimental setup (Morris, 1984).

Rats were tested a total of five times, including a probe trial where the platform was removed. Testing was initialized at five different, equidistant starting points for each testing series. Every rat was placed into the pool tail-first and facing the center of the pool to alleviate anxiety. Trials for each rat were sequentially arranged from a given starting point, followed by sequential testing at the second starting point, third starting point, fourth starting point, and the probe trial. If a rat failed to locate the hidden

platform within 90 seconds, it was taken from the water and placed on the platform for approximately 3 seconds. The total time that a rat swam in the water was 13 minutes or less. Each rat swam 13 times of 1 minute each. After each swimming trial, the rat was dried with dry towel immediately; the swimming trials were interspersed with rest periods. The trajectories of the rats were recorded using a digital camcorder mounted above the water tank. Rats were tracked and measured by Ethovision software (Noldus Information Technology, Inc) installed in a computer workstation.

“Latency” and “Path-length” during the spatial task acquisition trials were used as the parameters to measure cognitive functions such as spatial learning and recognition; and the “Probe time” during the probe trials was used as the parameter to measure the cognitive function such as spatial memory.

MEMRI scanning

At week 5 after blast exposure, 41 rats (12 from control group, 12 from tinnitus negative group, and 17 from tinnitus positive group) that had stable gap/PPI performance at the baseline were scanned with a 7.0 T Siemens ClinScan MRI scanner (Siemens Medical Solutions USA, Inc. Malvern, PA). Awake rats were injected with MnCl₂ (MnCl₂·4H₂O, 67 mg/kg) intraperitoneally. After the injection, rats were placed in a soundproof room for 8 hours before scanning. Accumulating uptake of manganese for 8 hours was adequate for functional imaging, and utilization of anesthesia during scanning did not affect manganese uptake (Bissig and Berkowitz, 2009; Lee et al., 2005). Before the scanning, rats were induced with 4% isoflurane/air mixture in induction chamber. Subsequently, general anesthesia was maintained with 2% isoflurane/air mixture via a commercially made MRI compatible nose cone. During

the scanning, the rat was placed on a heated re-circulating water pad with a rectal thermometer to monitor and maintain core body temperature. A whole-body transmit-only coil and a 4-element Burker mouse-brain receive-only surface coil, which were placed dorsally to animal's head, were used for scanning. Individual image-sets were acquired with 2 sets of MPRAGE (TR: 2500 msec, TE: 3 msec, TI: 1500 msec) and PDGE (TR: 1000 msec, TE: 3 msec) sequences with flip angle of 3 and total scanning time of 23 min. The field of view (FoV) was 25X25 section of space (192 pixel X192 pixel or 130 μm X 130 μm). The thickness of the slice was 260 μm . At the end of the scan, the rat was emerged and monitored until awake on a heated pad. Fully awake rats were returned to their home cages. They were closely monitored for another 8 hours after the scanning before they were returned to vivarium.

Images were processed with R (v2.12.1, <http://www.r-project.org>) scripts developed by Dr. D. Bissig at the department of anatomy, school of medicine, Wayne State University. The addition of two sets of MPRAGE images was divided by the addition of two sets of PDGE images to mitigate the *intensity field bias*. The corrected image sets were used for further analysis. Regions of interest (ROIs) were manually drawn using MRICro v.1.60 with gingerly referencing the Paxinos and Watson (4th Edition; 1998) rat brain atlas (Figure 15). Average signal intensity of ROIs was obtained with MRICro. Next, the signal intensity (SI) of ROIs was normalized with that of adjacent noise. The ratio of signal intensity of ROI and Noise was used to normalize SI. The formula to calculate the normalized signal intensity was as following:

$$\text{Ratio_ROI/Noise} = \text{SI of ROI} / \text{SI of Noise}$$

Noise normalization further mitigated the effects of intensity field bias related to the differences in the body habitus of the animals. The following structures were

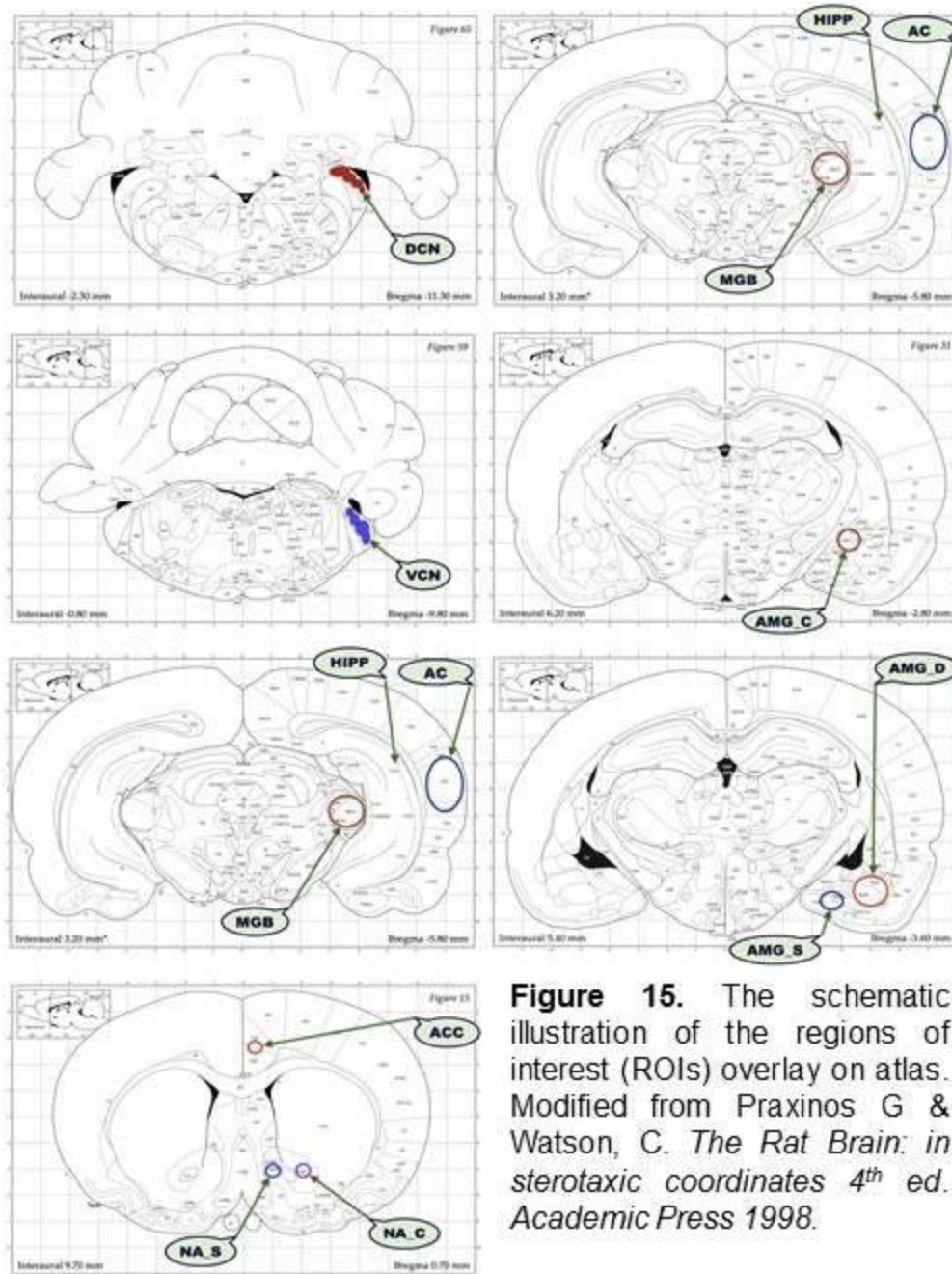


Figure 15. The schematic illustration of the regions of interest (ROIs) overlay on atlas. Modified from Praxinos G & Watson, C. *The Rat Brain: in stereotaxic coordinates 4th ed.* Academic Press 1998.

included for analysis at this point: Medial geniculate body (MGB), external cortex of inferior colliculus (ECIC), dorsal cortex of inferior colliculus (DCIC), central nucleus of inferior colliculus (CIC), dorsal cochlear nucleus (DCN), ventral cochlear nucleus (VCN), amygdala (AMG), nucleus accumbens (NA), anterior cingulate cortex (ACC), and hippocampus (HIPP). Spherical ROIs were used to characterize the CIC and MGB

(radius: 520 mm). For most structures, hand-drawn ROIs span 3-4 consecutive coronal slices. The ROIs were drawn in the way that they are placed at the rostrocaudal center of each anatomical region, and drawn to occupy the entire coronal profile of each region, excluding a buffer (≥ 1 voxel wide, depending on the ROI) at borders with neighboring brain regions and tissues (e.g. choroid plexus). Appropriate ROI placement was confirmed in parasagittal and transverse views. A colleague, who was not involved in the imaging portion of this project, coded image sets. Two people, who were unaware of the identity of the image sets, analyzed the corrected images independently to avoid subjectivity. The two sets of results were analyzed with Pearson correlation

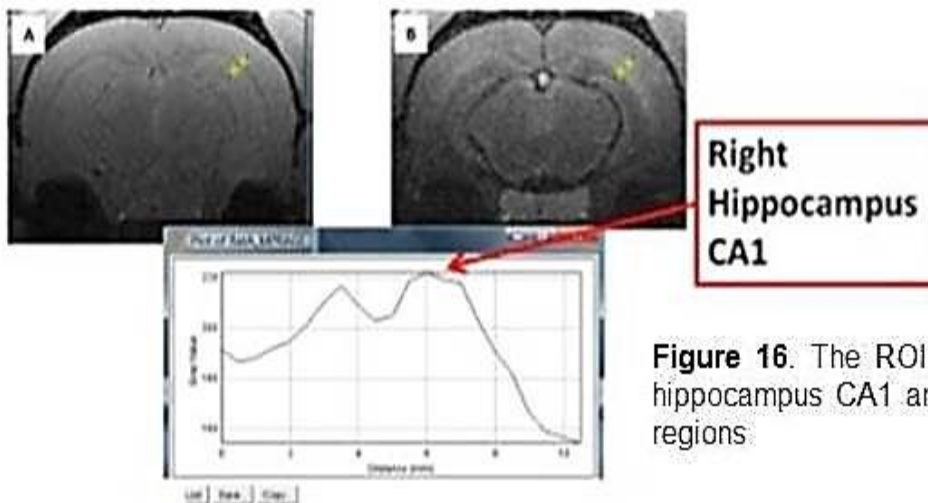


Figure 16. The ROI of the hippocampus CA1 and CA2 regions

analysis. The Pearson correlation coefficients were over 60% for all structures. The detailed methods of obtaining the raw signal intensity are described as following:

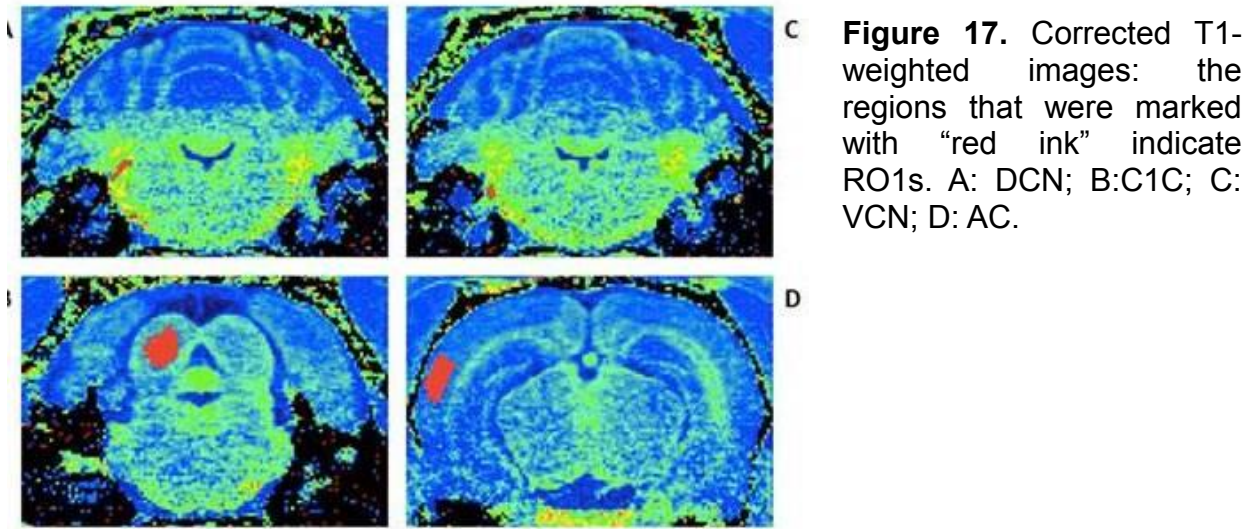
1) Hippocampus (HIPP):

Intensity of hippocampus was obtained with ImageJ. Three consecutive slices caudally onward were used on each side. The first slice was caudal to the slice where the dentate gyrus became evident. 4 lines were drawn on each side perpendicular to the curvature of forceps major corpus callosum in the fashion that the midpoint of the

line aligned with the border of forceps major corpus callosum and the direction of line was toward the center of the parenchyma (Figure 16, A). The lines were hand-drawn on the PDGE image set, then the computer copied the placement of the lines to the MPRAGE image set on the same corresponding coronal slice. A gray value linear plot was generated from each line copied to the MPRAGE image (Figure 16, B). The x-axis represents the distance the line “travels”, and y-axis represents the signal intensity along the line in the form of “gray value”. The peak whose distance just passed midpoint represented the position of hippocampus CA1 and CA2 neurons. The tenfold of the average of the 12 peak values on one side of hemisphere was used to represent signal intensity of ROI for that side of the hippocampus.

2) Dorsal cochlear nucleus (DCN), ventral cochlear nucleus (VCN), medial geniculate body (MGB), external cortex of inferior colliculus (ECIC), dorsal cortex of the inferior colliculus (DCIC), central nucleus of inferior colliculus (CIC), and auditory cortex (AC):

The ROIs of DCN and VCN were hand-drawn on 3 consecutive coronal cross-sections. The ROIs of ECIC and DCIC were hand-drawn on 4 consecutive coronal cross-sections. The ROIs of CIC, MGB and AC were 3D spheres with radius of 4, 3 and 4, respectively. Figure 17 showed the pictures of some of the ROIs of these regions.



3) Amygdala (AMG), anterior cingulate cortex (ACC), and nucleus accumbens (NA):

Amygdala was divided into three subdivisions: centromedial nuclei (AMG_C), the superficial or cortical-like nuclei (AMG_S), and deep or basolateral nuclei complex (AMG_D). Spherical 3D ROIs were used to characterize amygdala (AMG), anterior cingulate cortex (ACC), and nucleus accumbens (NA) (radius: 260 micron). The ROIs were drawn in the way that they were placed at the rostrocaudal center of each anatomical region in the coronal profile of each region, excluding a buffer (≥ 1 voxel wide, depending on the ROI) at borders with neighboring brain regions and tissues (e.g. choroid plexus). Appropriate ROI placement was confirmed in parasagittal and transverse profiles. Figure 18 showed pictures of the same ROIs on different profiles.

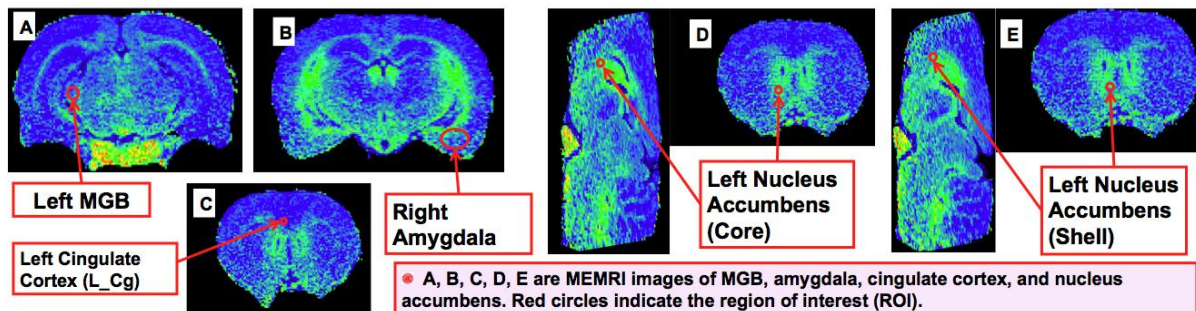


Figure 18. Corrected T1-weighted images; the regions that were marked with “red ink” indicate ROIs. A: MGB; B: AMG; C: ACC; and D&E: NA

Recording, ACES and acoustic masking

Surgeries were performed under general anesthesia with isoflurane using aseptic techniques. Rats' body temperature was maintained at 37°C with a thermo-controlled heating pad (Harvard Apparatus). Custom-made hollow bars were used for delivering sound. Anesthesia was induced with 5% isoflurane/air mixture then maintained with 2% isoflurane/air mixture at 0.4 l/min (Figure 19).

(1) Insert electrode to the left DCN: after the head was fixed to a stereotaxic device (Kopf Model 1350), craniotomy was performed; subsequently, the dura mater was removed. The cerebellum tissue overhanging the left DCN was partially aspirated. Under the microscope, a microwire electrode array consisted of 16 polyimide-insulated platinum/iridium microwires (Clunbury Scientific) or 32 channel NeuroNexus probe was lowered about 150-200 μm below the DCN surface, corresponding to the fusiform cell layer. Prior to insertion, the array was dipped 3% Di-I solution (1,1'-dioctadecyl-3,3,3',3'-tetramethylindocarbocyanine perchlorate, Invitrogen) prepared with DMF to label the location of the electrodes. Each electrode array consisted of 16 polyimide insulated platinum/iridium microwires that were arranged in 2 rows with 8 microwires in each row (diameter 50 μm ; electrode spacing 200 μm ; row spacing 100 μm ; impedance \sim 50 k Ω) or a 32 channel NeuroNexus probe. Impedance was measured with microelectrode meter (Ω mega-Tip Z, WPI instruments). To fit the curvature of the DCN, the shortest wires were placed at the most medial position and longest wires at the most lateral position, with a gradient height difference of 180 μm along the medial–lateral axis of the DCN (A, Figure 19; Figure 20).

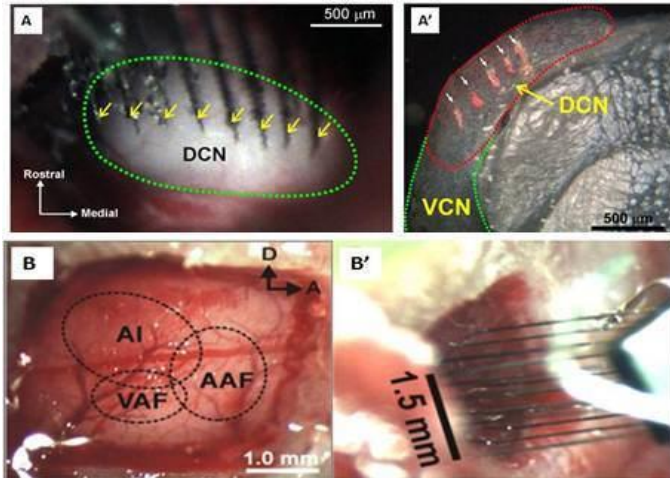


Figure 19. (A) Surgical view of the left DCN of a rat, showing the implanted electrodes; (A') Fluorescent confocal microscope photo of the DCN showing the insertion tracks; (B) Photo of surgical site of AC; (B') photo of custom-made array

(2) Insert electrode into right AC: microscopic craniotomy was performed at 4 mm lateral and 5 mm posterior to the bregma (Figure 19B; Figure 20). The dura mater was subsequently removed. The auditory core and belt regions were identified with stereotaxic coordinates and their close proximity to anterior and posterior dorsoventral vessels, using physiological responses to tone bursts stimuli. After taking photographs to record the surgical view, a 2 x 8, 16-channel microwire electrode array (B', Figure 19) was inserted in the AC and a silver wire was connected to neighboring tissue for grounding (B', Figure 19). The array was lowered into the layers 4-5. Each array consisted of 16 polyimide insulated platinum/iridium microwires that are arranged in 2 rows with 8 wires in each row (diameter = 50 μm ; electrode spacing = 500 μm ; row spacing = 500 μm ; impedance = 0.2-0.5 M Ω).

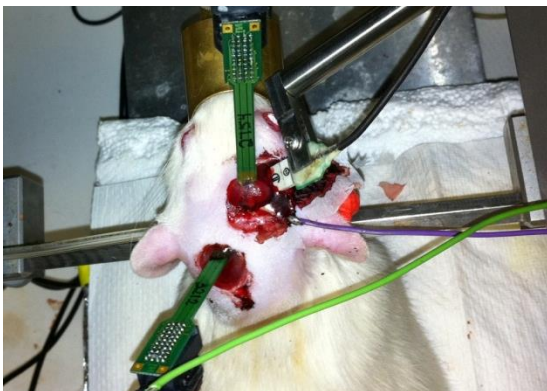


Figure 20. Photograph showing surgical placement of 3 electrode arrays in left DCN, right IC and AC

(3) Insert electrode array into right IC: under the microscope, a 5mm craniotomy was opened posterior and lateral to lambda to the right of the sagittal sinus (Figure 20). Cortex was partially aspirated to enable insertion of electrode without obstruction. A 2x16-channel linear microelectrode array (NeuroNexus, Ann Arbor, MI) with a thickness of 15 μm and recording contact surface of 20X20 μm was inserted in a parasagittal plane at 23° posterior-inferior angle to optimally span the tonotopic lamina of the IC. The electrode was incrementally advanced under the guidance of physiological response of IC to tone burst stimuli.

(4) ACES and acoustic masking: arrays were mounted on a switching headstage (SH16, TDT) for electrical stimulation to the AC and recording at the DCN, IC, and AC. All the headstages were connected to an auditory workstation (TDT system 3). The neural output was fed into a neurophysiology base station (RX5 Pentusa, TDT) with OpenEx platform. Multiunit signals were preamplified, band-pass filtered (300-1000 Hz) and threshold set at 1.5X root mean square (RMS) level. The gain of the preamplifier was fixed at 255X; the resolution of the preamplifier was 16-bits on the AD converters; and the input range of the preamplifier was ± 4.5 mV. The recording sampling rate was 24.4 kHz.

First, spontaneous activities were recorded, followed by the tone burst at 0.5 sec and 5 sec interval, followed by tuning curve recording; raw spontaneous activity and tone burst data also collected for analyzing coherence among structures. Next, the right AC was stimulated. Electrical stimuli were charge-balanced biphasic pulse at 120 μsec per phase for width and 1-100 μA for amplitude. The stimuli were incrementally increased at 2 μA increments. The rate of the stimulation was 2 pulses per second (pps). After the stimulation, same recording protocol was repeated for comparison. Coherence

analysis was utilized for statistical analysis before and after ACES and acoustic masking. ANOVA was used to compare spontaneous activity among 3 structures and among groups as well.

Histology study

After completion of all electrophysiology recording, each animal was deeply anesthetized with 5% isoflurane and euthanized. The animal then was perfused transcardially with 100 ml saline followed by 300 ml 4% paraformaldehyde in 0.1 M phosphate buffer (pH 7.4). The cranium was isolated and removed. The brain was removed and post-fixed for 4–6 h in the same fixative and subsequently cryoprotected by immersion in 30% sucrose in 0.1 M PB (pH 7.4) at 4°C overnight. Brain sections of 100- μ m thickness were cut coronally with a sliding microtome (Microm HM 400) at -20°C, which was controlled by a BFS-MP Freezing Stage. The tracks of electrodes in the DCN, IC, and AC were verified under a Nikon PCM2000 via fluorescent confocal microscope (A', Figure 19).

CHAPTER 4

RESULTS

Due to the limited capacity to handle the volume of the tasks at the same time, some rats underwent MEMRI only, and some of the rats underwent electrophysiology recording only, and some rats were able to participate in both studies. All 46 rats underwent ABR, gap/PPI, elevated plus maze, and Morris water maze. The results are reported in the following sections.

Part I: Blast-induced Tinnitus: findings related to auditory structures

ABR data

[[]: Thresholds

1. Data from all rats that finished ABR testing sessions (n=46):

ABR data were obtained before exposure, immediate following exposure (post-blast day 1), and before MEMRI (post-blast day 35) for rats in the experimental group (the blast group); and ABR data were collected before sham exposure and before MEMRI for the control group. For group average click threshold of left ears, at the baseline, the average threshold tinnitus positive group (n=15), tinnitus negative group (n=14), and the control group (n=17) were 10, 11.3 and 11.7, respectively ($p>0.05$); on post-blast day 1, the average threshold for tinnitus positive group and tinnitus negative group were 52.5 and 41.7, respectively ($p<0.05$); before MEMRI scan, the average threshold for control, tinnitus positive and tinnitus negative groups were 5.4, 5 and 6.7, respectively ($p>0.05$). Figure 21 showed the comparison of the ABR thresholds of the tinnitus positive group, the tinnitus negative group, and the control group at 3 time points (baseline, within 24 hours after the blast exposure, and before MEMRI). For the unexposed ear, the thresholds after the exposure were not significantly increased from

the baseline ($p>0.05$). However, for the exposed ears, compared to the baseline values, the thresholds increased significantly for the blast groups immediately after the blast exposure ($p<0.001$). At the time of the MRI scanning, all the thresholds returned to the baseline level or lower for both ears and for all 3 groups.

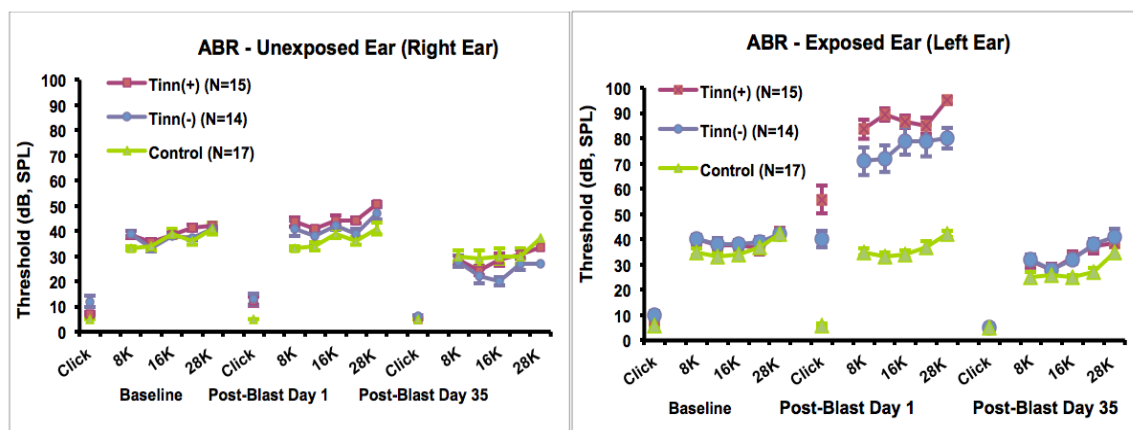


Figure 21. ABR data at baseline, post-blast day 1 and post-blast day 35 (right before MEMRI scanning).

2. Data from all rats that underwent all MEMRI tests and whose data were included for MEMRI analysis ($n=19$):

19 rats that finished MEMRI scanning and whose data were included for the analysis. Figure 22 illustrated the ABR thresholds of these rats at the baseline and at the time of MRI scanning, which was around post-exposure day 35. Among 3 groups, the average thresholds of click and tone burst at ≈ 8 KHz, ≈ 12 kHz, ≈ 16 kHz, ≈ 20 kHz, ≈ 28 kHz bands ranged from 5 dB SPL to 40 dB SPL. There was no significant differences at the baseline among 3 groups and between 2 ears ($p>0.05$); and there was no significant differences at the time of the MRI scanning among 3 groups and between 2 ears ($p>0.05$); however, the thresholds of the exposed ear of the sham group and the unexposed ears of all 3 groups at the time of the scanning were significantly lower than that of at the baseline ($p<0.05$).

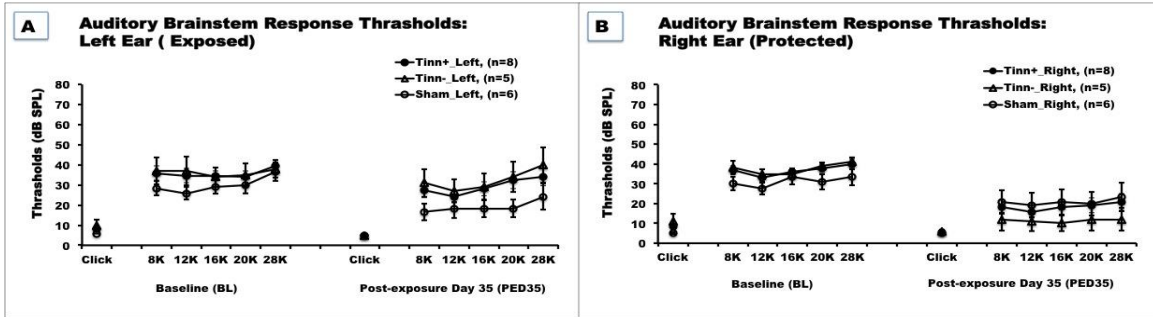


Figure 22. ABR Thresholds for 19 rats that underwent MRI scanning; A: Thresholds of exposed ears at the baseline and at the time of MRI scanning; B: Thresholds of unexposed ears at the baseline and at the time of MRI scanning

[[I]]: Amplitude of P1N1 waveform of the ABR tone burst at ≈28 kHz band

Compared to the average amplitude of the P1N1 of the ABR at the baseline, the

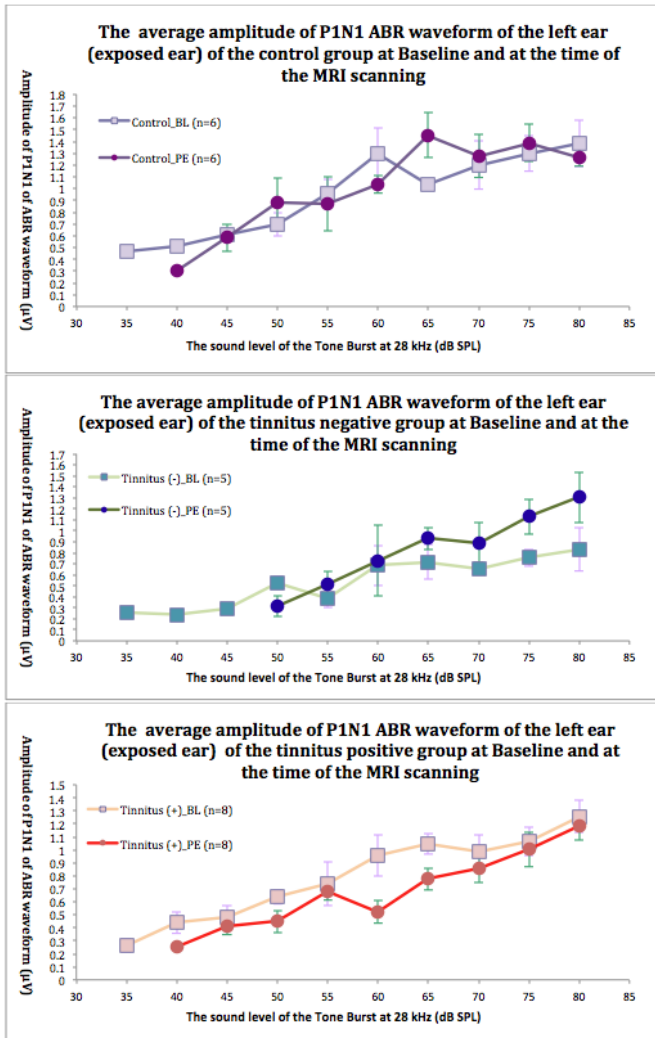


Figure 23. The average amplitude of the P1N1 ABR waveform of the left ears at baseline and at the time of the MRI scanning. Top: the control group; middle: the tinnitus negative group; bottom: the tinnitus positive group

control group did not show significant changes at the time of the MRI scanning ($p > 0.05$); the average amplitude of the P1N1 of the tinnitus negative group was significantly higher at sound levels of 75 dB SPL and 80 dB SPL ($p < 0.05$); and the average amplitude of the P1N1 of the

tinnitus positive group was significantly lower at sound levels 50 dB SPL, 60 dB SPL, and 65 dB SPL ($p < 0.05$). Figure 23 showed the group average of the amplitude of P1N1 of the ABR data from the 19 rats that were included in MEMRI study at 28 kHz tone burst band. Figure 24 showed a picture of the ABR waveform. The amplitude of the first wave (wave I) on an ABR waveform is defined as P1N1-amplitude. In Figure 24, the short red line between 2 blue lines indicates the P1N1-amplitude.

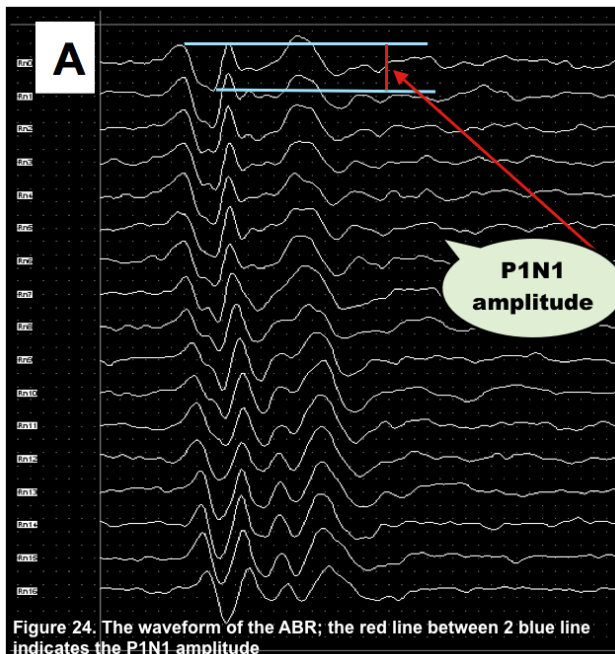


Figure 24. ABR waveform

Diagnostic gap/PPI behavioral data

Gap/PPI behavioral data for rats that underwent MEMRI imaging:

At baseline, all groups showed behavioral evidences of normal hearing (Figure 25). There was no difference among 3 groups ($p > 0.05$). Four weeks after the exposure, which was at the time of MEMRI scanning, the tinnitus positive group ($n=8$) still exhibited robust behavioral evidences of tinnitus at ≈ 28 kHz band ($p < 0.05$); whereas the tinnitus negative group ($n=5$) and the control group ($n=6$) exhibited behavioral evidences of normal hearing ($p > 0.05$). The PPI ratios of all 3 groups were consistently

low at these 2 time points; there was no significant difference among 3 groups and between 2 time points in terms of rats' PPI ratios ($p>0.05$).

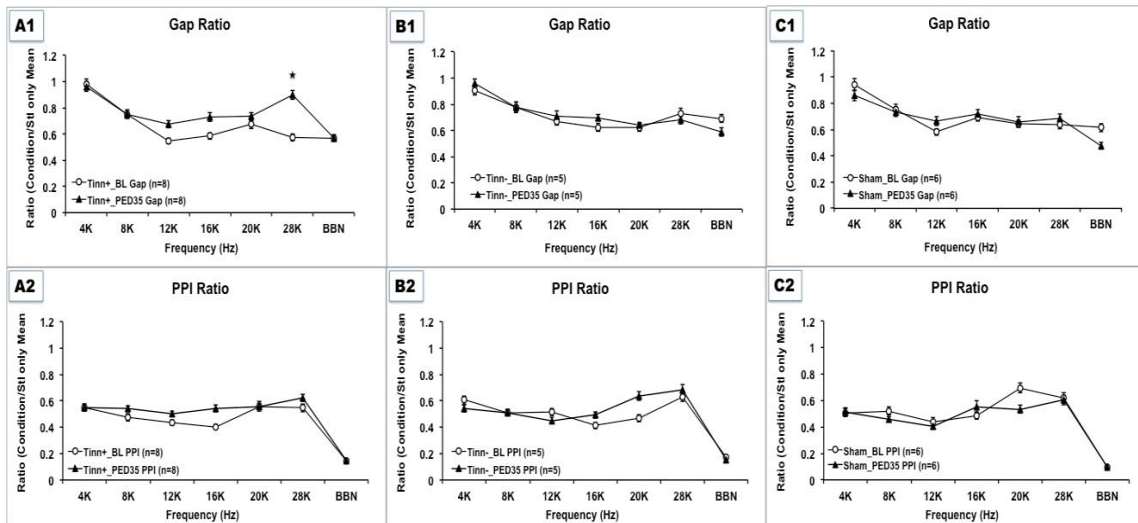


Figure 25. Gap and PPI Ratios; A1: gap ratio of tinnitus positive group before and after blast; A2: PPI ratio of tinnitus positive group before and after blast; B1: gap ratio of tinnitus negative group before and after blast; B2: PPI ratio of tinnitus negative group before and after blast; C1: gap ratio of sham group before and after blast; C2: PPI ratio of sham group before and after blast

MEMRI data

41 rats finished the MEMRI scanning. 30 rats survived the scanning and had manganese uptake into the cerebral parenchyma. Data from the rats with extreme uptake values (“extreme uptake was defined” as that the intensity ratios (ROI/Noise) were higher than the mean+2SD or lower than mean-2SD) was excluded. Image data from 19 rats were included for the MEMRI analysis. Tinnitus positive group exhibited neuronal hyperactivity in bilateral VCN, ipsilateral MGB, and contralateral DCN, DCIC, as well as ECIC; and the differences were significant ($p<0.05$). Figure 26 showed the intensity ratios of ROI/Noise for the auditory brain structures.

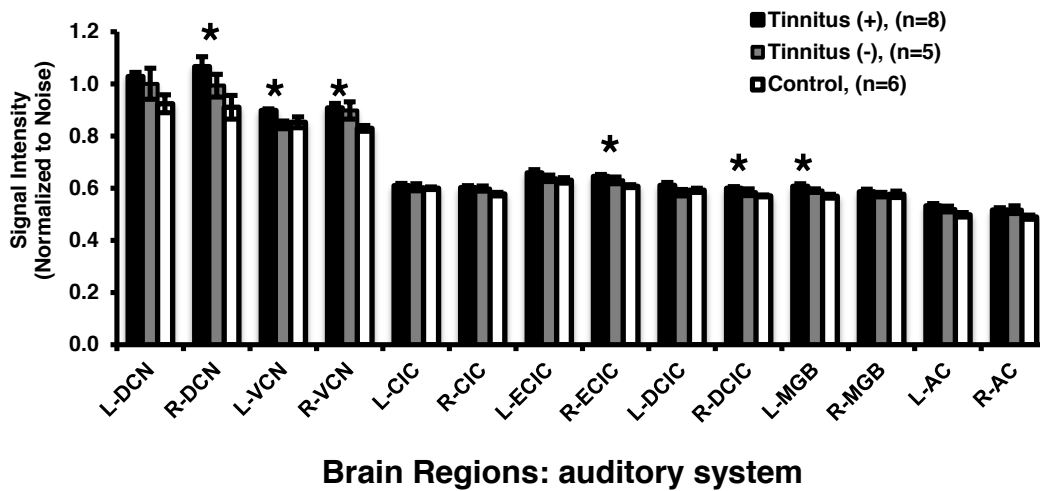


Figure 26. The intensity ratio of ROIs over nearby noise; compared to the tinnitus negative group and the control group, the tinnitus positive group showed significantly higher uptake of manganese into bilateral VCN, contralateral DCN, DCIC as well as ECIC, and ipsilateral MGB ($p < 0.05$).

Electrophysiology data

24 rats finished electrophysiological recordings. For tinnitus positive group, the absolute spontaneous firing rate was highest in the DCN and lowest in the IC (Figure 27).

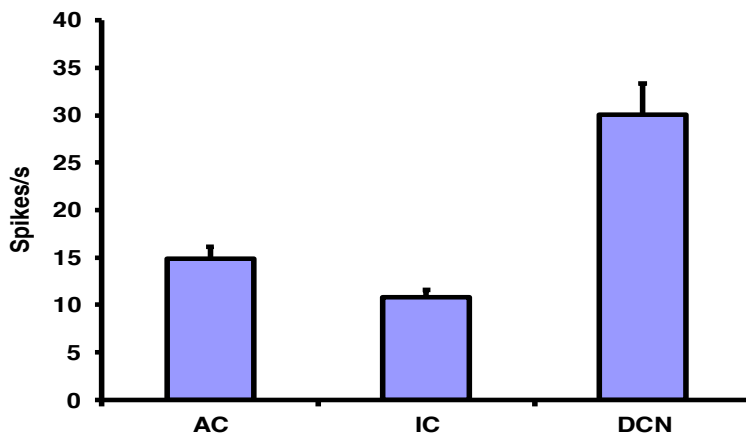


Figure 27. Spontaneous multiunit firing rate in the rat's DCN, IC and AC following blast; data from tinnitus positive group (this graph was obtained from a representative rat in tinnitus positive group)

After ACES, both spontaneous activity and tone burst activity decreased in AC and DCN, but increased in IC (Figure 28), which could be signs of recovery from tinnitus.

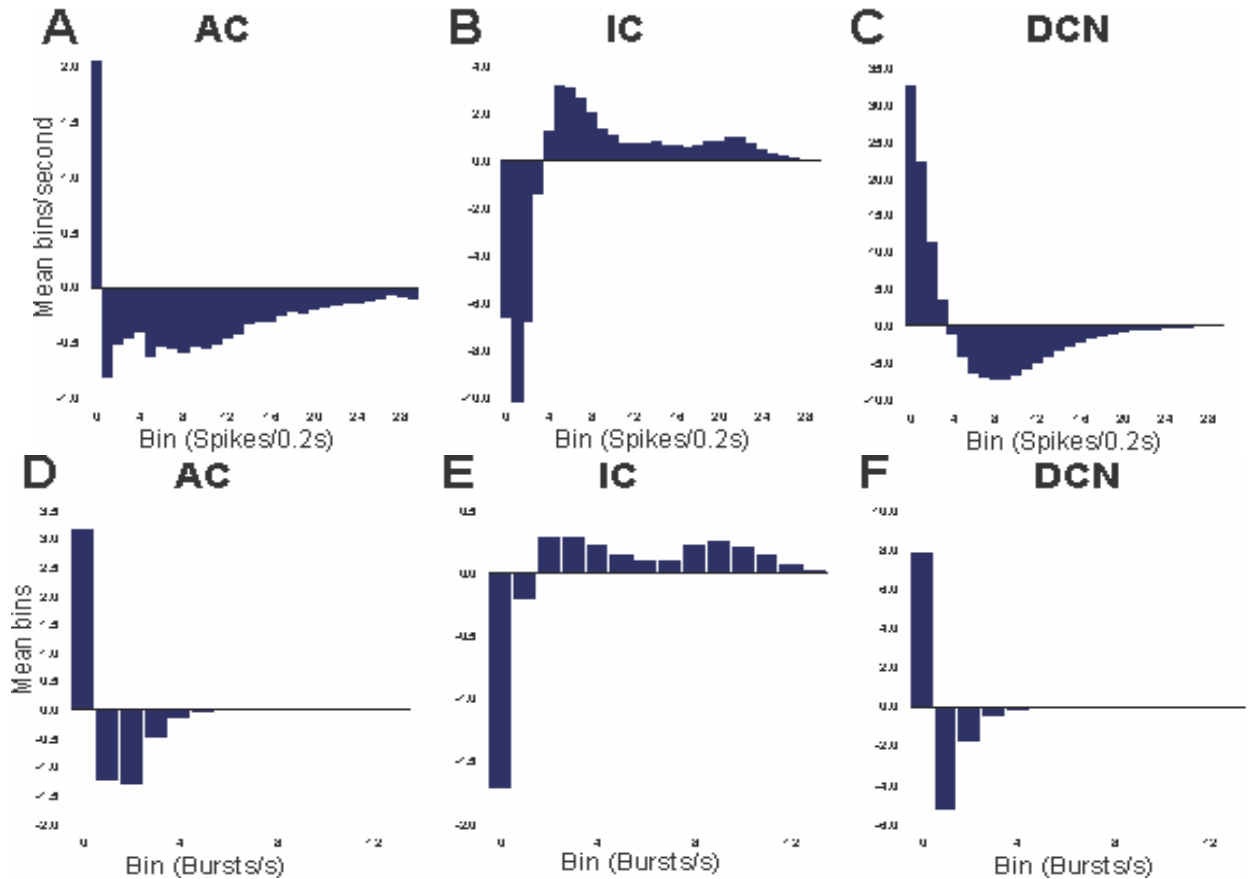


Figure 28. A-C. Firing pattern plot showing that, compared to spontaneous baseline activity, auditory cortex electrical stimulation (ACES) decreased discharge rates in the AC and DCN, but increased in the IC. D-F. At the same time, ACES decreased the counts of bursting events in the AC and DCN, but increased the bursting counts in the IC. The results suggest that ACES modulation-induced tinnitus suppression involve neuromodulation along the auditory axis. (these graphs were obtained from the same rat in Figure 27)

Figure 29 shows that after acoustic masking, coherence coefficient within IC increased, whereas that of other regions were decreased. The masking effect was the strongest if the stimulating acoustic sound was in low frequency range of 6-57 Hz (Figure 29).

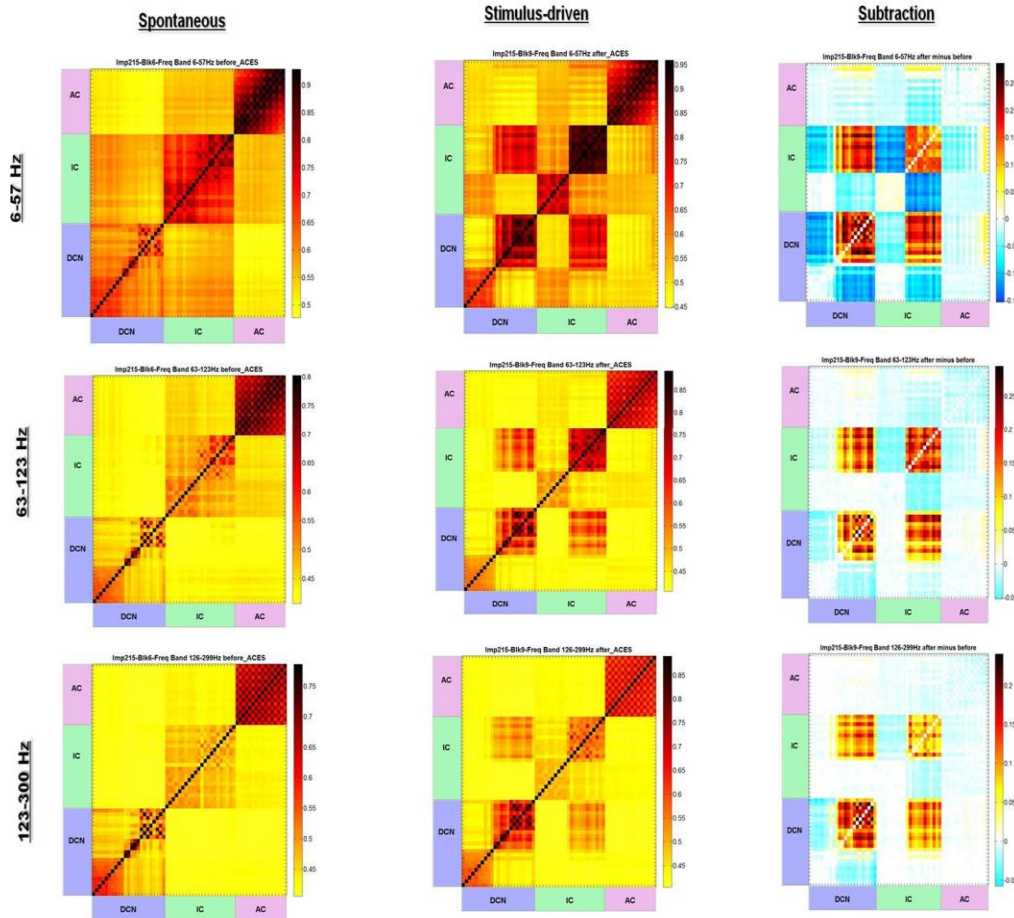


Figure 29. Acoustic masking, coherence coefficient matrix of a rat in tinnitus positive group (the same rat in Figure 27 and 28)

Part II: Blast-related Tinnitus: findings related to non-auditory structures

Elevated Plus Maze

Rats in the sham group made average of $32.6 \pm 7.7\%$ of the entries to the open arms and spent average of $26.2 \pm 6.8\%$ of time on the open arms. Rats in the blast group made average $9.8 \pm 4.7\%$ of entries to the open arms and spent average of $4.8 \pm 2.8\%$ of time on the open arms. Compared rats in the blast group, rats in sham group spent significantly more time on the open arms ($p < 0.05$) and made significantly more entries to the open arms ($p < 0.05$).

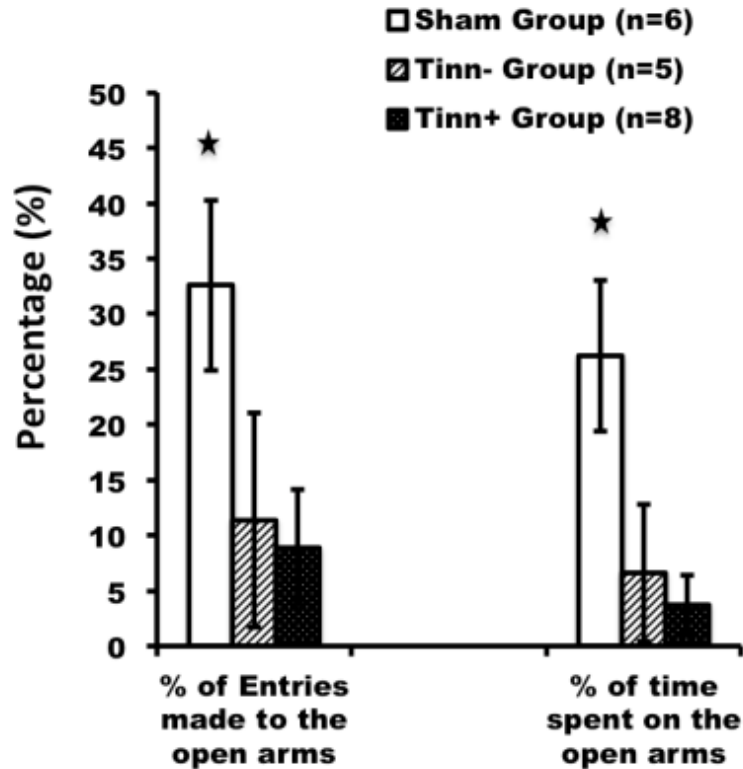


Figure 30. Elevated Plus Maze (2 days before MRI scanning).

Morris Water Maze

(1) Spatial task acquisition: The first three blocks were spatial task acquisition trials, which consisted of four trials for each block. For block 1, 2, and 3, the average time rats in sham group swam before they escaped to the platform were 44.3 ± 4.1 sec, 31.1 ± 4.3 sec, and 22.3 ± 2.8 sec, respectively; and the average escape latencies of rats in the blast group were 47.8 ± 3 sec, 27.9 ± 3 sec, and 22.7 ± 3 sec, respectively. The average velocity at which rats in sham group swam during block 1, 2 and 3 were 32 ± 3.3 cm/s, 37.3 ± 3.1 cm/s, and 35.7 ± 3.7 cm/s, respectively. The average velocity at which rats in the blast group swam during block 1, 2 and 3 were 36.4 ± 3.2 cm/s, 35.2 ± 3.6 cm/s, and 29.7 ± 1.3 cm/s, respectively. The differences in the latency and velocity between 2 groups were statistically insignificant ($p > 0.05$).

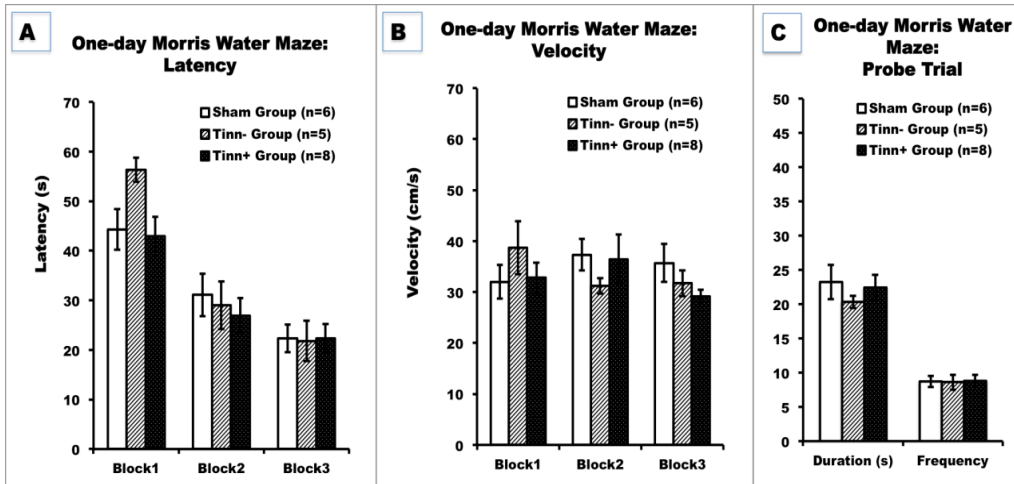


Figure 31. Data from One-day Morris water maze trials; there was no significant difference among 3 groups ($p>0.05$).

(2) Probe trial acquisition: During the probe trial, the rats in the sham group made 8.7 ± 0.8 times of entry to the zone where the platform used to be and spent average 23.2 ± 2.5 sec in that zone; whereas rats in the blast group made 9.7 ± 0.7 times of entry to that zone and spent average 21.6 ± 1.2 sec at where the platform used to be. The difference between groups in terms of numbers of entry and time spent in that zone was insignificant ($p>0.05$).

MEMRI data

From injection to scanning, the average time of manganese uptake for sham group and the blast groups were 648.2 ± 3.2 min and 640.3 ± 2.1 min, respectively. The differences of time for manganese uptake between groups were not statistically significant ($p>0.05$). Table 2 listed the Signal-to-Noise Ratio (SNR)s for the regions of interest. Compared to rats in the sham group, rats in the tinnitus positive groups demonstrated higher manganese uptake in contralateral superficial group and ipsilateral basolateral group of amygdaloidal complex ($p<0.05$).

Table 2. Signal-to-noise intensity ratio of regions of interest

Limbic and Paralimbic Structures			Mean SNR	SD of SNR	sig. (p)		Pearson's correlation coefficient	
Amygdaloidal Complex	AMG_S (superficial group)	Left	Tinn+	0.664	0.033	Tinn+ vs. sham	0.067	0.678
			Tinn-	0.649	0.051	Tinn- vs. sham	0.339	
			Sham	0.605	0.049	Tinn+ vs. Tinn-	1	
		Right	Tinn+	0.668	0.053	Tinn+ vs. sham	0.020	0.706
			Tinn-	0.657	0.050	Tinn- vs. sham	0.081	
			Sham	0.578	0.058	Tinn+ vs. Tinn-	1	
	AMG_D (deep group)	Left	Tinn+	0.716	0.042	Tinn+ vs. sham	0.015	0.456
			Tinn-	0.676	0.038	Tinn- vs. sham	0.713	
			Sham	0.647	0.037	Tinn+ vs. Tinn-	0.280	
		Right	Tinn+	0.686	0.045	Tinn+ vs. sham	0.050	0.324
			Tinn-	0.664	0.061	Tinn- vs. sham	0.353	
			Sham	0.615	0.045	Tinn+ vs. Tinn-	1	
AMG_C (central group)	Left	Tinn+	0.673	0.042	Tinn+ vs. sham	0.215	0.726	
		Tinn-	0.627	0.039	Tinn- vs. sham	1		
		Sham	0.629	0.043	Tinn+ vs. Tinn-	0.222		
	Right	Tinn+	0.665	0.057	Tinn+ vs. sham	0.595	0.718	
		Tinn-	0.670	0.080	Tinn- vs. sham	0.591		
		Sham	0.622	0.043	Tinn+ vs. Tinn-	1		
Nucleus Accumbens	Acb_C (core)	Left	Tinn+	0.697	0.061	Tinn+ vs. sham	0.082	0.505
			Tinn-	0.650	0.040	Tinn- vs. sham	1	
			Sham	0.629	0.045	Tinn+ vs. Tinn-	0.416	
		Right	Tinn+	0.691	0.060	Tinn+ vs. sham	0.156	0.492
			Tinn-	0.666	0.038	Tinn- vs. sham	0.823	
			Sham	0.627	0.063	Tinn+ vs. Tinn-	1	
	Acb_S (shell)	Left	Tinn+	0.681	0.050	Tinn+ vs. sham	0.388	0.706
			Tinn-	0.649	0.020	Tinn- vs. sham	1	
			Sham	0.642	0.052	Tinn+ vs. Tinn-	0.717	
		Right	Tinn+	0.679	0.047	Tinn+ vs. sham	0.894	0.603
			Tinn-	0.622	0.087	Tinn- vs. sham	1	
			Sham	0.643	0.053	Tinn+ vs. Tinn-	0.366	
ACC (anterior cingulate cortex)	Left	Tinn+	0.478	0.023	Tinn+ vs. sham	0.593	0.638	
		Tinn-	0.482	0.030	Tinn- vs. sham	1		
		Sham	0.461	0.015	Tinn+ vs. Tinn-	1		
	Right	Tinn+	0.481	0.022	Tinn+ vs. sham	0.183	0.671	
		Tinn-	0.481	0.014	Tinn- vs. sham	0.273		
		Sham	0.460	0.020	Tinn+ vs. Tinn-	1		
Hippocampus	Left	Tinn+	0.623	0.079	Tinn+ vs. sham	1	N/A	
		Tinn-	0.652	0.138	Tinn- vs. sham	1		
		Sham	0.589	0.070	Tinn+ vs. Tinn-	1		
	Right	Tinn+	0.620	0.060	Tinn+ vs. sham	0.552	N/A	
		Tinn-	0.599	0.128	Tinn- vs. sham	1		
		Sham	0.557	0.070	Tinn+ vs. Tinn-	1		

When the tinnitus positive group and tinnitus negative group was combined into the blast group (n=13), the blast group had significantly higher uptake of the manganese into bilateral superficial and deep groups of the amygdaloidal complex as well as

contralateral anterior cingulate cortex ($p < 0.05$). Figure 32 showed the comparison of the signal-to-noise ratio (SNR) between the blast group ($n=13$) and the control group ($n=6$).

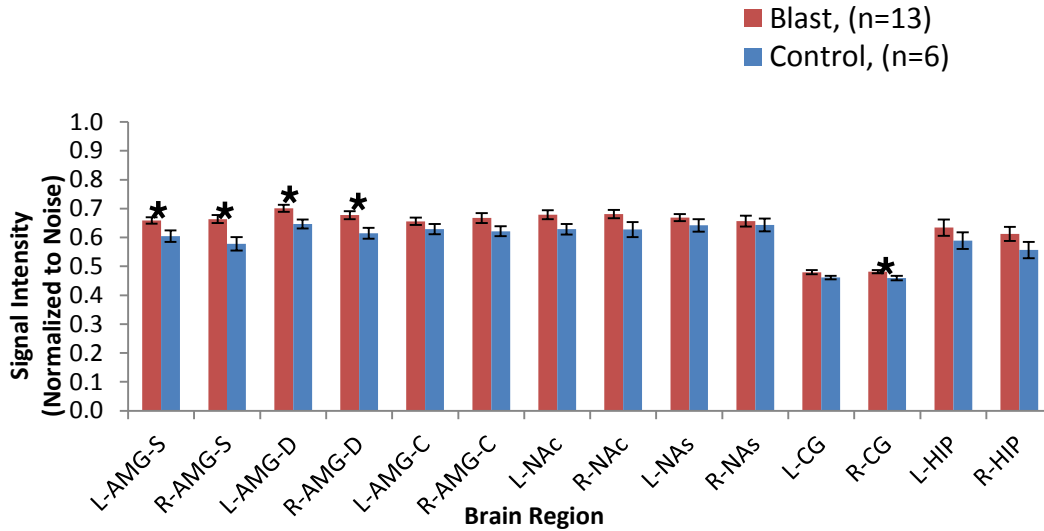


Figure 32. Signal-to-Noise Ratio (SNR) of limbic structures between the blast group and the control group.

The averages of manganese uptake of both sides of the structures among 3 groups were compared. The tinnitus positive group exhibited significantly higher uptake of manganese in DCN, VCN, ECIC, AMG_S and AMG_D ($p < 0.05$). Figure 33 listed the SNRs of the average of both sides for the investigated structures.

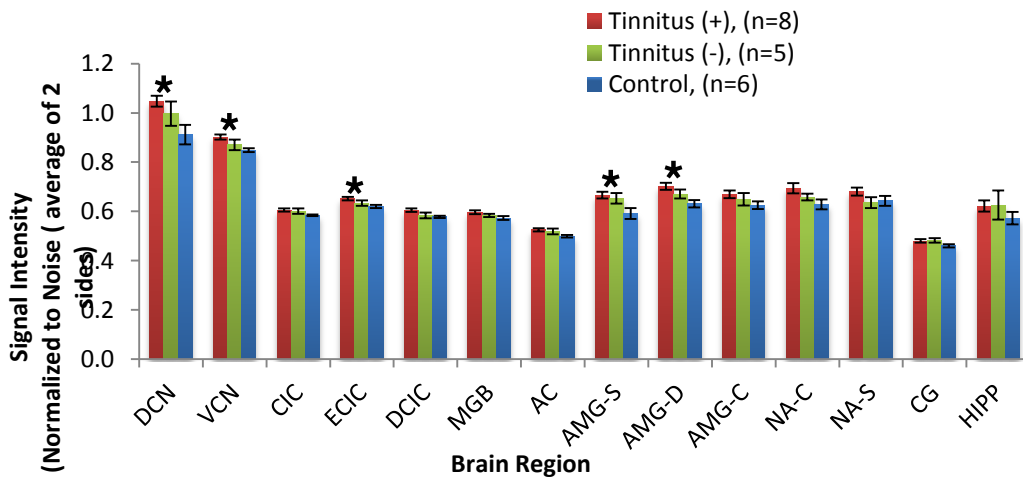


Figure 33. The average of the SNRs for both sides among 3 groups

Part III: The Impacts of Isoflurane and Sevoflurane on Auditory Electrophysiological Signals

Electrophysiology data: Coherence Analysis

Ten rats finished the electrophysiological recording for the anesthetic project. The increase of the dosage of the volatile anesthetics was achieved by increasing the concentration of gas mixture. The deepening of isoflurane was achieved by increasing inhaling concentration of isoflurane from 1.5% to 2.5%; and the deepening of isoflurane was achieved by increasing inhaling concentration of sevoflurane from 3% to 5%. Figure 34 showed the side-by-side comparison of the change of the coherence coefficients after the deepening of the anesthesia with 2 different agents, namely isoflurane and sevoflurane. The panel on the left shows the data from the recording under isoflurane, and the panel on the right shows the data from the recording under sevoflurane. In each of the panel, the matrixes on the left were the pictures of the coherence coefficient matrixes from a single rat; and the matrixes on the right were the pictures of the group average coherence coefficient.

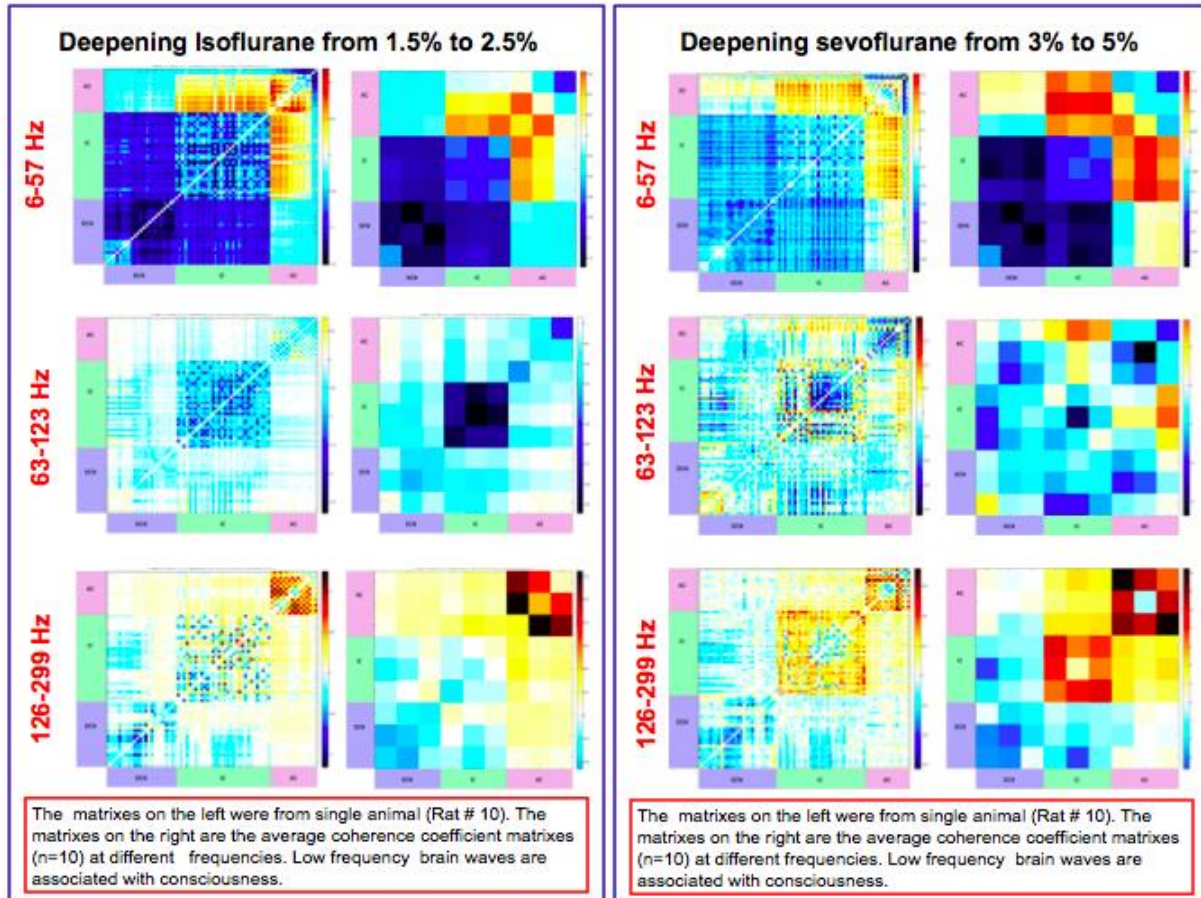


Figure 34. The coherence analysis matrixes; the panel on the left shows the data from the recording under isoflurane, and the panel on the right shows the data from the recording under sevoflurane. In each of the panel, the matrixes on the left were the pictures of the coherence coefficient matrixes from a single rat; and the matrixes on the right were the pictures of the group average coherence coefficient.

This low frequency γ oscillation (6-57 Hz) has been chosen to be the focus of the coherence analysis due to the fact that previous studies have indicated that anesthesia was associated with γ oscillation. Figure 35 showed the summary of our finding: (1) when anesthesia under volatile anesthetics was deepened, the group average coherence coefficients between and within dorsal cochlear nucleus (DCN) and inferior colliculus (IC) were decreased, indicating dissociation and dyssynchrony of these two structures; (2) the group average of coherence coefficients between the IC and auditory cortex (AC) were increased, indicating increased synchrony and connectedness

between these two structures; (3) the deepening of the anesthesia with sevoflurane was associated with dyssynchrony within AC yet the deepening of isoflurane was associated with slightly more synchronized AC; and (4) deepening isoflurane was associated with dissociation between AC and DCN whereas deepening sevoflurane did not affect the connection between AC and DCN.

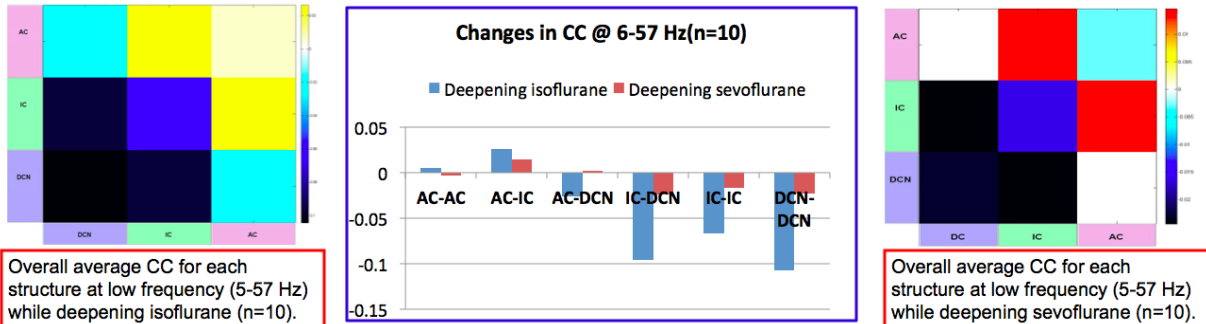


Figure 35. The change of coherence coefficient associated with deepening isoflurane or sevoflurane; the matrix on the left depicts deepening isoflurane; the matrix on the right depicts deepening sevoflurane.

CHAPTER 5

DISCUSSION

Summary of major findings

(1) All rats showed normal ABR hearing thresholds and behavioral evidences of normal hearing at the baseline. (2) One month after the blast exposure, ABR thresholds returned to the baseline level, yet the group average of the amplitude of P1-N1 on the ABR wave I for the tinnitus positive group (n=8) was higher than that of baseline ($p<0.05$). (3) Compared to rats in the sham group, the rats in the blast group (n=13) spent less time on the open arms, and they made less entries to the open arms on the elevated plus maze as well ($p<0.05$). (4) Compared to the sham group (n=6), the blast group (n=13) showed significantly higher uptake of Mn^{2+} in bilateral dorsal cochlear nucleus (DCN) as well as amygdala (AMG-S and AMG-D), contralateral ventral cochlear nucleus (VCN), inferior colliculus (IC), anterior cingulate cortex, as well as auditory cortex (AC), and ipsilateral medial geniculate body (MGB) ($p<0.05$). (5) The auditory cortex electric stimulation and acoustic masking suppressed the spontaneous firing of DCN and AC; and acoustic masking changed the coherence between the DCN and IC. (6) Deepening anesthesia with isoflurane or sevoflurane was associated with dissociation of DCN from IC while strengthening the connection and synchrony between AC and IC.

Part I: Blast-induced Tinnitus and its associated PTSD

Blast-induced tinnitus and its related PTSD affect tens and millions of veterans, men and women who put their lives on the line for the country. The psychological ramifications of these annoying conditions hinder them from successfully returning to civilian life, holding jobs, and maintaining intimate relationships. The gap between the

need of efficacious treatments and the lack of understanding of their underlying mechanisms prompted us to investigate the brain structures involved in their mechanisms using MEMRI technique. Our results indicated that (1) after a single blast exposure at 14-psi overpressure, 8 out of 13 rats developed chronic tinnitus at post-exposure week 5; (2) blasted rats showed evidence of elevated anxiety level; (3) tinnitus positive group showed hyperactivity in the deep and superficial groups of the amygdaloidal complex; and (4) blasted rats showed hyperactivity in amygdala and anterior cingulate cortex.

Collectively, the prefrontal cortex, amygdala (AMG), anterior cingulate cortex (ACC), hippocampus, and insula are the major components of referred to the limbic system (Roxo et al., 2011). Along with the central auditory system, structures in the limbic system are indicated in the etiology of tinnitus especially the maintenance of the presence of tinnitus (Goble et al., 2009; Landgrebe et al., 2009; Lockwood et al., 1998; Mirz et al., 2000b). Human functional neuroimaging studies of patients with chronic tinnitus have shown that neuronal hyperactivity in amygdala, hippocampus, as well as nucleus accumbens, and neuronal hypoactivity in ACC have been associated with chronic tinnitus (De Ridder et al., 2006; Landgrebe et al., 2009; Leaver et al., 2011; Plewnia et al., 2007b; Scheckmann et al., 2011; Shulman et al., 1995; Vanneste et al., 2011). Results from mapping the expression of proto-oncogene *c-fos* in central nerve system using immunocytochemistry in both noise-induced and salicylates-induced tinnitus rat model provided evidences that amygdala is activated in animals exhibited tinnitus (Mahlke and Wallhausser-Franke, 2004; Wallhausser-Franke et al., 2003; Zhang et al., 2003).

(1) Amygdala

Deep within the temporal lobe, the amygdala has been showed to be the pivotal component in the network that underpins fear-related responses. Amygdala assigns emotional significance and yields responses to external stimuli (Pitkanen et al., 2000). Based on its cytoarchitectonic and connectional characteristics, amygdala, a.k.a. amygdaloidal complex, is commonly divided into four groups: the deep or basolateral group (AMG-D), the superficial or cortical-like group (AMG-S), the centromedial group (AMG-C), and the amygdalohippocampal area (AHA) (Sah and Lopez De Armentia, 2003). The amygdaloidal complex networks reciprocally with other brain regions such as prefrontal cortex, anterior cingulate cortex and hippocampus. The basolateral group of the amygdala receives afferent signals from prefrontal cortex, then the signals are projected to central nuclei, hippocampus, and nucleus accumbens among others; and the centromedial group relays cholinergic projections from and to striatal, hypothalamus, and basal forebrain (Sah et al., 2003).

Amygdala is a key structure in the mechanism of several stress-related disorders. In the case of chronic tinnitus, the tinnitus triggers emotional stress; the amygdala consolidates tinnitus-induced stress; then it facilitates the release of stress hormones through hypothalamus-pituitary-adrenal (HPA) axis, and the consolidation of tinnitus-related memory through hippocampus (Kraus and Canlon, 2012). Based on this notion, treatments that targeted some limbic structures were developed and proven to be efficacious. In one such clinical trial, when a GABA agonist (amobarbital) was unilaterally injected into anterior choroidal artery, which supplies amygdalohippocampal region, the contralateral tinnitus was suppressed (De Ridder et al., 2006). In the case of PTSD, amygdala as the hub of fear conditioning plays vital roles in the mechanism of

PTSD. Closely related, fear conditioning and PTSD share similar neural circuitry and molecular mechanisms; and the animal models for studying fear conditioning have been used to study the mechanisms of PTSD (Mahan and Ressler, 2012). Auditory fear conditioning, a subtype of fear conditioning, requires the participation of two amygdala-associated pathways, which are thalamo-amygdala pathway and thalamo-cortico-amygdala pathway. The centromedial group of amygdala is the center of thalamo-amygdala pathway; and the basolateral group of amygdala is the center of thalamo-cortico-amygdala pathway (Romanski and LeDoux, 1992). Studies from fear conditioning have provided compelling evidences that the acquisition and storage of fear-related memory is mediated by lateral nucleus of amygdala through NMDA receptor-mediated synaptic plasticity (Maren, 1999).

Based on Elder's blast-induced PTSD rat model (Elder et al., 2012), we conducted elevated plus maze, one of the many cognitive/psychological tests in Elder's protocol, to test the anxiety level. Our blasted rats showed significantly higher level of anxiety, compared to the rats in the sham group. In Elder's model, rats were exposed with three blast exposures at 10.8-psi under general anesthesia, and the rats have exhibited increase level of anxiety, enhanced contextual fear conditioning, and an abnormal response in a predator scent assay along with elevated level of protein stathmin 1 in amygdala. We used one blast exposure at higher energy level (14-psi). Even though we did not test open field activity post-exposure of predator scent, and we did not test contextual fear conditioning; our results mirrored Elder's findings of elevated anxiety level and hyperactivity in amygdala. It is possible that the rats in the blast group of the current study exhibited PTSD-related traits chronically. Our result of elevated level of neuronal activity as evidenced by elevated neuronal uptake of Mn^{2+} in the

basolateral (deep) and cortical-like (superficial) but not centromedial group indicates that the thalamo-cortico-amygdala pathway may be a key component of the network that underpins the mechanism of blast-induced tinnitus and its associated PTSD.

(2) Anterior cingulate cortex (ACC)

Anterior cingulate cortex plays a vital role in both cognitive and emotional processes. It has extensive reciprocal connections with the prefrontal cortex, and the latter is the key player in the cognitive network whose functions include motivation, error detection, complex motor control, and working memory; furthermore, it networks with amygdala, nucleus accumbens, hypothalamus, insula, hippocampus, and orbitofrontal cortex to participate in the regulation of emotional and stress responses (Bush et al., 2000; Lazar et al., 2000). Based on its anatomy and cytoarchitecture, the ACC can be divided into the ventral portion and dorsal portion. The ventral portion of the ACC involves in the regulation of the emotional and stress responses (Etkin et al., 2006). Hyperactivity in the ACC has been demonstrated to associate with chronic. Our findings, that blast-induced tinnitus was associated with hyperactivity in amygdala and ACC, have resonated with these previous findings.

“ACC-amygdala coupling” refers to the connectivity between the amygdala and the anterior cingulate cortex. In the thalamo-cortico-amygdala pathway, fear-related sensory signals pass through thalamus then relay to an elaborate network of sensory cortices before reach to lateral nucleus of the amygdala for explicit processing (Das et al., 2005). This pathway is regulated by anterior cingulate cortex in a glucocorticoid-dependent manner (Stutzmann et al., 1998). Different regions of the ACC exert different regulatory effects on the amygdala. In human, the dorsal portion of the ACC positively modulates amygdala whereas the ventral portion of the ACC exerts an

inverse effect on the amygdala (Das et al., 2005; Yamasaki et al., 2002). Breakdown of this dynamic interplay between ACC and amygdala has been postulated to give rise to a range of neuropsychiatric disorders (Cremers et al., 2010; Lu et al., 2012; Schultz et al., 2012). Clinical functional imaging studies have demonstrated altered ACC-amygdala coupling in patients with PTSD from both civilian and combat veteran population (Fonzo et al., 2010; Nardo et al., 2010; Rauch et al., 2006; Sripada et al., 2012; Yin et al., 2011). One of the limitations of the current study is that the possible disruption of ACC-amygdala coupling was not addressed. Our findings of hyperactivity in both amygdala and ACC of blasted rats imply that altered ACC-amygdala coupling is possible, but it is unlikely that the net effect of ACC on amygdala for the blasted rats is negative modulation.

(3) Nucleus accumbens and hippocampus

Located adjacent to the caudate and the putamen, the nucleus accumbens (NA) regulates stress and reward responses. In stressed animals, the NMDA receptors mediated stimulation from medial prefrontal cortex (mPFC) directly modulates stress-induced dopamine release in ventral tegmental area of the NAc, from which projections to amygdala and hippocampus participate in the process of coping (Cabib and Puglisi-Allegra, 2012). Moreover, mPFC regulates the stress responses indirectly through regulating the local GABA feedback system in nucleus NAc (Doherty and Gratton, 2007; Pascucci et al., 2007). In this “check and balance” manner, mPRC regulates the coping aspect of the emotional stress responses through NAc.

The hippocampus receives inputs indirectly from the auditory system. The hippocampus is made of entorhinal cortex, dentate gyrus (DG), *Cornu ammonis* (CA) 1 region, CA3 region and subiculum. Auditory inputs and hippocampal outputs are relayed

into and from hippocampus through temporal association area, perirhinal cortex, as well as parahippocampal cortex. It has been established that the storage of memory depends on the hippocampus (Mizuno and Giese, 2005).

Previous studies have indicated the participation of nucleus accumbens and hippocampus in the mechanism of tinnitus or PTSD (Karl et al., 2006; Rauschecker et al., 2010; Schecklmann et al., 2013; Werner et al., 2009). Our results of Mn^{2+} uptake did not reflect this phenomenon, partly due to the complexity of the pathophysiology of the blast-induced neurotrauma. Blast-induced traumatic brain injury has profound and diffused impacts on all brain structures (Svetlov et al., 2009). Blast-induced tinnitus with related PTSD may thus have different pathological characteristics from tinnitus or PTSD rooted from other causes. In a combined behavioral, proteomics and histological study utilizing a stressed rat model, Kwon et. al. compared the differences between the blasted and stressed rats and the stressed-only rats. The one-time blast was delivered at 20-psi overpressure, and 2-week chronic stress was delivered with stresses such as fox urine, loud noises, and cage movements. The results showed that blasted and stressed rats exhibited lasting neuronal and glial cell loss, inflammation and gliosis in pre-frontal cortex and hippocampus whereas stressed-only rats did not (Kwon et al., 2011). The interplay of neuronal apoptosis and synaptic plasticity renders the uncertainty of the direction of the net result of Mn^{2+} uptake in hippocampus and other paralimbic structures such as nucleus accumbens. Our findings from Morris water maze indicated that blast-induced tinnitus and related PTSD did not affect spatial memory; this finding resonates previous similar study of noise-induced tinnitus (Zheng et al., 2011), which has shown that acoustic trauma induced tinnitus was associated with impaired impulse control but not performance accuracy in 5-choice serial reaction

time task, reflecting possible impairment in executive decision making; and that acoustic trauma induced tinnitus did not impair spatial memory (Zheng et al., 2011a; Zheng et al., 2011b).

Evidences from animal studies with rat models showed that DG and CA3 subregions support spatial memory functions; whereas CA1 subregion involves in the processes associated with intermediate-term memory, temporal pattern association and temporal pattern completion as well (Kesner et al., 2004). Current study is the first study to investigate the limbic structures in blast-induced tinnitus rat model, utilizing both behavioral tests and MEMRI; and the ROI in hippocampus of the current study was from CA1. It is possible that intermediate-term memory, temporal pattern association, and temporal pattern completion are not strongly associated with the mechanism of blast-induced tinnitus. Additionally, encoding episodic memory may not require the participation of cognitive function, such as spatial memory; though encoding spatial memory may not be feasible without episodic representation to form a spatial environment map (Eichenbaum et al., 1999).

Conclusion: *Involvement of limbic and paralimbic structures in the mechanisms of blast-induced tinnitus and related PTSD*

After having carefully examined the evidences from the current study and other studies, we proposed the following limbic mechanisms of blast induced tinnitus and related PTSD:

Traumatic injuries inflicted by blast shock wave exposure include but not limit to perforation of the tympanic membrane, shear injury of the middle ear, axonal injury, and hypoperfusion to hippocampus. Following deafferentation of auditory inputs due to the blast trauma, hyperactive signals in the dorsal cochlear nucleus (DCN), generated by

the plastic changes in the DCN, are relayed to brainstem followed by thalamus then auditory cortex to generate “phantom” perception. These signals are also relayed to the basolateral nucleus of amygdala, and high neuronal activities are projected to efferent amygdala, the central nucleus. Central nucleus projects inhibitory inputs to the ACC and stimulatory inputs to hypothalamus-pituitary-adrenal system, resulting in the altered ACC-amygdala coupling, and the release of catecholamines; and the latter triggers the hyperactivity in the dopaminergic NAc. If the functions of NAc are intact, this hyperactivity could indirectly inhibit the MGB therefore mitigates tinnitus. If the functions of the NAc are impaired, tinnitus would manifest. Malfunction of NAc directly affects the coping ability of patients with blast induced tinnitus from the stress of unpleasant sounds. The fact that the neuronal activity in NAc was normal indicates the NA impairment. The dynamic interplay of blast-related neuronal apoptosis, traumatic brain injury, inflammation affect the functions of hippocampus.

It is clear that hyperactivity of amygdala and the ACC are indicated in the mechanism of blast induced tinnitus and/or co-existing PTSD. The roles of the hippocampus, vmPFC, and NAc remain yet to be elucidated. To further investigate the roles of the NAc and vmPFC in the mechanisms of blast induced tinnitus and co-existing PTSD, other hemodynamically independent methods, such as *in vivo* electrophysiology study with microwire electrodes inserted to amygdala, NAc and vmPFC, coherence analysis of these three structures, and/or pharmacological manipulation of NAc using GABA agonists and antagonists, may be complementary.

Part II: The Impacts of Isoflurane and Sevoflurane on Auditory Electrophysiological Signals

The fact; that even though enormous cognitive differences exist between the

states of awareness and unconsciousness, no gross structural changes are observed during the transition of these states; inspires the notion, that the transition through different states of consciousness relies on brain's ability to change computationally (Llinas et al., 1998b). High frequency thalamocortical oscillations are associated with the wakefulness, and γ -band (35-45 Hz) oscillations are associated with non-REM sleep and anesthetized states (Cotillon-Williams and Edeline, 2004a; Hudetz and Imas, 2007; Imas et al., 2005). With insights gained from analyzing the human magnetoencephalography (MEG) recording when study subjects were in various states of consciousness, Llinas et al. proposed that the resonance of the thalamocortical loop may be the substrate for consciousness (Llinas et al., 1998b). Previous neuroimaging study also demonstrated that the functional disconnection at level of thalamus was associated with anesthesia (Alkire et al., 2000b).

Based on this "thalamocortical loop theory of consciousness", Ching et al. utilized 64-channel EEG recording and demonstrated that propofol (2,6-di-isopropylphenol), a GABA_A agonist that renders general anesthesia when administered intravenously, enhanced synchrony between cortex and thalamus, resulting a well-coordinated α -oscillation (10-13 Hz) between these regions (Ching et al., 2010). The current study utilized in-vivo real-time 80-channel microwire electrodes to record electrophysiology data of three structures along the auditory pathway. Compared to EEG, the implanted electrophysiology study yielded more detailed and robust data. And because of that, we were able to utilize coherence analysis to reveal the connectivity among the three structures.

In the coherence analysis, the transient oscillations of spontaneous activities were quantified by applying a time-frequency decomposition technique called "short-

time Fast Fourier Transform (FFT)” (Elisevich et al., 2011b). Coherence is a measure of synchrony between signals from different regions for each FFT frequency component. The phase relationships between signals were extracted with “Hilbert transform” (Mormann, 2000). The mean phase coherence was used to represent the synchronization between regions. The signals were divided into segments based on their frequency domains. For each frequency domain, FFTs from 80 channels formed a matrix, and Coherence coefficient was calculated using the following formula:

$$CC_{(dcn-ac)} = \frac{|F_{dcn} \cdot F_{ac}|}{|F_{dcn}| \cdot |F_{ac}|}$$

(CC: coherence coefficient; Fdcn: FFT of 32 channels of DCN signals; Fac: FFTs of 16 channels of AC signals.) Coherence coefficient represents the connectivity of the brain regions. It ranges from 0 to 1. For highly connected brain regions, their CC between them is closer to be 1. The results from the current study showed that with deepening anesthesia by increasing the inhaled concentration of isoflurane or sevoflurane, the CC between AC and IC increased while the CC between IC and DCN decreased. There was no difference in the direction of the changes between two agents; and the direction of the changes resonates with the previous research using propofol. Microinjection to thalamus with acetylcholine has reversed the halogenated ether induced general anesthesia, indicating that mechanism of anesthesia by halogenated ethers may involve cholinergic blockade at thalamus (Schneider and Kochs, 2007). The current study further provided evidences to support the “thalamocortical loop theory of consciousness”. The extent of the changes was different between two agents, possibly due to the difference in potency between the two agents.

In vivo electrophysiology study with coherence analysis is proven to offer robust and in-depth information regarding the computational information, synchronization information, and connectivity among brain regions independent of hemodynamic changes of the brain. To further test the “thalamocortical loop theory of consciousness”, anesthetic agents that act on different target receptors, such as benzodiazapines, narcotics, ketamine, etc. should be used in the future investigation using *in vivo* electrophysiology study with coherence analysis.

APPENDIX I

IACUC approval



INSTITUTIONAL ANIMAL CARE AND USE COMMITTEE
101 E. Alexandrine St.
Detroit, MI 48201-2011
Telephone: (313) 577-1629
Fax Number: (313) 577-1941

ANIMAL WELFARE ASSURANCE # A 3310-01

PROTOCOL # A 01-10-10

Protocol Effective Period: March 9, 2010 – January 31, 2013

TO: Jessica Ouyang, MS
Physiology
264 Lande Medical Research Building

FROM: Lisa Anne Polin, Ph.D. *Lisa Anne Polin*
Chairperson
Institutional Animal Care and Use Committee

SUBJECT: Approval of Protocol # A 01-10-10
"Impact of isoflurane and sevoflurane on cortical activity: in vivo multi-channel electrophysiology studies and implications in monitoring consciousness"

DATE: March 9, 2010

Your animal research protocol has been reviewed by the Wayne State University Institutional Animal Care and Use Committee, and given final approval for the period effective **March 9, 2010** through **January 31, 2013**. The listed source of funding for the protocol is **AANA Foundation**. The species and number of animals approved for the duration of this protocol are listed below.

<u>Species</u>	<u>Strain</u>	<u>Qty.</u>	<u>Cat.</u>	<u>USDA</u>
RATS	Long-Evans, male at 60-70 days, 200-300 grams	22		D

Be advised that this protocol must be reviewed by the IACUC on an annual basis to remain active. Any change in procedures, change in lab personnel, change in species, or additional numbers of animals requires prior approval by the IACUC. Any animal work on this research protocol beyond the expiration date will require the submission of a new IACUC protocol form and full committee review.

The Guide for the Care and Use of Laboratory Animals is the primary reference used for standards of animal care at Wayne State University. The University has submitted an appropriate assurance statement to the Office for Laboratory Animal Welfare (OLAW) of the National Institutes of Health. The animal care program at Wayne State University is accredited by the Association for Assessment and Accreditation of Laboratory Animal Care International (AAALAC).

REFERENCES

1. Abbas, P.J., 1988. Electrophysiology of the auditory system. *Clinical physics and physiological measurement : an official journal of the Hospital Physicists' Association, Deutsche Gesellschaft fur Medizinische Physik and the European Federation of Organisations for Medical Physics.* 9, 1-31.
2. Adoga, A.A., Adoga, A.S., Obindo, J.T., 2008. Tinnitus and the prevalence of co-morbid psychological stress. *Nigerian journal of medicine : journal of the National Association of Resident Doctors of Nigeria.* 17, 95-7.
3. Alkire, M.T., Haier, R.J., Fallon, J.H., 2000a. Toward a unified theory of narcosis: brain imaging evidence for a thalamocortical switch as the neurophysiologic basis of anesthetic-induced unconsciousness. *Consciousness and cognition.* 9, 370-86.
4. Alkire, M.T., Haier, R.J., Fallon, J.H., 2000b. Toward a unified theory of narcosis: brain imaging evidence for a thalamocortical switch as the neurophysiologic basis of anesthetic-induced unconsciousness. *Conscious Cogn.* 9, 370-86.
5. Army, U., 2009. Investigation of Homicides at Fort Carson, Colorado. Executive Summary, Vol., U.A.C.f.H.P.a.P. Medicine, ed.^eds., Aberdeen Proving Ground, MD, pp. 126.
6. Aschner, J.L., Aschner, M., 2005. Nutritional aspects of manganese homeostasis. *Molecular aspects of medicine.* 26, 353-62.
7. ATA, 2011. Facts About Our Active Military, Vets and Tinnitus. Vol. 2011, ed.^eds.
8. Baguley, D.M., 2002. Mechanisms of tinnitus. *British medical bulletin.* 63, 195-212.

9. Basak, B.K., 1984. Isoflurane as a general anesthetic: Will it displace all other volatile anesthetics? *Journal of the American Association of Nurse Anesthetists*. 614-618.
10. Bissig, D., Berkowitz, B.A., 2009. Manganese-enhanced MRI of layer-specific activity in the visual cortex from awake and free-moving rats. *Neuroimage*. 44, 627-35.
11. Brozoski, T.J., Bauer, C.A., 2005. The effect of dorsal cochlear nucleus ablation on tinnitus in rats. *Hearing research*. 206, 227-36.
12. Bush, G., Luu, P., Posner, M.I., 2000. Cognitive and emotional influences in anterior cingulate cortex. *Trends Cogn Sci*. 4, 215-222.
13. Butler, A.B., Cotterill, R.M., 2006. Mammalian and avian neuroanatomy and the question of consciousness in birds. *The Biological bulletin*. 211, 106-27.
14. Cabib, S., Puglisi-Allegra, S., 2012. The mesoaccumbens dopamine in coping with stress. *Neuroscience and biobehavioral reviews*. 36, 79-89.
15. Cernak, I., Noble-Haeusslein, L.J., 2010. Traumatic brain injury: an overview of pathobiology with emphasis on military populations. *Journal of cerebral blood flow and metabolism : official journal of the International Society of Cerebral Blood Flow and Metabolism*. 30, 255-66.
16. Ching, S., et al., 2010. Thalamocortical model for a propofol-induced alpha-rhythm associated with loss of consciousness. *Proc Natl Acad Sci U S A*. 107, 22665-70.
17. Chuang, K.H., et al., 2009. Manganese enhanced MRI reveals functional circuitry in response to odorant stimuli. *NeuroImage*. 44, 363-72.
18. Cohen, J.T., et al., 2002. Blast injury of the ear in a confined space explosion:

- auditory and vestibular evaluation. The Israel Medical Association journal : IMAJ. 4, 559-62.
19. Cotillon, N., Nafati, M., Edeline, J.M., 2000. Characteristics of reliable tone-evoked oscillations in the rat thalamo-cortical auditory system. Hearing research. 142, 113-30.
 20. Cotillon-Williams, N., Edeline, J.M., 2004a. Evoked oscillations in unit recordings from the thalamo-cortical auditory system: an aspect of temporal processing or the reflection of hyperpolarized brain states? Acta Neurobiol Exp (Wars). 64, 253-70.
 21. Cotillon-Williams, N., Edeline, J.M., 2004b. Evoked oscillations in unit recordings from the thalamo-cortical auditory system: an aspect of temporal processing or the reflection of hyperpolarized brain states? Acta neurobiologiae experimentalis. 64, 253-70.
 22. Cremers, H.R., et al., 2010. Neuroticism modulates amygdala-prefrontal connectivity in response to negative emotional facial expressions. Neuroimage. 49, 963-70.
 23. Crossgrove, J.S., Yokel, R.A., 2005. Manganese distribution across the blood-brain barrier. IV. Evidence for brain influx through store-operated calcium channels. Neurotoxicology. 26, 297-307.
 24. Darley, D.S., Kellman, R.M., 2010. Otologic considerations of blast injury. Disaster medicine and public health preparedness. 4, 145-52.
 25. Das, P., et al., 2005. Pathways for fear perception: modulation of amygdala activity by thalamo-cortical systems. Neuroimage. 26, 141-8.
 26. Davies, P.W., Erulkar, S.D., Rose, J.E., 1956. Single unit activity in the auditory

- cortex of the cat. *Bulletin of the Johns Hopkins Hospital*. 99, 55-86.
27. Dawson, G.R., Tricklebank, M.D., 1995. Use of the elevated plus maze in the search for novel anxiolytic agents. *Trends in pharmacological sciences*. 16, 33-6.
 28. De Ridder, D., et al., 2006. Amygdalohippocampal involvement in tinnitus and auditory memory. *Acta oto-laryngologica. Supplementum*. 50-3.
 29. Detsch, O., et al., 1999. Isoflurane induces dose-dependent changes of thalamic somatosensory information transfer. *Brain research*. 829, 77-89.
 30. Doherty, M., Gratton, A., 2007. Differential involvement of ventral tegmental GABA(A) and GABA(B) receptors in the regulation of the nucleus accumbens dopamine response to stress. *Brain research*. 1150, 62-8.
 31. Dong, H.L., et al., 2006. Excitatory and inhibitory actions of isoflurane on the cholinergic ascending arousal system of the rat. *Anesthesiology*. 104, 122-33.
 32. dos Santos, A.P., et al., 2010. Rat brain endothelial cells are a target of manganese toxicity. *Brain research*. 1326, 152-61.
 33. Downman, C.B., Woolsey, C.N., Lende, R.A., 1960. Auditory areas I, II, and Ep: cochlear representation, afferent paths and interconnections. *Bulletin of the Johns Hopkins Hospital*. 106, 127-42.
 34. Drummond, J.C., 2000. Monitoring depth of anesthesia: with emphasis on the application of the bispectral index and the middle latency auditory evoked response to the prevention of recall. *Anesthesiology*. 93, 876-82.
 35. Eggermont, J.J., 2001. Between sound and perception: reviewing the search for a neural code. *Hearing research*. 157, 1-42.
 36. Eggermont, J.J., 2003. Central tinnitus. *Auris, nasus, larynx*. 30 Suppl, S7-12.
 37. Eggermont, J.J., 2007. Correlated neural activity as the driving force for

- functional changes in auditory cortex. *Hearing research*. 229, 69-80.
38. Elder, G.A., et al., 2012. Blast exposure induces post-traumatic stress disorder-related traits in a rat model of mild traumatic brain injury. *J Neurotrauma*. 29, 2564-75.
 39. Elisevich, K., et al., 2011a. An assessment of MEG coherence imaging in the study of temporal lobe epilepsy. *Epilepsia*.
 40. Elisevich, K., et al., 2011b. An assessment of MEG coherence imaging in the study of temporal lobe epilepsy. *Epilepsia*. 52, 1110-9.
 41. Eschenko, O., et al., 2010a. Mapping of functional brain activity in freely behaving rats during voluntary running using manganese-enhanced MRI: implication for longitudinal studies. *NeuroImage*. 49, 2544-55.
 42. Eschenko, O., et al., 2010b. Behavioral, electrophysiological and histopathological consequences of systemic manganese administration in MEMRI. *Magnetic resonance imaging*. 28, 1165-74.
 43. Etkin, A., et al., 2006. Resolving emotional conflict: a role for the rostral anterior cingulate cortex in modulating activity in the amygdala. *Neuron*. 51, 871-82.
 44. Fagelson, M.A., 2007. The association between tinnitus and posttraumatic stress disorder. *American journal of audiology*. 16, 107-17.
 45. Fausti, S.A., et al., 2009. Auditory and vestibular dysfunction associated with blast-related traumatic brain injury. *Journal of rehabilitation research and development*. 46, 797-810.
 46. Fitch, R.H., et al., 2008. Use of a modified prepulse inhibition paradigm to assess complex auditory discrimination in rodents. *Brain research bulletin*. 76, 1-7.
 47. Folmer, R.L., et al., 1999. Tinnitus severity, loudness, and depression.

- Otolaryngology--head and neck surgery : official journal of American Academy of Otolaryngology-Head and Neck Surgery. 121, 48-51.
48. Fonzo, G.A., et al., 2010. Exaggerated and disconnected insular-amygdalar blood oxygenation level-dependent response to threat-related emotional faces in women with intimate-partner violence posttraumatic stress disorder. *Biol Psychiatry*. 68, 433-41.
 49. Goble, T.J., Moller, A.R., Thompson, L.T., 2009. Acute high-intensity sound exposure alters responses of place cells in hippocampus. *Hear Res*. 253, 52-9.
 50. Haenggeli, C.A., et al., 2005. Projections from the spinal trigeminal nucleus to the cochlear nucleus in the rat. *The Journal of comparative neurology*. 484, 191-205.
 51. Hazell, J.W., Jastreboff, P.J., 1990. Tinnitus. I: Auditory mechanisms: a model for tinnitus and hearing impairment. *The Journal of otolaryngology*. 19, 1-5.
 52. Hermer-Vazquez, R., Hermer-Vazquez, L., Srinivasan, S., 2009. A putatively novel form of spontaneous coordination in neural activity. *Brain research bulletin*. 79, 6-14.
 53. Hinton, D.E., et al., 2006. Tinnitus among Cambodian refugees: relationship to PTSD severity. *Journal of traumatic stress*. 19, 541-6.
 54. Hoa, M., et al., 2008. Tonotopic responses in the inferior colliculus following electrical stimulation of the dorsal cochlear nucleus of guinea pigs. *Otolaryngology--head and neck surgery : official journal of American Academy of Otolaryngology-Head and Neck Surgery*. 139, 152-5.
 55. Holt, A.G., et al., 2010. Evidence of key tinnitus-related brain regions documented by a unique combination of manganese-enhanced MRI and acoustic startle reflex testing. *PloS one*. 5, e14260.

56. Hosek, J.R.a.F.M., 2009. How have deployments during the war on terrorism affected reenlistment? . Vol., ed.^eds. RAND Corporation, Santa Monica, CA.
57. House, J.W., Brackmann, D.E., 1981. Tinnitus: surgical treatment. Ciba Foundation symposium. 85, 204-16.
58. Huber, M., et al., 2002. [Different patterns of regional brain activation during emotional stimulation in alexithymics in comparison with normal controls]. Psychotherapie, Psychosomatik, medizinische Psychologie. 52, 469-78.
59. Hudetz, A.G., Imas, O.A., 2007. Burst activation of the cerebral cortex by flash stimuli during isoflurane anesthesia in rats. Anesthesiology. 107, 983-91.
60. Ibrahim, A.E., Taraday, J.K., Kharasch, E.D., 2001. Bispectral index monitoring during sedation with sevoflurane, midazolam, and propofol. Anesthesiology. 95, 1151-9.
61. Imas, O.A., et al., 2005. Volatile anesthetics enhance flash-induced gamma oscillations in rat visual cortex. Anesthesiology. 102, 937-47.
62. IOM, 2005. Noise and Military Service: Implications for Hearing Loss and Tinnitus. Vol., L.E.J. Humes, L.M.; Durch, J.S., ed.^eds. Institute of Medicine of the national academies, Washington, DC.
63. IOM, 2010. Returning Home from Iraq and Afghanistan: Preliminary Assessment of Readjustment Needs of
64. Veterans, Service Members, and Their Families. Vol., ed.^eds. Institute of Medicine of National Academies, Washington, DC.
65. Jackson, S.J., et al., 2011. Manganese-enhanced magnetic resonance imaging (MEMRI) of rat brain after systemic administration of MnCl: hippocampal signal

- enhancement without disruption of hippocampus-dependent behavior. *Behavioural brain research*. 216, 293-300.
66. Kaltenbach, J.A., et al., 2002. Cisplatin-induced hyperactivity in the dorsal cochlear nucleus and its relation to outer hair cell loss: relevance to tinnitus. *Journal of neurophysiology*. 88, 699-714.
67. Kaltenbach, J.A., Zhang, J., Finlayson, P., 2005. Tinnitus as a plastic phenomenon and its possible neural underpinnings in the dorsal cochlear nucleus. *Hearing research*. 206, 200-26.
68. Karl, A., et al., 2006. A meta-analysis of structural brain abnormalities in PTSD. *Neurosci Biobehav Rev*. 30, 1004-31.
69. Kelly, S.D., 2007. Monitoring consciousness using the Bispectral Index during Anesthesia. In: Aspect Medical Systems, Inc., Vol., ed. eds., pp. 5-10.
70. Kesner, R.P., Lee, I., Gilbert, P., 2004. A behavioral assessment of hippocampal function based on a subregional analysis. *Reviews in the neurosciences*. 15, 333-51.
71. Kraus, K.S., Canlon, B., 2012. Neuronal connectivity and interactions between the auditory and limbic systems. Effects of noise and tinnitus. *Hear Res*. 288, 34-46.
72. Kwon, S.K., et al., 2011. Stress and traumatic brain injury: a behavioral, proteomics, and histological study. *Front Neurol*. 2, 12.
73. Landgrebe, M., et al., 2009. Structural brain changes in tinnitus: grey matter decrease in auditory and non-auditory brain areas. *Neuroimage*. 46, 213-218.
74. Lazar, S.W., et al., 2000. Functional brain mapping of the relaxation response and meditation. *Neuroreport*. 11, 1581-5.

75. Leaver, A.M., et al., 2011. Dysregulation of limbic and auditory networks in tinnitus. *Neuron*. 69, 33-43.
76. Lee, J.H., et al., 2005. Manganese-enhanced magnetic resonance imaging of mouse brain after systemic administration of MnCl₂: dose-dependent and temporal evolution of T1 contrast. *Magnetic resonance in medicine : official journal of the Society of Magnetic Resonance in Medicine / Society of Magnetic Resonance in Medicine*. 53, 640-8.
77. Leonardi, A.D., et al., 2011. Intracranial pressure increases during exposure to a shock wave. *Journal of neurotrauma*. 28, 85-94.
78. Levine, R.A., Abel, M., Cheng, H., 2003. CNS somatosensory-auditory interactions elicit or modulate tinnitus. *Experimental brain research. Experimentelle Hirnforschung. Experimentation cerebrale*. 153, 643-8.
79. Lindholm, M.L., et al., 2009. Mortality within 2 years after surgery in relation to low intraoperative bispectral index values and preexisting malignant disease. *Anesthesia and analgesia*. 108, 508-12.
80. Llinas, R., et al., 1998a. The neuronal basis for consciousness. *Philosophical transactions of the Royal Society of London. Series B, Biological sciences*. 353, 1841-9.
81. Llinas, R., et al., 1998b. The neuronal basis for consciousness. *Philos Trans R Soc Lond B Biol Sci*. 353, 1841-9.
82. Lockwood, A.H., et al., 1998. The functional neuroanatomy of tinnitus: evidence for limbic system links and neural plasticity. *Neurology*. 50, 114-20.
83. Lockwood, A.H., 2005. Tinnitus. *Neurologic clinics*. 23, 893-900, viii.
84. Lowry, L.D., Eisenman, L.M., Saunders, J.C., 2004. An absence of tinnitus.

- Otology & neurotology : official publication of the American Otological Society, American Neurotology Society [and] European Academy of Otology and Neurotology. 25, 474-8.
85. Lu, Q., et al., 2012. Impaired prefrontal-amygdala effective connectivity is responsible for the dysfunction of emotion process in major depressive disorder: a dynamic causal modeling study on MEG. *Neurosci Lett.* 523, 125-30.
 86. Mahan, A.L., Ressler, K.J., 2012. Fear conditioning, synaptic plasticity and the amygdala: implications for posttraumatic stress disorder. *Trends in neurosciences.* 35, 24-35.
 87. Mahlke, C., Wallhausser-Franke, E., 2004. Evidence for tinnitus-related plasticity in the auditory and limbic system, demonstrated by arg3.1 and c-fos immunocytochemistry. *Hear.Res.* 195, 17-34.
 88. Man, A., Naggan, L., 1981. Characteristics of tinnitus in acoustic trauma. *Audiology : official organ of the International Society of Audiology.* 20, 72-8.
 89. Maren, S., 1999. Long-term potentiation in the amygdala: a mechanism for emotional learning and memory. *Trends in neurosciences.* 22, 561-7.
 90. Miller, I.S., McGahey, D., Law, K., 2002. The otologic consequences of the Omagh bomb disaster. *Otolaryngology--head and neck surgery : official journal of American Academy of Otolaryngology-Head and Neck Surgery.* 126, 127-8.
 91. Mills, R.P., Cherry, J.R., 1984. Subjective tinnitus in children with otological disorders. *International journal of pediatric otorhinolaryngology.* 7, 21-7.
 92. Mirz, F., et al., 2000a. Cortical networks subserving the perception of tinnitus--a PET study. *Acta Otolaryngol Suppl.* 543, 241-3.
 93. Mirz, F., et al., 2000b. Cortical Networks subserving the perception of tinnitus--a

- PET study. *Acta Otolaryngol. Suppl.* 543, 241-243.
94. Mizuno, K., Giese, K.P., 2005. Hippocampus-dependent memory formation: do memory type-specific mechanisms exist? *Journal of pharmacological sciences.* 98, 191-7.
 95. Moller, A.R., 2006. Neural plasticity in tinnitus. *Progress in brain research.* 157, 365-72.
 96. Moller, A.R., 2007. The role of neural plasticity in tinnitus. *Progress in brain research.* 166, 37-45.
 97. Moran, J.E., Drake, C.L., Tepley, N., 2004. ICA methods for MEG imaging. *Neurology & clinical neurophysiology : NCN.* 2004, 72.
 98. Mormann, F.L., K; David, P; Elger, C.E., 2000. Mean phase coherence as a measure for phase synchronization and its application to the EEG of epilepsy patients. *Physica D.* 144, 358-369.
 99. Morris, R., 1984. Developments of a water-maze procedure for studying spatial learning in the rat. *Journal of neuroscience methods.* 11, 47-60.
 100. Mrena, R., et al., 2004. Otologic consequences of blast exposure: a Finnish case study of a shopping mall bomb explosion. *Acta oto-laryngologica.* 124, 946-52.
 101. Muhlau, M., et al., 2006. Structural brain changes in tinnitus. *Cerebral cortex.* 16, 1283-8.
 102. Murphy, V.A., et al., 1991. Saturable transport of manganese(II) across the rat blood-brain barrier. *Journal of neurochemistry.* 57, 948-54.
 103. Nardo, D., et al., 2010. Gray matter density in limbic and paralimbic cortices is associated with trauma load and EMDR outcome in PTSD patients. *J Psychiatr Res.* 44, 477-85.

104. Nondahl, D.M., et al., 2002. Prevalence and 5-year incidence of tinnitus among older adults: the epidemiology of hearing loss study. *Journal of the American Academy of Audiology*. 13, 323-31.
105. Norena, A.J., Eggermont, J.J., 2003. Changes in spontaneous neural activity immediately after an acoustic trauma: implications for neural correlates of tinnitus. *Hearing research*. 183, 137-53.
106. Nunez, A., Amzica, F., Steriade, M., 1993. Electrophysiology of cat association cortical cells *in vivo*: intrinsic properties and synaptic responses. *Journal of neurophysiology*. 70, 418-30.
107. Pascucci, T., et al., 2007. The medial prefrontal cortex determines the accumbens dopamine response to stress through the opposing influences of norepinephrine and dopamine. *Cerebral cortex*. 17, 2796-804.
108. Patterson, J.H., Jr., Hamernik, R.P., 1997. Blast overpressure induced structural and functional changes in the auditory system. *Toxicology*. 121, 29-40.
109. Perrine, S.A., Hoshaw, B.A., Unterwald, E.M., 2006. Delta opioid receptor ligands modulate anxiety-like behaviors in the rat. *British journal of pharmacology*. 147, 864-72.
110. Pitkanen, A., et al., 2000. Reciprocal connections between the amygdala and the hippocampal formation, perirhinal cortex, and postrhinal cortex in rat. A review. *Ann N Y Acad Sci*. 911, 369-91.
111. Plewnia, C., et al., 2007a. Moderate therapeutic efficacy of positron emission tomography-navigated repetitive transcranial magnetic stimulation for chronic tinnitus: a randomised, controlled pilot study. *J Neurol Neurosurg Psychiatry*. 78, 152-6.

112. Plewnia, C., et al., 2007b. Moderate therapeutic efficacy of positron emission tomography-navigated repetitive transcranial magnetic stimulation for chronic tinnitus: a randomised, controlled pilot study. *J.Neurol.Neurosurg.Psychiatry*. 78, 152-156.
113. Probst, R., et al., 1987. Otoacoustic emissions in ears with hearing loss. *American journal of otolaryngology*. 8, 73-81.
114. Puel, J.L., et al., 1998. Excitotoxicity and repair of cochlear synapses after noise-trauma induced hearing loss. *Neuroreport*. 9, 2109-14.
115. Rauch, S.L., Shin, L.M., Phelps, E.A., 2006. Neurocircuitry models of posttraumatic stress disorder and extinction: human neuroimaging research--past, present, and future. *Biol Psychiatry*. 60, 376-82.
116. Rauschecker, J.P., Leaver, A.M., Muhlau, M., 2010. Tuning out the noise: limbic-auditory interactions in tinnitus. *Neuron*. 66, 819-26.
117. Richmond, D.R., et al., 1989. Physical correlates of eardrum rupture. *The Annals of otology, rhinology & laryngology*. Supplement. 140, 35-41.
118. Ridgway, J.P., 2010. Cardiovascular magnetic resonance physics for clinicians: part I. *Journal of cardiovascular magnetic resonance : official journal of the Society for Cardiovascular Magnetic Resonance*. 12, 71.
119. Romanski, L.M., LeDoux, J.E., 1992. Equipotentiality of thalamo-amygdala and thalamo-cortico-amygdala circuits in auditory fear conditioning. *The Journal of neuroscience : the official journal of the Society for Neuroscience*. 12, 4501-9.
120. Romon, Y.C., S., 1911. *Histologie du Système Nerveux de l'Homme et des Vertébrés Vol.*, Maloine, Paris.
121. Roxo, M.R., et al., 2011. The limbic system conception and its historical

- evolution. *TheScientificWorldJournal*. 11, 2428-41.
122. Sah, P., et al., 2003. The amygdaloid complex: anatomy and physiology. *Physiological reviews*. 83, 803-34.
 123. Sah, P., Lopez De Armentia, M., 2003. Excitatory synaptic transmission in the lateral and central amygdala. *Ann N Y Acad Sci*. 985, 67-77.
 124. Saunders, J.C., 2007. The role of central nervous system plasticity in tinnitus. *Journal of communication disorders*. 40, 313-34.
 125. Schecklmann, M., et al., 2011. Neural correlates of tinnitus duration and Distress: A positron emission tomography study. *Hum Brain Mapp*.
 126. Schecklmann, M., et al., 2013. Neural correlates of tinnitus duration and distress: a positron emission tomography study. *Hum Brain Mapp*. 34, 233-40.
 127. Schneider, G., Kochs, E.F., 2007. The search for structures and mechanisms controlling anesthesia-induced unconsciousness. *Anesthesiology*. 107, 195-8.
 128. Schultz, D.H., Balderston, N.L., Helmstetter, F.J., 2012. Resting-state connectivity of the amygdala is altered following Pavlovian fear conditioning. *Front Hum Neurosci*. 6, 242.
 129. Sebel, P.S., et al., 2004. The incidence of awareness during anesthesia: a multicenter United States study. *Anesthesia and analgesia*. 99, 833-9, table of contents.
 130. Seidman, M.D., et al., 2008. Direct electrical stimulation of Heschl's gyrus for tinnitus treatment. *The Laryngoscope*. 118, 491-500.
 131. Shiomi, Y., et al., 1997. Characteristics of DPOAE audiogram in tinnitus patients. *Hearing research*. 108, 83-8.
 132. Shulman, A., et al., 1995. SPECT Imaging of Brain and Tinnitus-

- Neurotologic/Neurologic Implications. *Int.Tinnitus.J.* 1, 13-29.
133. Silva, A.C., Bock, N.A., 2008. Manganese-enhanced MRI: an exceptional tool in translational neuroimaging. *Schizophrenia bulletin.* 34, 595-604.
 134. Smith, I., Nathanson, M., White, P.F., 1996. Sevoflurane--a long-awaited volatile anaesthetic. *Br J Anaesth.* 76, 435-45.
 135. Sripada, R.K., et al., 2012. Altered resting-state amygdala functional connectivity in men with posttraumatic stress disorder. *J Psychiatry Neurosci.* 37, 241-9.
 136. Steriade, M., 2001. Impact of network activities on neuronal properties in corticothalamic systems. *Journal of neurophysiology.* 86, 1-39.
 137. Stutzmann, G.E., McEwen, B.S., LeDoux, J.E., 1998. Serotonin modulation of sensory inputs to the lateral amygdala: dependency on corticosterone. *J Neurosci.* 18, 9529-38.
 138. Svetlov, S.I., et al., 2009. Biomarkers of blast-induced neurotrauma: profiling molecular and cellular mechanisms of blast brain injury. *J Neurotrauma.* 26, 913-21.
 139. Tucciarone, J., et al., 2009. Layer specific tracing of corticocortical and thalamocortical connectivity in the rodent using manganese enhanced MRI. *NeuroImage.* 44, 923-31.
 140. Tungsinmunkong, S., et al., 2007. Blast injury of the ears: the experience from Yala Hospital, Southern Thailand. *Journal of the Medical Association of Thailand = Chotmaihet thangphaet.* 90, 2662-8.
 141. Turner, J.G., et al., 2006. Gap detection deficits in rats with tinnitus: a potential novel screening tool. *Behavioral neuroscience.* 120, 188-95.
 142. Tyler, R., et al., 2008. Identifying tinnitus subgroups with cluster analysis.

- American journal of audiology. 17, S176-84.
143. Urban, B.W., 2002. Current assessment of targets and theories of anaesthesia. *British journal of anaesthesia*. 89, 167-83.
 144. Van de Moortele, P.F., et al., 2009. T1 weighted brain images at 7 Tesla unbiased for Proton Density, T2* contrast and RF coil receive B1 sensitivity with simultaneous vessel visualization. *NeuroImage*. 46, 432-46.
 145. Vanneste, S., Van de Heyning, P., De Ridder, D., 2011. Contralateral parahippocampal gamma-band activity determines noise-like tinnitus laterality: a region of interest analysis. *Neuroscience*. 199, 481-90.
 146. Wallhausser-Franke, E., et al., 2003. Expression of c-fos in auditory and non-auditory brain regions of the gerbil after manipulations that induce tinnitus. *Exp.Brain Res*. 153, 649-654.
 147. Watanabe, T., Frahm, J., Michaelis, T., 2008. Manganese-enhanced MRI of the mouse auditory pathway. *Magnetic resonance in medicine : official journal of the Society of Magnetic Resonance in Medicine / Society of Magnetic Resonance in Medicine*. 60, 210-2.
 148. Werner, N.S., et al., 2009. Hippocampal function during associative learning in patients with posttraumatic stress disorder. *J Psychiatr Res*. 43, 309-18.
 149. Yamasaki, H., LaBar, K.S., McCarthy, G., 2002. Dissociable prefrontal brain systems for attention and emotion. *Proc Natl Acad Sci U S A*. 99, 11447-51.
 150. Yin, Y., et al., 2011. Altered resting-state functional connectivity of thalamus in earthquake-induced posttraumatic stress disorder: a functional magnetic resonance imaging study. *Brain Res*. 1411, 98-107.
 151. Yu, X., et al., 2008. Statistical mapping of sound-evoked activity in the mouse

- auditory midbrain using Mn-enhanced MRI. *NeuroImage*. 39, 223-30.
152. Zhang, J., Guan, Z., 2007. Pathways involved in somatosensory electrical modulation of dorsal cochlear nucleus activity. *Brain research*. 1184, 121-31.
 153. Zhang, J., Guan, Z., 2008. Modulatory effects of somatosensory electrical stimulation on neural activity of the dorsal cochlear nucleus of hamsters. *Journal of neuroscience research*. 86, 1178-87.
 154. Zhang, J., Zhang, X., 2010. Electrical stimulation of the dorsal cochlear nucleus induces hearing in rats. *Brain research*. 1311, 37-50.
 155. Zhang, J., Zhang, Y., Zhang, X., 2011. Auditory cortex electrical stimulation suppresses tinnitus in rats. *Journal of the Association for Research in Otolaryngology : JARO*. 12, 185-201.
 156. Zhang, J.S., et al., 2003. Fos-like immunoreactivity in auditory and nonauditory brain structures of hamsters previously exposed to intense sound. *Exp Brain Res*. 153, 655-60.
 157. Zheng, Y., et al., 2011. The effects of acoustic trauma that can cause tinnitus on spatial performance in rats. *Neuroscience*. 186, 48-56.
 158. Zhou, J., Shore, S., 2004. Projections from the trigeminal nuclear complex to the cochlear nuclei: a retrograde and anterograde tracing study in the guinea pig. *Journal of neuroscience research*. 78, 901-7.
 159. Zhou, J., Nannapaneni, N., Shore, S., 2007. Vesicular glutamate transporters 1 and 2 are differentially associated with auditory nerve and spinal trigeminal inputs to the cochlear nucleus. *The Journal of comparative neurology*. 500, 777-87.
 160. Zucchi, R., Ronca-Testoni, S., 1997. The sarcoplasmic reticulum Ca²⁺ channel/ryanodine receptor: modulation by endogenous effectors, drugs and

disease states. Pharmacological reviews. 49, 1-51.

ABSTRACT**BLAST-INDUCED TINNITUS: A COMBINED BEHAVIORAL, MEMRE, AND ELECTROPHYSIOLOGY STUDY**

by

JESSICA OUYANG

May 2014

Advisor: Drs. Steve Cala & Jinsheng Zhang**Major:** Physiology**Degree:** Doctor of Philosophy

Tinnitus and hearing loss are the frequent auditory-related co-morbidities of blast trauma. The etiology of blast-induced tinnitus is also muddled by brain mechanisms associated with emotional and cognitive problems such as anxiety, memory loss, and depression. We set out to develop a realistic and ecologically valid model to address changes of cognitive status and psychological state that are associated with blast-induced tinnitus. In this study, 19 adult rats were randomly divided into the sham group (n=6) and the blast group (n=13). Blast exposure (14-psi overpressure) was conducted via a shock wave tube to expose the left ears of the rats in the blast group, and a sham exposure was conducted to the rats in the sham group. Blast-induced tinnitus was evaluated with gap detection and pre-pulse inhibition (PPI) acoustic startle reflex paradigms; the changes of thresholds of the hearing was evaluated with auditory brainstem response (ABRs), the change in the level of anxiety was evaluated with elevated plus maze; and the change in the status of memory was evaluated with one-day Morris water maze. To investigate blast-induced neuronal changes in the limbic structures, we utilized MEMRI technique. Obtained with MRicro, MR intensity signal-to-

noise ratios (SNRs) of selected limbic structures were measured to represent the level of synaptic activity. Of the 13 rats that were exposed to blast shock wave, 8 rats developed chronic tinnitus on post-exposure day 35 (PED35) and 5 rats did not. Our results showed that compared to rats in the sham group (n=6), (1) rats in the blast group with or without tinnitus demonstrated higher level of anxiety ($p<0.05$); (2) rats that exhibited behavioral evidences of tinnitus (n=8) demonstrated neuronal hyperactivity in basolateral (deep) and cortical-like group (superficial) of the amygdaloidal complex ($p<0.05$); and (3) rats in the blast group demonstrated neuronal hyperactivity in basolateral and cortical-like groups of amygdala along with anterior cingulate cortex ($p<0.05$). In conclusion, the elevated level of neuronal activity in the amygdala and anterior cingulate cortex core indicates central plasticity associated with blast-induced tinnitus and related PTSD; the thalamo-cortico-amygdala pathway likely underpins the blast-induced tinnitus; and altered ACC-amygdala coupling likely underpins the blast-related PTSD.

AUTOBIOGRAPHICAL STATEMENT

JESSICA OUYANG

Education

2014: Ph.D. in Physiology, Wayne State Univ., School of Medicine, Detroit, MI
 2008: M.S. in Nurse Anesthesiology (CRNA), Wayne State University, Detroit, MI
 2002: B.S. in Nursing, Wayne State University, Detroit, MI

Experience

Nurse Anesthetist: Detroit Receiving Hospital, Wayne State Univ., 2009-present
Licensed Nurse: Providence Hospital, Southfield, MI, 2005-2008.
Licensed Nurse: Beaumont Hospital, Troy MI. 2003-2005.
Licensed Nurse: Henry Ford Hospital, Detroit MI. 2003.

Scholarships and Fellowships

American Association of Nurse Anesthetists Foundation (AANA) grant for: *"Impact of isoflurane and sevoflurane on cortical activity: in vivo multi-channel electrophysiology studies and implications in monitoring consciousness"*
 American Association of Nurse Anesthetists Foundation (AANA) fellowship (2010 & 2011)

Awards (selected)

2006 Graduate Professional Scholarship, Graduate School, WSU
 2006 Chair's Honor List in Chemistry, WSU
 2002 Dean's List College of Nursing, WSU

Grant and fellowship awards:

- 2009 American Association of Nurse Anesthetists Foundation (AANA) grant for: *"Impact of isoflurane and sevoflurane on cortical activity: in vivo multi-channel electrophysiology studies and implications in monitoring consciousness"*
- 2010 American Association of Nurse Anesthetists Foundation (AANA) fellowship
- 2011 American Association of Nurse Anesthetists Foundation (AANA) fellowship

Presentations at national and international conferences

- 2011 Ouyang J, Zhang X, VandeVord P, Zhang J. Blast-induced tinnitus: *in vivo* MEMRI and electrophysiology studies. Abstract and poster. Association for Research in Otolaryngology.
- 2011 Ouyang J, Zhang X, Moran J, Zhang, J. Isoflurane and sevoflurane on cortical activities: *in vivo* multi-channel electrophysiology studies and their implications on monitoring consciousness. Abstract and poster. American Association of Nurse Anesthetists.
- 2012 Ouyang J, Lepczyk L, Pace E, VandeVord P, and Zhang J. Blast-induced tinnitus: *in vivo* MEMRI study of extra-lemniscal auditory structures. Abstract and poster. Association for Research in Otolaryngology.
- 2012 Ouyang J, Pace E, Lepczyk L, Zhang W, Zhang J. Blast-induced tinnitus and its related "invisible wounds" in limbic structures: a combined behavioral and MEMRI study. Abstract and Poster. Wayne State University Physiology Symposium.

Peer-reviewed publications

1. **Ouyang J**, Pace E, Lepczyk L, Kaufman M, Zhang W, Zhang J. The involvement of the amygdala in blast-induced tinnitus, anxiety and related traumatic brain injury in rats. PLOS ONE (under review)